STUDIES IN SOL-GEL CHEMISTRY

A thesis submitted in partial fulfilment of the requirements of the Nottingham Trent University for the degree of Doctor of Philosophy

by

Martin Gardener

November 2000

Department of Chemistry and Physics
The Nottingham Trent University

To my parents,
Patrick and Dilys Gardener

"Thieve other flowers"

"If I had my life to live over again, I'd be a plumber. "
– Albert Einstein

ACKNOWLEDGEMENTS

I would like to thank Dr. Carole Perry for the opportunity to carry out this research and helpful advice, guidance and encouragement over the years.

I also thank Mr. Fabrice Martin of the Nottingham Trent University for producing interdigital electrodes on glass substrates by photolithography and Dr. Mike Newton (second supervisor) and Dr. Glen McHale for assistance and advice on acoustic wave device testing.

Also I would like to thank Dr. Frank Mabbs, Dr. Xing Zhao and Mr. John Friend at the EPSRC funded ESR service at Manchester University for recording all ESR spectra in this work and also to Prof. Martyn Symmons for useful discussions on ESR.

I would also like to thank Dr. Alex Slawin, formerly of Loughborough University, and now at St. Andrews University for single crystal structure analysis.

Finally I would also like to thank members of the Inorganic Research group, past and present, - Ms. Linda Heath, Dr. Severine Aubonnet, Dr. Ana Maria-Caballero, Mr. Christopher McLean-Tooke, Dr. Melanie Webb, Mr. David Eglin, Mr. Kirill Shafran and Mr. Simon Thompson - for help in various matters.

Abstract

The aim of this work was twofold. Firstly the incorporation of thermochromic bis(diammine)copper(II) chloride complexes and the derived diammoniumtetrachlorocuprate(II) salts, into silica sol-gel materials was investigated examining the differences in thermochromic behaviour including mechanisms of interaction between the free compounds and the doped materials. Secondly the aqueous sol-gel chemistry of zinc acetate was studied examining the nature of condensed phases from low (0.1M) and high (saturated, 1.38M) concentration solutions. The effect of low levels of sulphate ions on the condensation products produced from saturated solutions was also investigated. Finally zinc oxide thin films were prepared from dispersions of zinc hydroxyacetate materials for acoustic wave devices.

Incorporation of bis(diammine)copper(II) chloride complexes in silica sol-gel by a two-step acid/ base process resulted in a material with differences in optical properties characteristic of a restriction of in-plane ligand motion arising from hydrogen bonding of soluble silica species to the hydrogen atoms of the $-NH_2$ groups. Thermal treatment of the materials to 80°C for 1 hour gave a similar purple → blue colour transition as for the free complexes. For bis(ethanediammine) and bis(1,2-propanediammine) complexes this resulted from the loss of water followed by chloride ion coordination to the Cu(II) ions while the bis(N,N'-diethylethylenediammine) complex changed from light blue to green as the bulky ligands crowd the axial positions and prevent coordination of the chloride. Prolonged thermal treatment of the doped silicas (24 hours) resulted in irreversible colour changes not found for the free compounds with bis(ethanediammine) and bis(1,2-propanediammine) complexes becoming green while the bis(N,N'-diethylethylenediammine) complex became yellow. This transition was found to result from the complex migrating into and being trapped in regions of strong electronic influence in the silica resulting in a twisting of the in-plane ligands towards a tetrahedral geometry. Incorporation of bis(1,2-propanediammine) into colloidal silica gel gave light blue coloured samples as differences in surface chemistry of the matrix resulted in a different degree of geometric distortion.

Doping of alkoxide silica sol-gel with 1,2-diammoniumpropanetetrachlorocuprate salts resulted in a pale green, transparent material that became yellow when thermally treated to 80°C for 1 hour corresponding to the colour for the low temperature phase to high temperature phase colour found for the free compound. The colouration of the high temperature phase could be preserved by desiccation of the material and was reversed upon exposure to humidity. Thermal treatment of the silica for longer periods (24 hours) gave deep green coloured samples as a proton was transferred intermolecularly to the matrix with coordination of the resulting $-NH_2$ groups to the Cu(II). Cooling and rehydration of these samples under ambient conditions gave light blue coloured samples with optical characteristics similar to those of solutions of the complex isolated from appropriately acidified solutions of the bis(1,2-propanediammine)copper(II) chloride complex containing two ammonium and two ammine groups. These samples became deep green when heated to 80°C for 1 hour even though the free compound did not show any thermochromic behaviour hence suggesting interaction with the silica. Thermal treatment of the samples to 150°C for 1 hour gave an irreversible red/ brown colouration. The reason for this is not clear but could not be attributed to decomposition of the complex.

Condensation products obtained from low (0.1M) concentration zinc acetate solution were found to be dependant upon the pH of the solution and pK_a of the alkali used for precipitation. A critical pH of 10.6 was found experimentally, and explained by theoretical calculations using the Partial Charge Model, above which ionic dissociation of acetate from zinc occurred resulting in formation of crystalline hydrous zinc oxide phases. Precipitation with ammonia formed rhombohedral particles of ε-$Zn(OH)_2$ (Wulfingite) from the 2-dimensional growth of $[Zn(OH_2)_4(OH)_2]^0$ precursors plus a small amount of zinc oxide. Increasing the pK_a of the alkali (KOH or NaOH) resulted in zinc oxide (zincite) formation through deprotonation of the acidic μ^3 bridging hydroxyl groups formed during olation. Condensation below pH10.6 resulted in an amorphous, polymeric material based upon μ^2 bridging acetate ligands and bridging hydroxyls. The slow reaction rates at the low Zn^{2+} concentration resulted in a polymer structure consisting of acetates with O-C-O angles close to that of free acetate with minimum strain. The polymeric structure was formed via a reaction pathway that was found to be independent of pH with solid phases resulting only from condensation between h=2 precursors.

Addition of small amounts of sulphate ions (ca. $1SO_4^{2-}$: $3400Zn^{2+}$) to saturated solutions of zinc acetate prior to ammonia addition resulted in zinc oxide formation when dispersions of zinc hydroxyacetate were warmed to temperatures above 40°C following a washing process to remove contaminating ions. A semi-qualitative catalytic mechanism for sulphate induced zinc oxide formation has been proposed to account for the observed results and is supported by calculations using the Partial Charge Model.

An initial study into the use of dispersions of zinc hydroxyacetate materials for zinc oxide thin film and acoustic wave device preparation showed that aqueous sol-gel routes to zinc oxide thin films are feasible although the coatings prepared on silica substrates were capable of supporting bulk acoustic waves and not surface acoustic waves.

CHAPTER 1 INTRODUCTION

This program of research focuses on two aspects of sol-gel chemistry – the incorporation and behaviour of thermochromic inorganic complexes in alkoxide derived silica sol-gel and the aqueous chemistry of zinc acetate.

Chapter 1 gives a brief introduction into the alkoxide and aqueous sol-gel processes and the structural information that may be obtained from the infrared spectra of metal acetates while a description of the methods and techniques used during this work is given in Chapter 2.

In Chapter 3 preparation and characterisation of thermochromic bis(diammine)copper(II) chloride complexes is presented that were used to prepare doped alkoxide derived silica sol-gels studied in Chapter 4.

Chapter 5 examines the materials that may be obtained from condensation in low concentration (0.1M) aqueous zinc acetate solution while Chapter 6 looks into condensation in saturated (1.38M) zinc acetate systems and the influence of small amounts of sulphate ions on the sol preparation process developed.

A method of preparing zinc oxide thin films using the sols prepared in Chapter 6 is presented in Chapter 7 along with the performance of the films as acoustic wave devices.

Finally Chapter 8 proposes further work to expand and develop the experiments presented in this thesis.

Introductions to specific areas will be covered separately at the start of the relevant chapter.

1.1 THE ALKOXIDE SOL-GEL PROCESS

"Conventional" processing of ceramic materials and glasses has for centuries involved very high temperatures (1000-2000°C). Dense glasses are produced by melting metal oxides in the desired stoichiometry and supercooling the melt without crystallisation. The main drawbacks

of the method are the problems of purity and homogeneity together with the cost of thermal processing.

The sol-gel process makes possible preparation of porous or dense ceramic glasses with high homogeneity, purity and optical quality as monolithic pieces or thin films[1,2]. Sol-gel derived materials have been used to prepare a large range of products for a wide range of applications such as lenses, mirrors, waveguides, fibres, laser materials, optical filters, sensors and catalysts. New types of ceramic materials – organic/inorganic hybrid composites – have been created using the sol-gel process by incorporating high temperature intolerant organic compounds, such as dyes and polymers, into the metal oxide matrix at low temperatures resulting in materials with a wide range of properties[1-3].

A *sol* is a colloidal dispersion of particles or macromolecules 1-500nm diameter in a liquid. A *gel* is formed when a dispersed substance forms a continuous solid network contacting two sides of the liquid container with a system of interpenetrating, liquid filled pores. Gels may further be classified. *Xerogels* are formed when the gel is allowed to dry through evaporation. These gels are monolithic and usually much denser than other prepared gels. Evaporation of the solvent to the point when the liquid meniscus begins to retreat into the gel pores results in the formation of a solid-gas interface. This interface is of higher free energy than a solid-liquid interface and so the energy of the system increases. To counter this the gel contracts to minimise surface area and so minimise energy. For this reason evaporation of solvent must be slow as rapid evaporation puts great stress on the solid network (typically 8Mpa/cm^2) and causes catastrophic failure. Slow evaporation allows time for slow structural relaxation and prevents cracking. *Aerogels* are obtained when the liquid is removed from the pores under supercritical conditions. This method removes the presence of a liquid meniscus and so

cracking and shrinkage do not occur. These gels typically have a large surface area (ca. $1000m^2g^{-1}$) and are very lightweight (ca. 3wt% silica).

1.1.1 The chemical process to alkoxide sol-gel silicas

The usual process for production of silica sol-gel materials involves dilution of a precursor – typically tetraethoxysilane (TEOS) or tetramethoxysilane (TMOS) – in alcohol with addition of water and an acid/base to catalyse hydrolysis or condensation. Hydrolysis begins with an S_N2 substitution via a five co-ordinate intermediate[4].

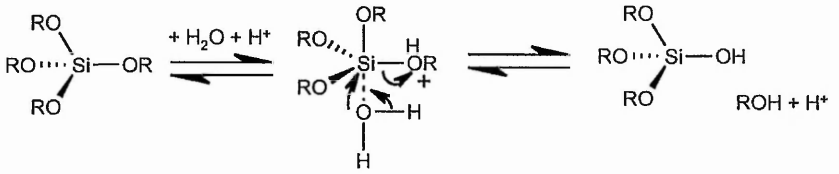

This acid catalysed reaction starts with the protonation of an O-R group with attack on the silicon by water. The penta-coordinate intermediate then loses an alcohol and a proton. This reaction is supported by radio labelled oxygen studies.

Base catalysis occurs by direct attack on the silicon atom by an OH^- ion resulting in an penta-coordinate intermediate with a negative charge on the silicon. This charge is then redistributed until a negative charge develops on an alkoxy group (the leaving group). This then dissociates from the intermediate and accepts a proton from a water molecule.

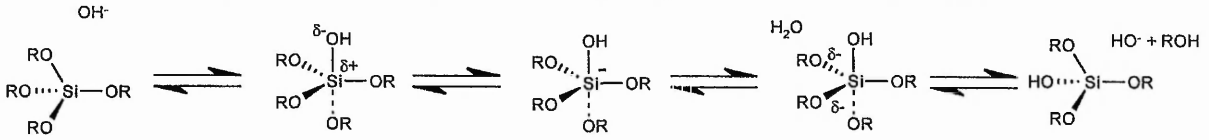

Reaction under acid or basic conditions leads, in general, to two types of silica structure; polymeric by the acid catalysed route or colloidal by the base catalysed route.

The moment reactive silanol groups are present in solution condensation processes can occur. The reaction is nucleophilic and water or alcohol, in low water content mixtures, may be released. Under low pH conditions silanols are protonated increasing the negative partial charge on the silicon atom in the $Si\text{-}OH_2^+$ bond. This renders the molecule susceptible to nucleophilic attack by other Si-OH groups[4].

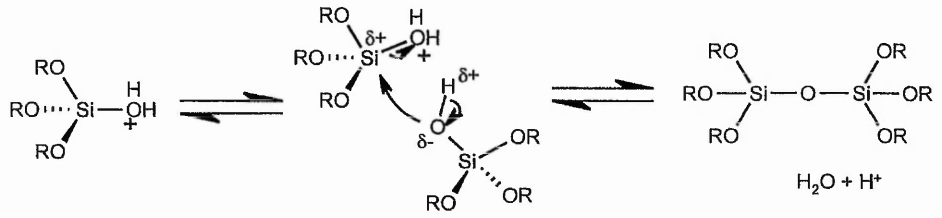

It has been suggested that the most likely route for base catalysed conditions is through the deprotonation of a silanol group forming a penta-coordinate intermediate. The negative charge on the oxygen is then capable of nucleophilic attack on a silicon atom forming Si-O-Si bonds and releasing OR^- groups that acquire protons from water molecules present.

Under acidic conditions the hydrolysis of TEOS occurs very rapidly but the condensation rate is much slower making the two processes distinct. Condensation does not cease at the gelation stage as uncondensed oligomers are still present. This slow condensation makes the probability of sol particles colliding, aggregating and ripening likely before growth to sufficient size to scatter visible light occurs. Gels prepared by this method are typically optically transparent. Conversely gels prepared under basic conditions – or even a two step acid hydrolysis, basic condensation process – results in gels that are usually optically opaque due to large particle sizes resulting from rapid polymerisation.

1.1.2 Gelation

The phenomenon of gelation occurs when the silica network extends from one side of the reaction vessel to the other causing a dramatic increase in viscosity and what visibly appears to be a freezing of the solution. The properties of the gel depend upon the properties of the sol (particle size etc.) prior to gelation. Chemical reactions do not cease upon gelation. In acid catalysed gels a large amount of unreacted, hydrolysed precursors and oligomers will be present. Condensation reactions between precursors and reactions between adjacent silanol groups on aggregated sol particles then continue. This is the process of *ageing*. During this period following gelation significant changes in the structure and physical properties of the gel continue. The dissolution/ re-precipitation processes (*coarsening*) results in the growth or inter-particle "necks" decreasing the porosity and surface area, and hence free energy, of the gel. This leads to an increase in the gel strength. *Syneresis* is an important reaction process during gel shrinkage as proximal Si-OH groups condense to form Si-O-Si bridges. A long ageing time of the gel prior to the drying stage results in a strong silica network that is more resistant to shrinkage but with a smaller surface area.

1.1.3 Drying

Evaporation of the solvent to produce *xerogels* removes the liquid from the pore network. The thermodynamically driven process of shrinkage occurs as a solid-gas interface develops. The presence of a meniscus in the small (<20nm) gel pores causes massive capillary stresses in the material. Cracking from these stresses can be controlled by addition of drying chemical control additives (such as oxalic acid or surfactants) that modify (lower) the surface energy of the solid-gas interface. Careful control of the process before drying in the hydrolysis, condensation, gelation and ageing stages can be used to eliminate small pores from the material. Scherer[5-8], in a detailed mathematical analysis of the drying process, suggested that

it is not the presence of small pores that causes capillary stresses but the presence of polydisperse pore sizes producing strain differentials. Use of templating techniques and other modifications to the process can be used to produce a gel with monodispersed pore sizes.

During the initial stages of drying the rate of loss of mass equals that of loss of mass due to evaporation of solvent and remains constant (figure 1.1).

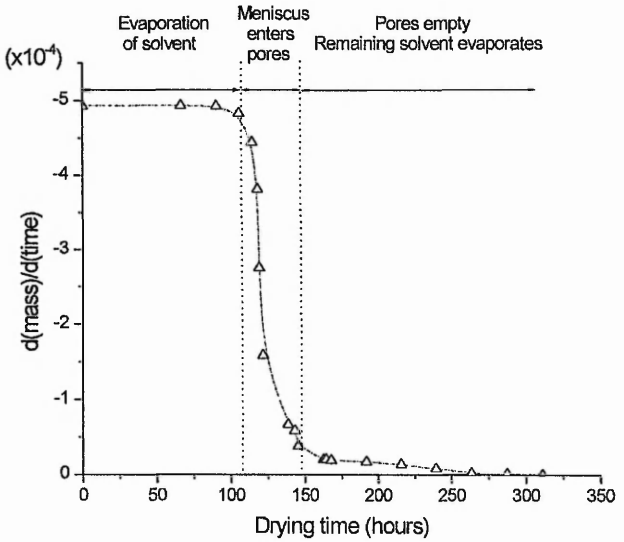

FIGURE 1.1: *EXAMPLE OF ACID CATALYSED SILICA SOL-GEL DRYING (THIS WORK). (1 TEOS: 4 ETOH: 4H_2O)*

As the gel contracts at this stage liquid is expelled from the pores and evaporates at a rate proportional to the gel volume decrease. Gel shrinkage causes the material to densify and the matrix is strengthened sufficiently to resist further contraction. The liquid in the pores at the external surface of the gel begins to move into the gel forming a meniscus and the rate of loss of mass decreases suddenly. It is as this stage that the gel is most susceptible to cracking. Eventually the pores empty of liquid leaving a "dry" gel that may be exposed to atmosphere or thermally treated without further cracking.

1.2 AQUEOUS SOL-GEL CHEMISTRY

1.2.1 Hydrolysis of metal ions

Metal cations (M^{z+}) in aqueous solution are solvated by dipolar water molecules giving rise to aquo complexes $[M(OH_2)_N]^{z+}$. Charge transfer occurs via the M-OH_2 σ bond[9] as electron density is transferred from the $3a_1$ molecular orbitals of the co-ordinated water ligands to the empty orbitals on the metal ion. This weakens the O-H bond in the water ligand and so becomes more acidic. The H_2O ligand then deprotonates by the reaction;

$$[M(OH_2)_N]^{z+} + hH_2O \longrightarrow [M(OH)_h(OH_2)_{N-h}]^{(z-h)+} + hH_3O^+$$

The mean electronegativity χ_p of the hydrolysed precursors $[M(OH)_h(OH_2)_{N-h}]^{(z-h)+}$ depends upon the metal cation M^{z+} and the hydrolysis ratio *h*. Correspondingly, for a given metal cation M^{z+}, a relationship can be established between χ_p and *h*. It is therefore possible to establish *h* for any given value of χ_p.

1.2.2 Condensation

Condensation of hydrolysed metal ions follows two main mechanisms[10, 11].

i) **Olation:** At least one water molecule must be in the metal co-ordination sphere for olation to occur. Olation is therefore observed with aquo-hydroxo complexes and leads to the formation of hydroxyl bridges through an intermediate $H_3O_2^-$ species[10].

this is followed by cleavage of the M-OH_2 bond.

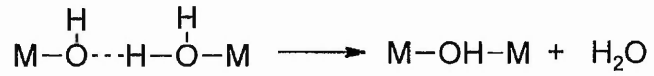

Removal of H_2O from the first co-ordination sphere of the metal is required so the reaction rates depend upon the lability of the H_2O ligand which in turn generally

increases with increasing ionic radius although crystal field stabilisation effects for ions such as Cr^{3+} and Ni^{2+} must be taken into account.

ii) **Oxolation:** High valency cations give rise to oxo-hydroxo anions in aqueous solution. These complexes contain only oxo or hydroxo ligands in the inner co-ordination sphere. No water molecules are co-ordinated to the metal ion making olation impossible. There are two mechanisms for oxide formation in aqueous solution.

a) *Nucleophilic addition* via M-OH or M=O groups occurs. No loss of water is required and so condensation is rapid[10].

b) *Nucleophilic substitution.* The reaction begins with nucleophilic addition of an OH group followed by a 1,3-proton transfer towards the leaving ligand. Formation of the water molecules during oxolation means that oxolation must be slower than olation.

$$M\text{-}OH\text{-}M\text{-}OH \longrightarrow M\text{-}O\text{-}M + H_2O$$

1.3 Infrared spectra of metal carboxylic acid complexes

Extensive infrared studies have been made on metal complexes of carboxylic acids, in particular acetates, and may be used to analyse bonding of acetate ligands to metal ions.

The infrared frequency assignment of sodium acetate and aqueous acetate has been made by Itoh and Bernstein[20]. This is shown in table 1.1.

Mode	Na salt	Aqueous solution
ν(CH)	*2936*	*2935*
δ(CH_3)	-	*1344*
ν(COO)	*1414*	*1413*
ν(CC)	*924*	*650*
ν(CH)	*2989*	*3010*
ν(COO)	*1578*	*1556*
δ(CH_3)	*1430*	*1429*
δ(CH)	*460*	*471*
ν(CH)	*2989*	*2981*
δ(CH_3)	*1443*	*1456*
π(COO)	*615*	*621*

TABLE 1.1: *IR ASSIGMENTS FOR SODIUM ACETATE AND AQUEOUS ACETATE ACCORDING TO ITOH AND BERNSTEIN*

The acetate ligand may co-ordinate in one of the following ways;

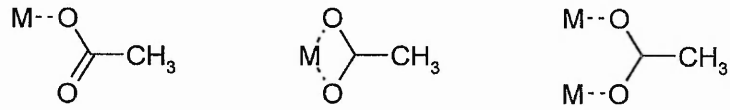

Unidentate Bidentate, chelated Bidentate, bridging

In determining bonding characteristics the difference between the band positions of the symmetric and antisymmetric carbonyl peaks [$\Delta = \nu_{as}(COO) - \nu_s(COO)$] is useful. A careful examination of the infrared spectra of salts of acetates and trifluoroacetates and comparison with x-ray crystal structures led to the conclusion that[13]:

(a) Unidentate complexes exhibit Δ values which are much greater than the ionic complexes

(b) Chelating complexes have Δ values significantly less than the ionic values

(c) The Δ values for bridging complexes are higher than those of chelating and are close to the ionic values.

It must be noted that these simplistic rules only hold true where the bidentates are symmetric[20]. For example asymmetric acetate complexes, such as $Ph_2Sn(CH_3COO)_2$, do not

adhere to these rules[13]. Unidentate complexes also exhibit a strong π(COO) band at 540cm^{-1} making co-ordination of this type easily distinguishable from the infrared spectra[13].

Linkage isomerism is another possible co-ordination mode in acetate complexes that can be distinguished by infrared spectroscopy. For example the (acac)Pd(PPh)$_3$(CH$_3$COO) complex has two isomers[21]:

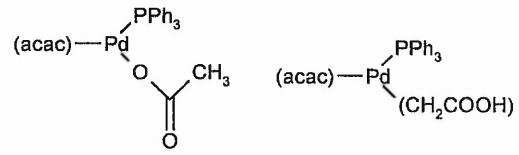

O-isomer C-isomer

In this complex the O-isomer exhibits ν(C=O) at 1640cm^{-1} whereas the C-isomer is shifted to 1670cm^{-1} and a ν(OH) band at 2700-2500cm^{-1} is present in the spectrum.

1.3.1 Infrared spectra of zinc acetates

Chapters 5 and 6 are concerned with the aqueous chemistry of zinc acetate. Previous work on the infrared spectra and x-ray structure of zinc acetate salts has showed that structural information on the co-ordination mode of the acetate ligands can be obtained from the infrared spectra[12-23].

Acetate salts of zinc(II) have five absorption bands associated with the carboxylate functionality. Zinc acetate dihydrate has a bridging bidentate structure[12, 14-17]. The bands associated with the acetate are the antisymmetric stretch (1558cm^{-1}), the symmetric stretch (1445cm^{-1}), the COO bend (696cm^{-1}) and the out of plane bend (622cm^{-1}). Anhydrous zinc acetate has the antisymmetric stretch (1559cm^{-1}), symmetric stretch (1441cm^{-1}), COO bend (695cm^{-1}), out of plane bend (612cm^{-1}) and COO rock (523cm^{-1})[12].

Infrared absorption peak assignments for zinc acetate dihydrate are shown in table 1.2.

Peak (cm^{-1})	Assignment	Peak (cm^{-1})	Assignment
3110	$\nu_{as}(OH_2)$	1020	CH_3 rock
1670	δ(HOH)	953	R(CC)
1558	ν_a(COO)	847	H_2O rock
1445	ν_s(COO)	750	H_2O twist
1390	$\delta_{as}(CH_3)$	696	α(COO)
1355	$\delta_{as}(CH_3)$	622	π(COO)
1057	$\delta_s(CH_3)$		

TABLE 1.2: *ASSIGNMENT OF ZINC ACETATE DIHYDRATE INFRARED SPECTRUM*

The acetate ligands in zinc acetate dihydrate are asymmetric with the difference between the two C-O bond lengths, δ_r, of 0.004Å and a COO angle of 117.5°[14, 17] whereas anhydrous zinc acetate has a δ_r of 0.0095 Å and a COO angle of 121.55°[17, 18]. The rules stated in 1.3 are therefore not strictly applicable to zinc acetate systems. However previous studies examining the infrared spectra of zinc acetates[19] concluded that the difference between antisymmetric and symmetric vibrational bands, Δ, may be used to determine the bonding mode of the acetate. When Δ is around 114cm^{-1} the ligand is chelated. Where Δ is approximately 160cm^{-1} or higher the ligand is μ^2 bridging, although it is difficult to differentiate between free acetate and μ^2 acetates. The position of the symmetric and antisymmetric carboxylate stretching frequencies is dependant upon the metal-oxygen bond ionicity[16,17,19] with the symmetric and antisymmetric peak positions moving to higher wavenumbers as the metal-oxygen bonds become more covalent.

The infrared spectra of the carboxylate is therefore a useful analytical tool in determination of the co-ordination of zinc acetate complexes.

References

1. L. L. Hench, *Ceramics International*, **17**, 206, (1990)

2. C. J. Brinker, T. W. Zerda, *J. Non-Cryst. Solids,* **183**, 243, (1995)

3. J. Zarzycki, *J. Sol-Gel Science and Tech.,* **8**, 17, (1997)

4. C. C. Perry, *Sol-Gel Technology – Sira Technology Center,* (1 day course, not published), (1998)

5. G. W. Scherer, *J. Non-Cryst. Solids*, **87**, 199, (1986)

6. G. W. Scherer, *J. Non-Cryst. Solids*, **89**, 217, (1987)

7. G. W. Scherer, *J. Non-Cryst. Solids,* **91**, 83, (1987)

8. G. W. Scherer, *J. Non-Cryst. Solids*, **99,** 324, (1988)

9. J. Livage, *Prog. In Solid State Chem.,* **18**, 259, (1988)

10. J Livage, M. Henry, J. P. Jolivet, *Structure and Bonding 64*, (rest??)

11. J. Livage, J. Lemerle, *Ann. Rev. Mater. Sci.,* **12**, 103, (1982)

12. M. K. Johnson, D. B. Powell, R. D. Cannon, **37**, 899, (1981)

13. K. Nakamoto, *Infrared spectra of inorganic and coordination compounds,* (New York, Chichester, Wiley), (1986)

14. M. K. Johnson, D. B. Powell, R. D. Cannon, *Spectrochim. Acta A,* **37**, 899, (1981)

15. V. Amirthalingham, *Acta. Crystallogr.,* **11**, 896, (1958)

16. S. C. Chang, *Acta Crystallogr.,* **26**, 673, (1970)

17. T. Ishioka, Y. Shibata, M. Takahashi, I. Kanesaka, *Spectrochim. Acta A,* **54**, 1811, (1998)

18. W. Clegg, I. R. Little, B. P. Straughan, *Acta Crystallogr. C,* **42**, 1701, (1986)

19. N. W. Alcock, V. M. Tracy, T. C. Waddington, *J. Chem. Soc. Dalton Trans.,* **72**, 2243, (1976)

20. K. Itoh, H. J. Bernstein, *Can. J. Chem.,* **34**, 170, (1956)

21. S. Baba, S. Kawaguchi, *Inorg. Nucl. Chem. Lett.,* **9**, 1287, (1973)

CHAPTER 2 METHODS

This chapter describes the methods of analysis, sample preparation and conditions of operation for the techniques used in this thesis.

2.1) FOURIER TRANSFORM INFRARED SPECTROSCOPY[1-7]

The design of the Fourier Transform Infrared (FTIR) spectrometer is based upon the Michelson interferometer (figure 2.1). Infrared radiation from a source (typically a heated element) is directed toward a beam splitter composed of a very thin film of germanium on a potassium bromide substrate.

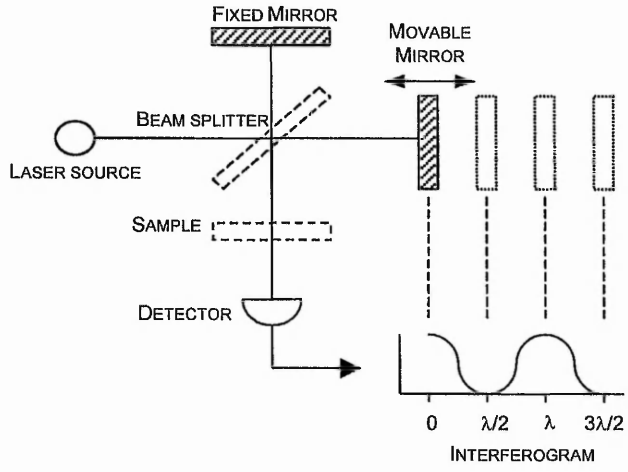

FIGURE 2.1: *BASIC DIAGRAM OF AN FTIR SPECTROMETER*

Ideally the beam splitter would reflect 50% of the incident radiation and transmit the other 50% creating two separate light paths. Along one path the light is reflected directly back to the beam splitter by the fixed mirror where 50% of this light is reflected to the source and 50% passed to the detector. On the other hand the radiation emitted from the source that passed through the beam splitter is reflected by a moving mirror where it is reflected back at the beam splitter and partially reflected to the detector. It is the sum of these two signals – part from the fixed mirror and part from the moving mirror – that reaches the detector. When both moving

mirror and fixed mirror are the same distance from the beam splitter both light paths take the same time to reach the detector. However, if the moving mirror distance increases by x the light along this path has to travel an extra distance. This places the two light waves out of phase and at an appropriate distance determined by wavelength they will cancel each other out (180° out of phase) and no signal is recorded by the detector. In this way is an interferogram constructed.

2.1.1) Construction of the FTIR spectrum

The interferogram, essentially intensity vs. time recorded by the detector, is itself of little use to chemistry. This information must be converted into the spectrum (intensity vs. wavenumber) by the mathematical technique known as Fourier Transform.

$$I(\delta) = \int_0^{\infty} B(\upsilon)\cos(2\pi\delta\upsilon)d\upsilon \qquad B(\upsilon) = \int_{-\infty}^{+\infty} I(\delta)\cos(2\pi\upsilon\delta)d\upsilon$$

Where δ = optical retardation (equal to twice the distance moved by the mirror), $I(\delta)$ = intensity of interferogram as a function of δ and ν = frequency in wavenumbers (cm^{-1}).

If no sample is present in the spectrometer the spectrum is composed of the emitting source modified by the absorption characteristics of the optical components and/ or the presence of water of carbon dioxide from the atmosphere (is not purged with dry gas). This is the background spectrum. With a sample in place the spectrum then contains absorbance bands superimposed on the background spectrum. The background absorbance can then be subtracted, using a computer, from the sample spectrum leaving only those absorbance bands due to the sample. Since the background is recorded at a different time to the sample it is therefore very important that no change to the system be made when scanning the sample.

2.1.2) Advantages of FTIR

The FTIR system also has a much higher accuracy than the dispersive system; an accuracy of $\pm 0.05 cm^{-1}$ can be achieved whereas the dispersive system can only hope at best for $2cm^{-1}$. The dispersive IR system can typically collect the $400\text{-}4000cm^{-1}$ spectrum in 2 or 3 minutes. The FTIR system passes *all* frequencies simultaneously and can collect the whole range in a single movement of a mirror (about 1 second), although several scans are usually averaged to increase the signal to noise ratio. Other factors, such as discontinuities in the dispersive IR spectrum with diffraction grating changes and polarisation by the diffraction gratings, are all eliminated by the FTIR technique resulting in a clearer spectra.

By far the most significant advantage of the FTIR instrument over the dispersive "dual beam" methods is the greatly increased signal to noise ratio. The increase in signal to noise of FTIR over dispersive IR is proportional to the square root of the number of resolution elements being scanned. This is termed Fellgett's advantage, where ν_1 and ν_2 are the range scanned and $\Delta\nu$ is the resolution.

$$F.A. = \sqrt{\frac{\upsilon_1 - \upsilon_2}{\Delta\upsilon}}$$

2.1.3) Diffuse Reflectance

One of the techniques, apart from transmission FTIR, used in this thesis is diffuse reflectance infrared spectroscopy (DRIFTS). This method is a problem because only a small amount of the incident radiation is reflected by the sample (typically 5-8%). The sample is contained in a small holder cup approximately 15mm diameter. The infrared energy is focussed by the optics onto the surface of the sample and the diffusely reflected beam is collected by a large ellipsoidal mirror and then focussed by the optics onto the detector (figure 2.2). The spectrum

acquired by the DRIFTS technique is very similar to that of the transmission spectrum with increases in band intensities of surface features. The spectrum is converted to units of Kubelka-Munk making it equivalent to an absorbance spectrum which can then be used for qualitative and quantitative analytical purposes. If the powder or sample particulates are very small the energy will enter the particle and be reflected multiple times from the surface. During these reflections the energy will be absorbed by surface groups so as to increase the intensity of these groups relative to the bands observed in the transmission spectrum. This technique can therefore be used to gain some information on the surface chemistry of solid particulates.

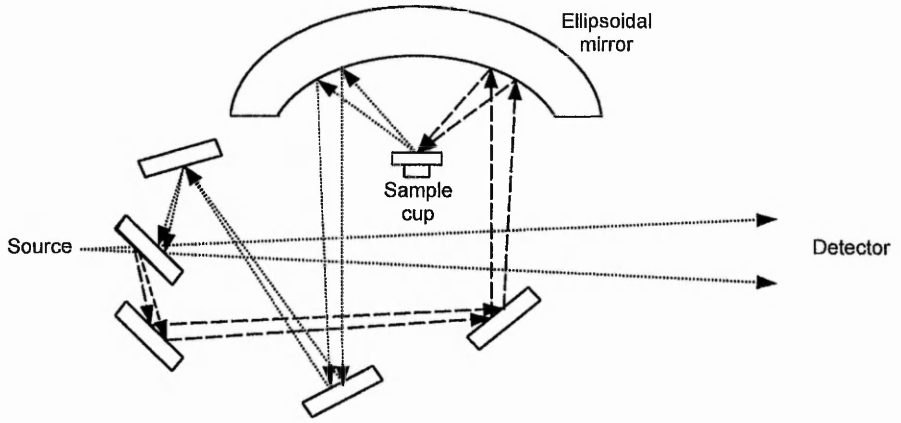

FIGURE 2.2: *SCHEMATIC OF DIFFUSE REFLECTANCE SAMPLING ACCESORY*

All spectra were recorded using a Nicolet Magna-IR 750 Fourier transform infrared spectrometer at $2cm^{-1}$ resolution, averaging 64 scans for transmission or 128 scans for DRIFTS techniques. DRIFTS spectra were recorded using a Spectra-tech^{TM} baseline diffuse reflectance accessory. Finely ground samples are mixed at 10wt% with KBr for DRIFTS analysis.

2.2) X-RAY DIFFRACTION[8-12]

X-ray tubes are constructed from tungsten metal filament and a water-cooled metal plate of high thermal conductivity separated by approximately 1cm. This is sealed inside an evacuated glass tube (figure 2.3).

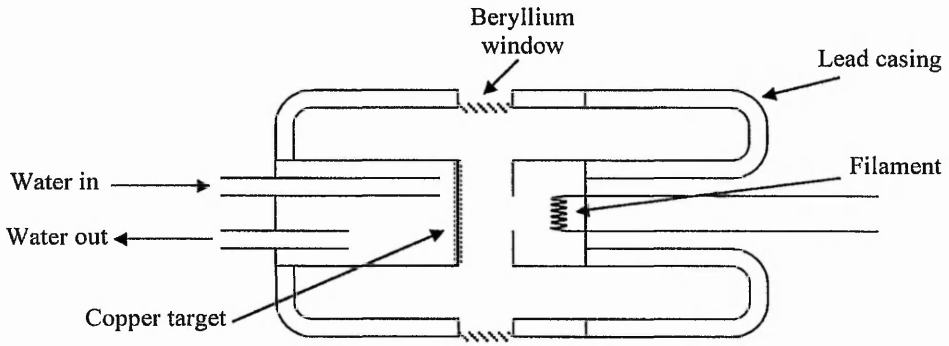

FIGURE 2.3: *SCHEMATIC DIAGRAM OF X-RAY TUBE*

The filament is heated by passing an electric current and emits electrons. The electrons are then accelerated from the filament to the metal target by applying a potential of around 50kV. As the high energy electrons stream from the filament they are focussed by the focussing hood (from ≈1cm to ≈0.01cm). This makes the target easier to cool and allows higher currents, and therefore higher x-ray intensities, to be produced. Most of the electron beam energy is converted into heat while around 2% results in the production of x-rays that are emitted in all directions. Narrow "windows", usually made of beryllium, in the sides of the x-ray tube allow radiation emitted at an angle of 3-6° to escape.

The x-rays leaving the tube are not monochromatic but cover a wide range of frequencies (so called *white radiation*). The reason for this is that as electrons strike the target it is unlikely they will lose all their energy in a single collision but rather in a series of collisions with each being of lower energy than the electron beam. If an electron strikes the target with adequate energy it can eject an electron from the target atoms. If an electron is ejected from the K-shell

an electron will then be transferred from a higher energy level to produce an x-ray photon of energy equal to the difference between the two levels. These x-rays (called *characteristic x-rays*) have a fixed wavelength characteristic of the target element and are quite intense emissions. Nomenclature of "K-lines", commonly used in x-ray powder diffractometry, is the transition from a higher energy L-shell to the lower energy K-shell is $K\alpha$ radiation while transition from an M-shell to the K-shell is $K\beta$. Powder x-ray diffraction patterns are most commonly run using Cu-Kα radiation (1.54051Å).

2.2.1) Diffraction of X-rays

X-rays in the 50-250pm wavelength range give rise to diffraction patterns because they are of the same length as the distances between adjacent atoms in crystalline solids.

Collection of powder diffraction patterns is made by grinding the sample to a fine powder and pressing it into a small depression (approx. 2mm wide) in glass coverslip sample holder. The completely random orientation of the individual crystallites in the sample generate cones of diffracted x-ray energy for each individual plane of atoms according to the Bragg equation.

$$\lambda = 2d \sin\theta$$

Where λ = wavelength of radiation, d = spacing between atomic planes and θ = angle between incident and diffracted radiation.

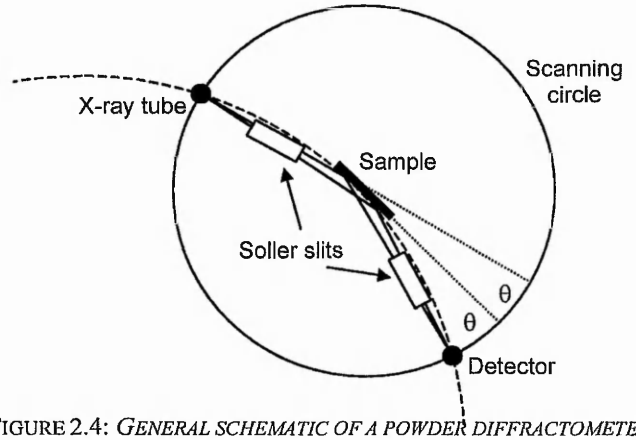

FIGURE 2.4: *GENERAL SCHEMATIC OF A POWDER DIFFRACTOMETER*

The diffraction pattern is scanned by rotating the detector around the specimen. The instrument makes use of the *parafocussing effect* (figure 2.4) whereby the focus line of the x-ray tube and that of the counter are held on the line of a circle. This ensures that the x-rays measured are reflected from the surface of the sample and are so focussed onto the detector. The diffraction pattern is further refined by restriction of beam divergence using *Soller slits* – packed thin metal plates – in the path of both incident and divergent beams. It is because of the use of the parafocussing effect that patterns are recorded as 2θ vs. intensity and not simply θ vs. intensity.

X-ray diffraction was performed on samples using a Hiltonbrooks modified Philips PW1050 Powder diffractometer with Cu-Kα (1.540562Å) radiation. Samples were scanned over variable ranges between 10 and 80° of 2θ with a step-size of 0.02° and a count time of 4 seconds per step.

Powder XRD patterns are used to qualitatively identify crystalline materials using the JCPDS (Joint Committee on Powder Diffraction Standards) Powder Diffraction Files. Quantitative

measurements of composition of crystalline phases in samples was made by mixing the material with 50wt% of α-Al_2O_3 (corundum).

2.3) ESR Spectroscopy[13-16]

If an atom or molecule contains unpaired electrons then it is paramagnetic. In the absence of a magnetic field the energy levels of these electrons are degenerate. When an external field, B_z, is applied they will normally align along the direction of the magnetic field (z) and the degeneracy of the ±½ states of the unpaired electron is removed. Flipping from one state to the other along the z-axis occurs (resonance) when the splitting induced by the applied field equals that of the applied microwaves (figure 2.5).

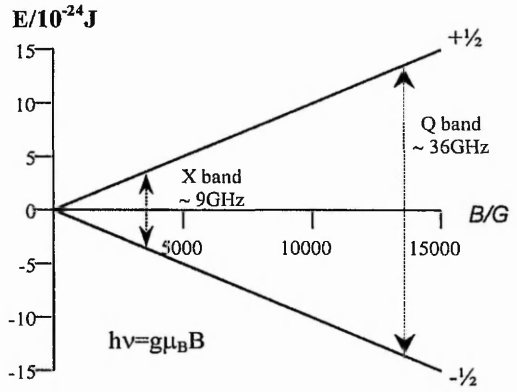

FIGURE 2.5: *SCHEMATIC REPRESENTATION OF THE SPLITTING OF M_S=±½ BY AN EXTERNAL, STATIC MAGNETIC FIELD*

The g value is a proportionality constant in the equation $h\nu=g\mu_B B$ for a S=1/2 and I=0 system where B is the magnitude of the static field at resonance in kG, ν is the frequency of the microwave radiation in MHz. Essentially this factor reflects the magnitude of the energy difference between the + and – states in a given magnetic field. Should the electron be the only source of magnetism then g_e=2.0023. In an atom there may also be orbital angular momentum in addition to the spin angular momentum of the electron and in such a situation these combine to give the total angular momentum, J, and it is the transition between J levels

that is monitored in ESR spectroscopy. The g-value is a property of the whole molecule and is independent of any electron-nuclear interactions. The g value is also anisotropic with three principal components usually defined as the values along the principal axes of an ellipsoid.

2.3.1) Spectra

The most common ESR spectrometers use a phase-sensitive detector and hence produce spectra as first derivatives of the absorption spectrum. The peaks are therefore measured easily from the crossing point of the baseline and the peak width measured from the maxima and minima of the line. In some cases inadequately resolved fine features may be better resolved by using a second derivative. Rare cases may use a difference spectrum where a sample reference is recorded concurrently. The spectra are also commonly displayed in Gauss (G), not Tesla, and most publications use this unit.

Quantitative determinations are difficult in ESR spectroscopy, as with NMR, since the transition moment (and so the area under the absorption curve) is a property of the electron, not the molecule and so the area is directly proportional to the number of unpaired electrons only. Even using calibration standards with narrow lines (such as the αα-diphenyl-β-picryl hydrazyl radical) only a ±20% accuracy can be obtained. When integrating ESR curves attention must be paid to the Lorentzian shape with narrow, but significant wing areas.

2.3.2) Hyperfine coupling

Hyperfine coupling occurs from magnetic coupling that may occur between the spin, S, of the unpaired electron and that of a nearby magnetic nucleus, I, and is similar to the spin-spin coupling observed in NMR spectroscopy.

The interaction results in four states arising from the $+M_s$ and $-M_s$ spin of the electron, namely $\{M_s=+1/2, M_I=+1/2\}$,$\{M_s=+1/2, M_I=-1/2\}$,$\{M_s=-1/2, M_I=+1/2\}$ and $\{M_s=-1/2, M_I=-1/2\}$. The first two states differ in energy and given that the nuclear spin does not reorientate, two lines are detected in the ESR spectrum. This is illustrated in figure 2.6.

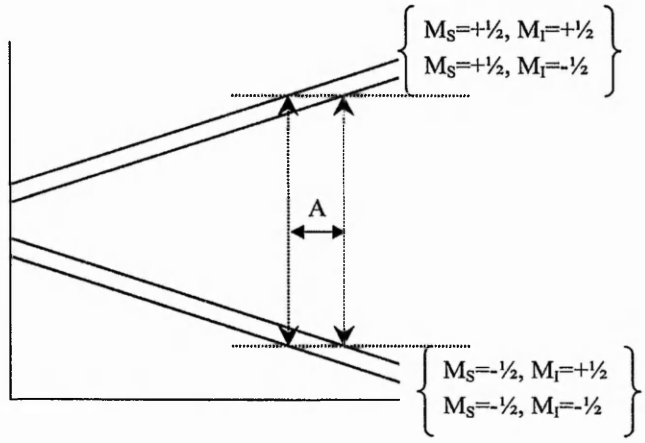

FIGURE 2.6: *SCHEMATIC REPRESENTATION OF HYPERFINE COUPLING TO I=1/2 NUCLEUS (e.g. ^{14}N)*

ESR spectra were recorded by Dr. Frank Mabbs at the EPSRC ESR service at UMIST on a Bruker™ ESR CW spectrometer at X-band frequencies (9.456785GHz). Solid samples were recorded as powders. Spectra of solutions were recorded as "glassy" solution from a water/ glycerol mixture at 110K. Microwave intensity was varied to obtain the best spectrum. Samples were held in a glass capillary tube of 2mm external diameter in the microwave cavity of the spectrometer and cooled to the required temperature by either liquid nitrogen or liquid helium.

2.4) ELECTRON MICROSCOPY[17-22]

The transmission electron microscope was first developed in the 1930's after it was found that wavelength has an effect on the theoretical resolution of a microscope where resolution=$f\lambda/a$ (f=focal length, λ=wavelength and a=aperture). Green light has a wavelength of 0.5μm has a

theoretical resolution of 0.2μm. Moving down the electromagnetic spectrum to shorter wavelengths reaches the ultraviolet region (<0.4μm). An ultraviolet microscope would therefore be 0.05μm. Unfortunately glass absorbs ultraviolet light so all optics would have to be made from quartz and would therefore be very expensive for only a small increase in resolution. X-ray microscopes could theoretically increase resolution dramatically but are not easily refracted to form an image. Electron waves are therefore the best alternative.

Electrons are charged particles and can therefore be refracted by magnetic fields and accelerated by an electric potential. The stronger the potential, the faster the electron is accelerated and, according to the de Broglie relationship ($\lambda=h/p$ where λ=wavelength of electrons, h=Planks constant and p=electron momentum) the shorter the wavelength the better the improvement of resolution. An electron accelerated by a 75kV potential has a wavelength of less than 5 picometers making the theoretical resolution of the order of 100,000 times better than a light microscope. In practice however the difficulty in forming stable magnetic fields makes the quality of magnetic lenses not as high as optical lenses and so very small apertures must be used resulting in a decrease of optimal resolution by approximately 100 times.

Table 2.1 shows a comparison between electron and optical microscopy.

	Electron Microscopy	**Optical Microscopy**
Illumination	*Electron beam*	*Light beam*
Wavelength	*0.0859Å (2.0kV)*	*7.500Å (visible)*
Medium	*Vacuum*	*Atmosphere*
Lens	*Magnetic lens*	*Optical lens (glass)*
Aperture angle	*≈35°*	*≈70°*
Resolution	*3Å*	*2000Å (visible)*
Magnification	*90-80,000x*	*10-2,000x*
Focusing	*Electrical*	*Mechanical*
Contrast	*Scattering, Absorption, Diffraction*	*Absorption, Reflection*

TABLE 2.1: *COMPARISON OF COMPONENTS IN ELECTRON AND OPTICAL MICROSCOPES*

When the electron beam encounters the sample the interaction results in the emission of all lower forms of energy such as x-rays, secondary electrons, ultra-violet radiation and heat.

The contrast of the image is produced by absorption or scattering of incident electrons by the specimen. The atomic number of the material determines the amount of contrast with higher atomic number having higher contrast. In order to create contrast in the image the scattered electrons must be separated from the undeviated beam otherwise they would recombine with the beam and result in a featureless image. Introduction of an objective aperture into the beam path accomplishes this and results in an image where areas of high mass and/ or density are darker.

2.4.1) Electron diffraction[23]

Diffraction patterns produced by the electron microscope can be of two types;

1) Ring patterns (polycrystalline specimen)
2) Spot pattern (single crystal region of sample)

Ring patterns may be used to identify crystalline phases. These diffraction patterns arise from very fine grain sizes in polycrystalline material. Spot patterns may be used to determine orientation of the samples and identify individual crystal planes resulting in individual spots.

2.4.2) EDAX[24]

High energy electrons incident on a sample may generate x-rays that can be counted by a suitable detector. The electrons of sufficient energy displace an inner shell electrons from an atom within the sample resulting in electrons from an outer shell dropping into the inner shell vacancy together with emission of characteristic x-rays. These x-rays are detected by a lithium drifted silicon detector attached to the microscope column. The signal produced by

the detector is then processed according to their energy and a spectrum of the different elements and their abundance in the sample is obtained.

TEM analysis were performed using a JEOL 2010 TEM with a LaB_6 electron gun filament operating at 200KeV. Energy dispersive X-Ray analysis was performed using the attached PentafetST X-ray detector and TEMQUANT function within the Link-ISIS software from Oxford instruments.

The TEM was calibrated to check the camera length using an aluminium standard. As the d-spacings are already known, diffraction patterns are obtained at the camera length to be used with samples and a back calculation performed to obtain the exact length.

2.5) COATING METHODS[25]

Two different coating methods were evaluated for production of thin films to determine which would be most suitable for the systems examined in this thesis.

2.5.1) Spin coating

Spin coating is a widely used method in the preparation of producing thin films. A simple apparatus may be constructed (figure 2.7) using a D.C. electrical motor or a more complex system of speed controls and clean environment may be used.

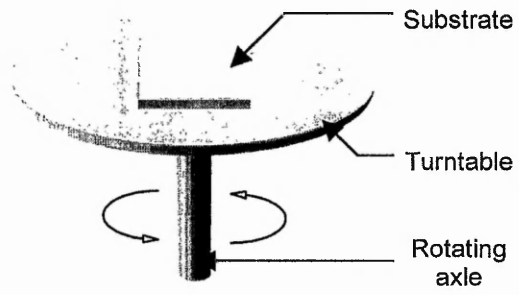

FIGURE 2.7: *ILLUSTRATION OF THE SPIN-COATING TECHNIQUE APPARATUS*

The surface of the substrate is covered with an excess of the coating liquid. The turntable is then accelerated and centrifugal forces throw off the excess liquid. The spinning motion of the turntable results in the downflow of air across the apparatus that both dries the film and attracts dust to the surface. A very clean environment must be ensured to prevent contamination. The film thickness is proportional to concentration of coating liquid and the turntable speed.

$$thickness \alpha \ {}^{1}/_{speed}$$

This coating method has the advantages that very small amounts of liquid are required, the coating process is very rapid and, as demonstrated by several workers, multiple coatings may be produced. The disadvantage of this method is that large substrates cannot easily be coated evenly and the films require a dust-free atmosphere to keep them clean.

2.5.2) Dip coating

The dip coating technique immerses the substrate in a volume of the coating liquid (figure 2.8). The substrate is gradually withdrawn from the liquid by a motor.

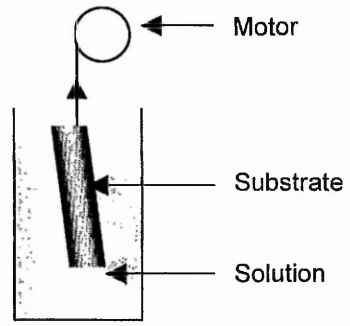

FIGURE 2.8: *ILLUSTRATION OF THE DIP-COATING TECHNIQUE APPARATUS*

At a constant temperature the film thickness is proportional to the viscosity, withdrawal rate and liquid density.

$$thickness \alpha \left[\frac{(viscocity)(withdrawalrate)}{(density)} \right]^{2/3}$$

This method allows the coating of any size or shaped sample and is relatively easy to construct. Unlike the spin coating method contamination is not a serious problem. The disadvantage is the large amount of solvent required for a coating compared with spin-coating. A similar method of *drain coating* may be used, particularly useful in the aqueous systems described in this thesis, where the substrate is held static and the liquid is slowly pumped away although this is essentially the same as dip-coating.

References

1. L. Glasser, *J. Chem. Ed.,* **64**, A228, (1987)

2. P. R. Griffiths, J. A. De Haseth, *Fourier Transform Infrared Spectroscopy*, (Wiley, New York), (1986)

3. K. Nakamishi, P. H. Solomon, *Infrared Spectroscopy 2nd Edition,* (Holden-Day, San Francisco), (1977)

4. W. D. Perkins, *J. Chem. Ed.,* **63** (1), A5, (1986)

5. W. D. Perkins, *J. Chem. Ed.,* **64** (12), A296, (1986)

6. W. D. Perkins, *J. Chem. Ed.,* **64** (11), A269, (1986)

7. J. P. Chesick, *J. Chem. Ed.,* **66** (5), 413, (1989)

8. B. D. Cullity, *Elements of X-ray Diffraction 2nd Edition,* (Addison-Wesley, Massachusetts), (1978)

9. J. H. Enemark, *J. Chem. Ed.,* **65**(6), 491, (1988)

10. R. Jenkins, R. Anderson, G. J. McCarthy, *Use of Powder Diffraction Files. An Education Resource Package,* (Pennsylvania, USA)

11. T H. P. Klug, L. E. Alexander, *X-ray Diffraction Procedures for Polycrystalline and Amorphous Materials 2nd Edition,* (John Wiley, New York), (1974)

12. C. G. Pope, *J. Chem. Ed.,***74**(1), 129, (1997)

13. D. Kivelson, R. Neiman, *J. Chem. Phys.,* **35**, 149, (1961)

14. M. Symons, *Chemical and Biochemical Aspects of Electron Spin Resonance,* (Van Nostrand Reinhold, New York), (1978)

15. P. B. Ayscough, *Electron Spin Resonance in Chemistry,* (Methuen, London), (1967)

16. N. M. Atherton, *Principles of Electron Spin Resonance,* (Ellis Horwood, New York-London), (1993)

17. B. E. P. Beeston, R. W. Horne, R. Markham, *Practical Methods in Electron Microscopy Vol.1,* (A. M. Glauert, Holland), (1987)

18. D. Chescoe, P. J. Goodhew, *The Operation of Transmission Electron Microscopes,* (Oxford C Science Publications, Oxford University Press), (1990)

19. J. R. Fryer, *The Chemical Applications of Transmission Electron Microscopes*, (Academic Press, London), (1979)

20. D. C. Joy, A. D. Roming Jr, J. I. Goldstein, *Principles of Analytical Electron Microscopy,* (Plenum Press, New York), (1986)

21. I. M. Watt, *The Principles and Practice of the Electron Microscope*, (Cambridge), (1985)

22. J. W. Eddington, *Electron Diffraction in the Electron Microscope in Practical Electron Microscopy in Materials Science,* (Phillips Technical Library)

23. D. B. Williams, *Practical Analytical Electron Microscopy in Materials Science,* (Verlag Chemie, International), (1984)

24. G. Lawes, *Scanning Electron Microscopy and X-Ray Microanalysis – Analytical Chemistry by Open Learning,* (Wiley, New York), (1987)

25. I. M. Thomas, *Optical Coating Fabrication in Sol-Gel Optics: Processing and Applications,* (Klein), (1994)

CHAPTER 3 COPPER DIAMMINE COMPLEX SYNTHESIS AND CHARACTERISATION

3.1 INTRODUCTION

The definition of thermochromism is rather loose. Normally it suggests a radical change in visible colour of a substance that takes place when heated to a specific temperature (discontinuous thermochromism) or over a range of temperature (continuous thermochromism). This change may be reversible (the original colour returning upon cooling) or irreversible.

The opinion may be held that true thermochromism may only be reversible since an irreversible colour change caused by heating are the results of chemical reaction. Indeed colour changes due to hydration/ dehydration may also be argued as non-thermochromic since these changes may be induced in a dry atmosphere in some cases and reverse not on cooling, but on exposure to moisture. These cases where dehydration is responsible for the thermochromism therefore seem to require no special terminology.

While these may not seem so clear cut, studying these cases more closely makes it more convenient to divide thermochromic phenomenon into two distinct classes – 1) Reversible thermochromism and 2) Irreversible thermochromism.

The phenomenon of irreversible thermochromism may also be classified further as "continuous", where the transition occurs over a range of temperature corresponding to gradual structural changes in the solid, or "discontinuous thermochromism" where the colour change occurs quite suddenly, corresponding to a abrupt change in structure. Although most compounds can be classified using these terms a few compounds still remain ambiguous.

A multitude of examples of thermochromic phenomena can be found in the literature and are observed in solids, liquids, solutions and gases. Many of these examples are also closely related to the other "chromisms" (*solvato*chromism, *electro*chromism, *photo*chromism, *piezo*chromism. etc). A thermochromic compound will often possess one or more of these other additional "chromism" properties.

It should be remembered that cooling of an optically absorbing substance does itself cause changes in band position and width, sometimes even resolving individual bands). This arises not from structural changes but from molecular vibrations that are weakened at lower temperature allowing better defined energies. In many cases it is this effect that results in a continuous thermochromism, although many examples exist where structural changes take place instead.

Of greatest interest to this work are thermochromic transition metal complexes. Transition metal complexes form the bulk of thermochromic compounds found in literature and the mechanism for observed phenomena are highly diverse[1]. The spectral changes that result from these phenomenon generally involve shifts and deformations of d-d electronic bands induced by changes in ligand field symmetry and/ or shape and often changes in charge transfer bands due to changes in metal ligand redox processes. Several examples showing the wide range of physiochemical reasons for thermally induced colour transition in a wide range of compounds are presented below to illustrate the diversity of the thermochromic phenomena.

A particular range of thermochromic compounds studied by Segal and co-workers[2-6] exhibit irreversible, discontinuous thermochromism by transfer of a ligand from the coordination sphere of one metal ion to another (termed *chromotropism*). Complexes with this mechanism

have the general formula $[M(L)_3][M'Cl_4]$ where M and M' are two dissimilar metal ions and L = 1,10-phenanthroline, bathophenanthroline or dipyridine. Upon heating a ligand exchange reaction occurs, with associated colour change, at 160-320°C, depending upon the complex:

$$[ML_3][M'Cl_4] \longrightarrow [ML_2(Cl)_2][M'L(Cl)_2]$$

A summary of different complexes investigated by Andruh *et al* [2-6] is shown below.

Complex	***Thermochromism observed***	***Temperature (°C)***	***Ref.***
$[Cu(phen)_3][ZnCl_4]$	green → light green	200 - 250	2
$[Cu(dipy)_3][ZnCl_4]$	blue → green	198	2
$[Ni(phen)_3][PdCl_4]$	pink/brown →green	220	3, 5
$[Ni(bathophen)_3][PdCl_4]$	pink → green	275	3, 5
$[Ni(phen)_3][CuCl_4]$	yellow/orange → green	250	4
$[Co(dipy)_3](SnCl_3)_2$	yellow → green	200	6
$[Ni(dipy)_3](SnCl_3)_2$	pink → yellow	250	6
$[Co(phen)_3][ZnCl_4]$	yellow → red	280-320	7
$[Ni(phen)_3][ZnCl_4]$	pink → green	315	7
$[Ni(dipy)_3][ZnCl_4]$	pink → green	235	7
$[Co(dipy)_3][ZnCl_4]$	yellow → red	160-200	7

TABLE 1: *CHROMOTROPIC COMPLEXES INVESTIGATED BY M. ANDRUH ET AL*
DIPY = DIPYRIDYL, PHEN = 1,10-PHENANTHROLINE, BATHOPHEN = 4,7-DIPHENYL-1,10-PHENANTHROLINE

Most notable is the effect of ligand type on the phase transition temperature. Complexes with the dipy ligand have a lower thermochromic temperature than the similar complex with phen ligands.

Thermochromism by dehydration/ hydration is possibly the most common mechanism. At the most simple level the thermal dehydration of copper sulphate heptahydrate shows a blue > green dehydration thermochromism when heated over a bunsen flame as coordination of sulphate to the copper takes place. The thermochromic complex $[NiL_2](Br)_2.3H_2O$ [8] (L = *N*'-Isopropyl-2-methyl-1,2-propanediamine) was synthesised by Pariya *et al* by the stoichiometric addition of the ligand to a 9:1 ethanol-water solution of nickel chloride. Heating of the complex to ≈130°C results in a yellow → green anation thermochromism that reverses in air,

but may be preserved by storing in a dessicator. The hydrated compound is square planar, changing to trigonal bipyramidal with the loss of water, so resulting in the yellow > green thermochromism.

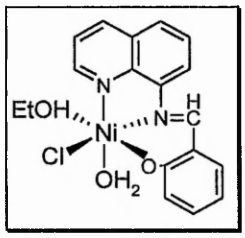

The Schiff-base Nickel(II) complex of salicylidene-8-aminoquinoline[9] (left) also provides an interesting example of an unusual, irreversible thermochroism by the thermal anation mechanism. The complex changes from a yellowish green colour to orange when heated to 170-250°C with a loss of mass equal to one molecule of water. The chloride ion also moves to the outer coordination sphere giving a square planar geometry.

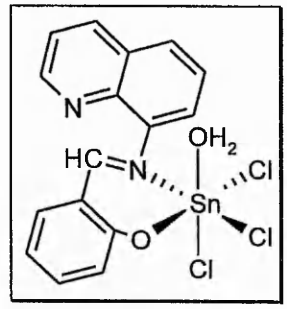

The Tin-Schiff base complex (right) investigated by Donia and El-Boraey[10] provides a more rare example of a thermochromic non-transition metal complex. Upon heating to 120-180°C the complex changes from yellow to orange and is reversible in air or silicon oil. No actual mechanism was proposed to account for the colour change, but conductivity measurements were made showing that the energy was consumed in a small phase change rather than the thermal agitation of electrons. It was assumed that a relatively small structural modification occurred upon heating.

Perturbation of electronic energy levels may occur without a ch*p-1Xange in the chemical structure or movement of the atoms at all. Such a range of compounds are 5, 10, 15, 20-Tetraarylporphyrin systems (see right) investigated by Mori *et al*[11]. Studies were made by varying the type of R groups to

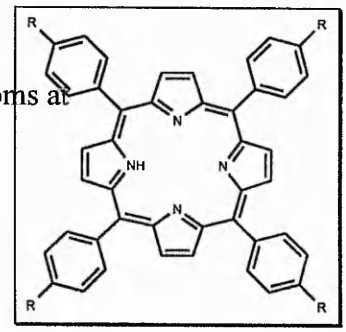

vary the electron donating/ withdrawing properties (i.e. $-NO_2$, -Me, -OMe, $-NH_2$). It was found that when R = $-NH_2$, the compound exhibited low temperature thermochromism in 2-methyltetrahydrofuran. Solvatochromism - the change of absorption with solvent - was also noted. It was determined that the thermochromism was also related to the solvatochromism by the enhanced electron donating abilities of the para-substituted $-NH_2$ group at lower temperatures by increased interaction with the solvent by hydrogen bonding. The ortho-substituted $-NH_2$ isomer was said to have little effect on electronic state of the porphyrin π-system since the ortho - substituted phenyl groups are nearly perpendicular to the porphyrin ring. Substitution of para $-NH_2$ with -OH shows a temperature dependence of free base / di-cation equilibrium; that is at lower temperatures (77K) protonation of the pyrrole nitrogen in the porphyrin ring occurs.

Definition of thermochromism

For the purposes of this thesis the definition of thermochromism will be wide ranging. Taking into account that the two terms in the word – thermo (heat) and chromic (colour) – *any* visual colour change in a substance that may be induced by heat, reversible or irreversible shall be termed thermochromic. If the change can be induced by other means (e.g. desiccation) then that does not necessarily make the compound invalid for the term "thermochromic". If a chemical reaction can be brought about by two different ways, then those two ways still follow a different path regardless of the paths ending in the same product. It is the *pathway* of change that will be named as "thermochromic" in this thesis, not the resulting colouration. If the product is visually different in colour from the reactants following a change in temperature above or below ambient then the process shall be termed as thermochromic.

3.2 EXPERIMENTAL

Bis(diammine)copper(II) chloride complex preparation

Diaquabis(1,2-ethanediammine)copper(II) chloride

2g (0.015 moles) of anhydrous copper(II) chloride was dissolved in 150ml of a 75:25 by volume mixture of diethylether and ethanol. 2.002ml of 1,2-ethanediamine (0.030 moles) was added drop-wise to the solution with stirring forming a blue precipitate. The precipitate was filtered under suction and washed with 100ml of diethylether. The precipitate was then crystallised from a 90:10 by volume mixture of diethylether and ethanol. Yield = 81%.

Diaquabis(1,2-propanediammine)copper(II) chloride

The complex was prepared as per diaquabis(1,2-ethanediammine)copper(II) chloride replacing the 1,2-ethanediamine with 2.553ml of 1,2-propanediamine (0.030 moles). Yield = 89%.

Diaquabis(N,N'-diethylethylenediamine)copper(II) chloride

The complex was prepared as per diaquabis(1,2-ethanediammine)copper(II) chloride replacing the 1,2-ethanediamine with 4.293ml of N,N'-diethylethylenediamine (0.030 moles). Yield = 76%.

Preparation of ammonium salts of Diaquabis(1,2-propanediammine)copper(II) chloride

The copper complex reacted readily with acid. Titration of a solution of diaquabis(1,2-propanediammine)copper(II) chloride complex with HCl resulted in a colour change from deep purple to light blue to pale green as more acid was added. The blue and green compounds were isolated for analysis. The green compound was prepared by dissolving 1g of $[Cu(pn)_2(H_2O)_2]Cl_2$ in 10ml of 3M HCl. This was then slowly evaporated (24h) from a watch glass resulting in a mixture of green and yellow crystals. The blue compound was prepared by dissolving the complex in a 50:50 by volume ethanol:diethylether mixture and visually titrating with a 50:50 by volume mixture of ethanol and 1M HCl. The blue complex

precipitated from the solution. This was filtered and washed with more of the ethanol/diethylether mixture to remove impurities. The blue compound was then dissolved in water and needle like crystals were formed by slow evaporation of the solvent from a watch glass.

Analysis of the compounds was made by UV/Visible spectroscopy, FTIR spectroscopy and thermogravimetric analysis.

3.3 RESULTS

3.3.1 UV/Visible spectroscopy

The UV/Visible spectra of the Cu(II) complexes prepared with the different diamines complexes are shown in figure 3.1. The spectra were run in water or ethanol but showed no changes dependent upon solvent.

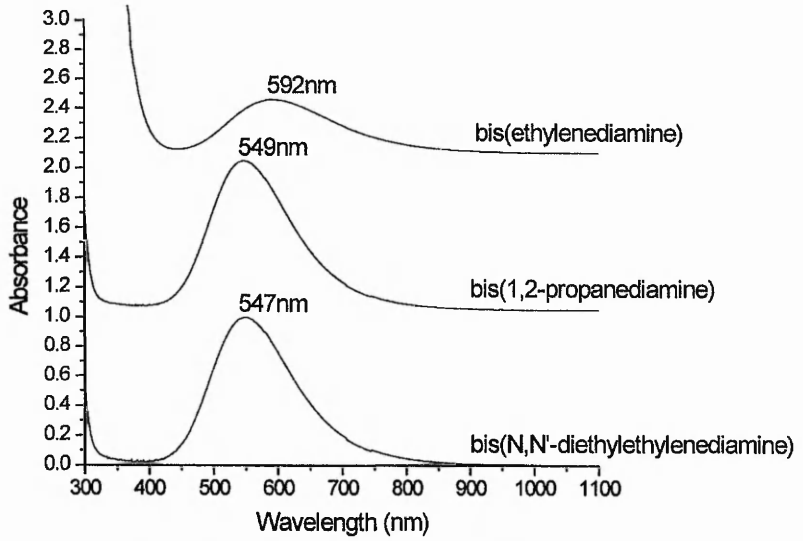

FIGURE 3.1: *UV/VISIBLE SPECTRA OF THE COMPLEXES PREPARED*

All the complexes are blue/ purple in colour suggesting a six co-ordinate environment for Cu^{2+}. The non-symmetrical shape of all spectra suggests that the complexes exist in a Jahn-Teller distorted crystal field (D_{2h} symmetry) with three broad overlapping bands present characteristic of these compounds.

3.3.2 Infrared analysis

The infrared spectra of the Cu complexes are shown in figure 2. The spectrum of the diamine compounds is shown in figure 3. Shifts of the ν(C-N) bands of the complex relative to the free amine (-14cm^{-1} for 1,2-ethanediamine, -5cm^{-1} for 1,2-propanediamine and -1cm^{-1} for N, N'-diethylethylenediamine) and narrowing of the bands indicates co-ordination of the ligands to the copper.

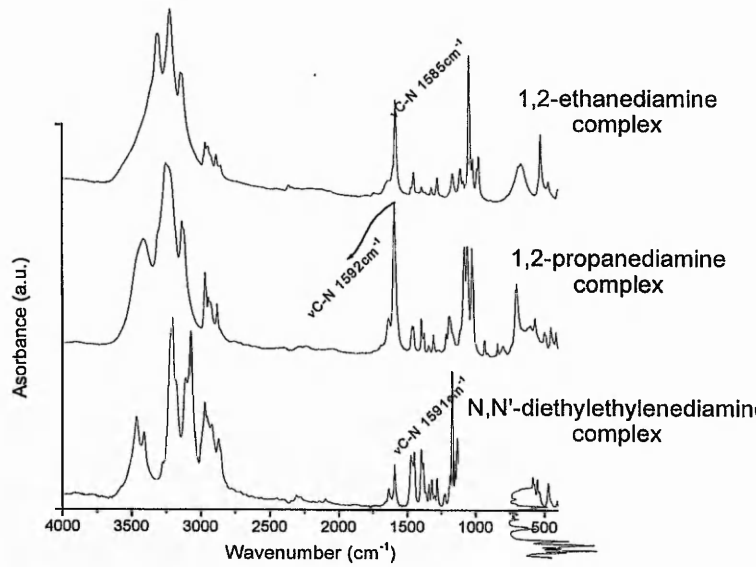

FIGURE 3.2: *FTIR SPECTRUM OF BIS(DIAMMINE) COPPER(II) COMPLEXES*

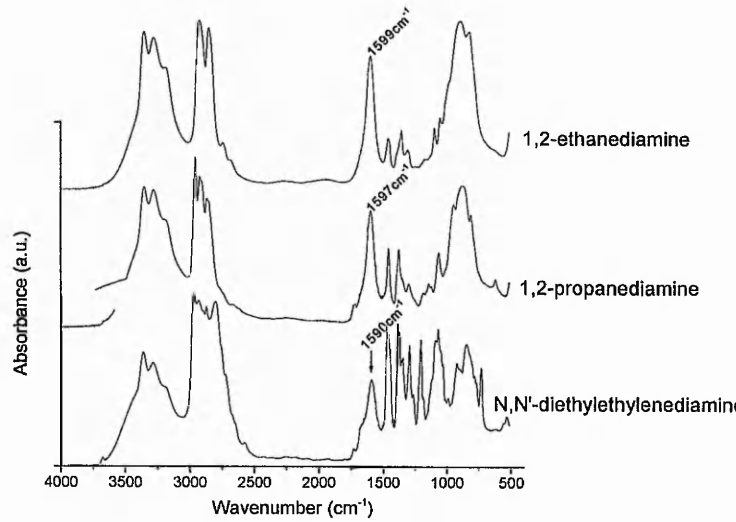

FIGURE 3.3: *FTIR SPECTRUM OF DIAMMINE COMPOUNDS*

3.3.3 Thermal analysis

Thermogravimetric analysis shows that 2 molecules of water are associated with each complex below 80°C.

COMPLEX	% MASS LOSS AT 80°C	EXPECTED % MASS LOSS
Cu(II) / bis(1,2-ethanediammine)	12.8	13.1
Cu(II) / bis(1,2-propanediammine)	11.7	11.9
Cu(II) / bis(N,N'-diethylethylenediamine)	9.5	10.1

TABLE 3.2: *MASS LOSSES OF COPPER COMPLEXES PREPARED AT 80 °C*

Microanalysis

	%C	%N	%H	%Cl
Bis(1,2-ethanediammine)	17.6 (16.5)	19.96 (19.3)	6.2 (6.9)	27.6 (24.1)
Bis(1,2-propanediammine)	23.0 (22.7)	17.5 (17.6)	6.8 (7.6)	23.5 (22.0)
Bis(N,N'-diethylethylenediammine)	36.4 (35.0)	14.4 (14.0)	8.3 (8.0)	20.1 (17.4)

MICROANALYSIS OF BIS(DIAMMINE)COPPER(II) CHLORIDE COMPLEXES.
VALUES IN BRACKETS INDICATE EXPECTED VALUES.

The empirical formulae for the complexes is therefore Cu(diammine)$_2$(H_2O)$_2$$Cl_2$.

Figure 3.4 shows colouration of the copper complexes before and after thermal treatment to 80°C for 1 hour.

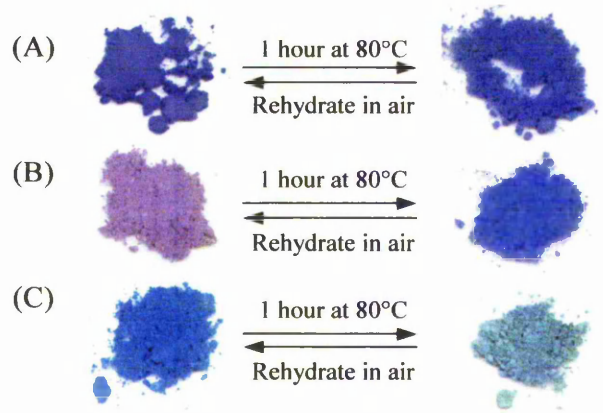

FIGURE 3.4: *THERMOCHROMIC TRANSITIONS OF COPPER(II) COMPLEXES AFTER THERMAL TREATMENT TO 80 °C FOR 1 HOUR*
(A) Cu(1,2-ethanediammine)$_2$(H_2O)$_2$$Cl_2$, (B) Cu(1,2-propanediammine)$_2$(H_2O)$_2$$Cl_2$
(C) Cu(N,N'-diethylethylenediammine)$_2$(H_2O)$_2$$Cl_2$

The bis(1,2-ethanediammine)copper complex shows a small visible colour change from deep purple colour to a deep blue. The bis(1,2-propanediammine)copper complex is purple and becomes blue after heating while the bis(N,N'-diethylethylenediammine)copper complex is initially light blue becoming green after heating.

3.3.4 Single crystal x-ray diffraction analysis

Single crystal analysis to determine complex structures was carried out by Dr. Alex Slawin at St. Andrews University. The results are shown in figure 3.5.

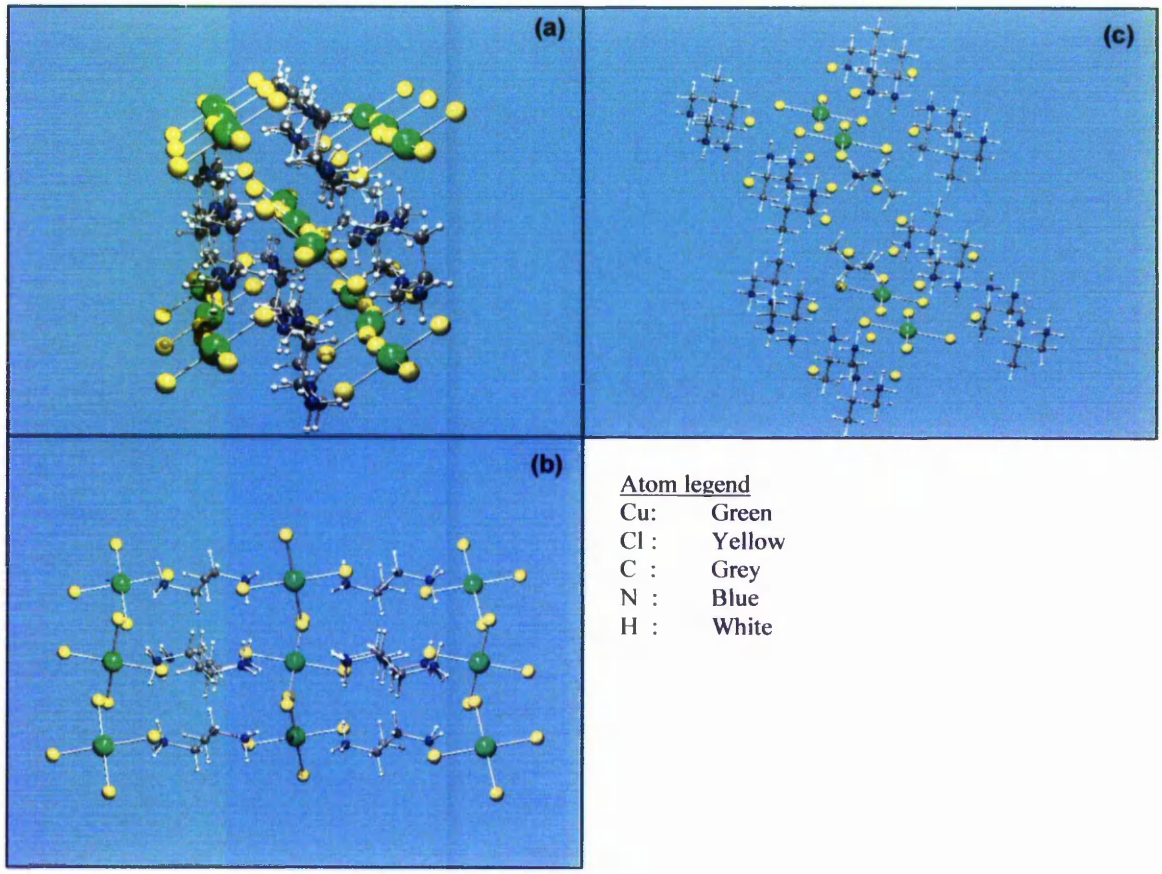

FIGURE 3.5: *SINGLE CRYSTAL STRUCTURES OF THE COMPLEXES ISOLATED FROM ACIDIFIED SOLUTIONS OF* $[Cu(pn)_2(H_2O)_2]Cl_2$ *(A) STRUCTURE OF GREEN COMPOUND CRYSTALLISED FROM 3M HCL, (B) STRUCTURE OF HIGH TEMPERATURE PHASE (YELLOW) OF GREEN CRYSTALS, (C) YELLOW CRYSTAL FROM SAME SOLUTION (STRUCTURES ORIENTED TO SHOW THE RELATIONSHIP BETWEEN VARIOUS* $CuCl_4^{2-}$ *SITES FOR EACH CRYSTAL)*

Tetrachlorocuprate(II) salts of ammonium ions typically crystallise in a two-dimensional layered structure with layers separated by the organic anions[12-14]. Crystals of this type have been synthesised by other workers[12-14] by addition of stoichiometric amounts of the appropriate diammonium hydrochloride to ethanolic solutions of copper(II) chloride and crystallising the compound by evaporation. The diammoniumtetrachlorocuprate(II) salts obtained in this work were prepared by crystallisation from acidified solutions of bis(1,2-propanediammine)copper(II) chloride. This gave two different types of crystals in approximately equal amounts. The empirical formulae of the two crystals was $C_3H_{12}N_2CuCl_4$ (green) and $C_9H_{48}N_6CuCl_{10}$ (yellow). For crystal structure data see appendix III.

	Green crystals (low temperature phase)	Yellow crystals (high temperature phase)	Yellow crystals
Empirical formula	$C_3H_{12}N_2CuCl_4$	$C_3H_{12}N_2CuCl_4$	$C_9H_{48}N_6CuCl_{10}$
R_{mm}	281.49	281.49	722.62
Crystal type	Monoclinic	Monoclinic	Triclinic

TABLE 3.3: *DATA FOR CRYSTALS OBTAINED FROM ACIDIFIED SOLUTIONS OF* $[Cu(pn)_2(H_2O)_2]Cl_2$

(1,2-diammonium)tetrachlorocuprate(II) - low temperature phase

The green crystals of (1,2-diammonium)tetrachlorocuprate(II) had two different Cu(II) co-ordination environments in the crystal structure. Both Cu(II) sites were distorted from perfect square planar symmetry by deviation of the in-plane Cl-Cu-Cl bonds from 90° by 1.34° for Cu(1) and 1.40° for Cu(2). The tetrachlorocuprate ions were hydrogen bonded via the chlorine ligands to hydrogen atoms on the ammonium groups of the 1,2-diammoniumpropane cations. The ions were also tipped slightly so that they were not co-planar. Unlike some other types of diammonium salts[15,16] no Cu...Cl hydrogen bonding or stacking of the tetrachlorocuprate ions into sheets was found, presumably because the tetrachlorocuprate anions were not co-planar. The tetrachlorocuprate ions were also oriented in two dimensions approximately 90° to each other giving a two dimensional crystal structure.

(1,2-diammonium)tetrachlorocuprate(II) - high temperature phase

When heated to 80°C for 1 hour the green crystals became yellow but retained the same crystal symmetry and showed no change in elemental composition. The crystal structure, like the low temperature phase, has two different tetrachlorocuprate geometries with both showing distortions of in-plane Cl-Cu-Cl geometry from perfect D_{4h} symmetry by 1.34° and 1.42° for Cu(1) and Cu(2) respectively. These angles are identical to those found in the green crystals although the Cu(2) centre shows a 0.02° change to the Cl-Cu-Cl bond angle following thermal treatment. The two Cu(II) centres are not co-planar and form disordered sheets with each tetrachlorocuprate anion being slightly tipped away from the other separated by layers of the 1,2-diammoniumpropane cations. The 1,2-diammoniumpropane cation also had only a small change in bond angles and distances. In the high temperature phase of the crystal the tetrachlorocuprate anions are not hydrogen bonded to the ammonium groups of the cation and the Cu-Cl bond distances show a small change. The thermochromic transition is therefore a result of a 2-D to 1-D transition of planar tetrachlorocuprate anions resulting in loss of hydrogen bonding to the ammonium groups on the cation causing small geometric and/ or electronic changes to the Cu(II) as an infinite sheet--like $CuCl_4$ structure is formed separated by the organic cations.

tri(1,2-diammoniumpropane)tetrachlorocuprate(II) hexachloride

The yellow crystals of tri(1,2-diammoniumpropane)tetrachlorocuprate(II) hexachloride had one Cu(II) site. The square planar geometry of the tetrachlorocuprate ion was distorted from perfect D_{4h} symmetry in the same way as for (1,2-diammoniumpropane)tetrachlorocuprate(II), although the in-plane Cl-Cu-Cl bond had a smaller deviation from 90° by 0.65°. Also in contrast with the (1,2-diammoniumpropane)tetrachlorocuprate(II) crystals, the tetrachlorocuprate anions were co-planar separated by the organic cations and chloride ions.

The (1,2-diammoniumpropane)tetrachlorocuprate(II) crystals were found to be thermochromic becoming yellow when heated to 80°C for 1 hour. This colour was reversed to green when cooled to room temperature and could not be preserved by desiccation. No mass loss was associated with this transition. The yellow tri(1,2-diammoniumpropane)tetrachlorocuprate(II) hexachloride crystals did not show any thermochromic behaviour.

Elemental analysis

The crystal structure of the blue crystals could not be solved by single crystal x-ray diffraction although the crystals were found to be rhombohedral with cell dimensions of a=6.836, b=5.783 and c=9.528 using either 0.71073Å or 1.54178Å radiation . Table 3.3 shows results of carbon, hydrogen, nitrogen and chloride elemental analysis of the blue crystals. Elemental analysis was performed by Mr. T. Spencer of the University of Nottingham.

	%C	%H	%N	%Cl
Blue crystals	16.3	5.14	12.33	52.24
Expected	17.12	5.50	11.90	50.32

TABLE 3.4: *PERCENT WEIGHT OF CARBON, NITROGEN AND CHLORINE OBTAINED BY MICROANALYSIS IN BLUE CRYSTALS OBTAINED FROM ACIDIFIED SOLUTIONS OF* $[Cu(pn)_2(H_2O)_2]Cl_2$.

From this data the empirical formula for two alkylammine ligands (assuming 3 carbons per ligand) in the blue crystals is $C_6H_{22}N_4$ with 6.5 chloride ions. This suggests that the diammine ligands in the complex have two ammonium and two ammine groups. The complex could therefore have either two $^{+}H_3NCH(CH_3)CH_2NH_2$ ligands bonded to the copper via the amine or one chelating 1,2-propanediammine ligand and one diammonium cation. As the exact structure, and hence nomenclature, of this compound is unknown it will hereafter be referred to as "(diammoniumdiammine)copper(II) chloride".

3.3.5 EPR analysis

EPR analysis of the three different complexes show identical spectra regardless of the ligand type used. Three copper sites are present in the solutions corresponding to the three copper sites found by crystallography (figure 3.6).

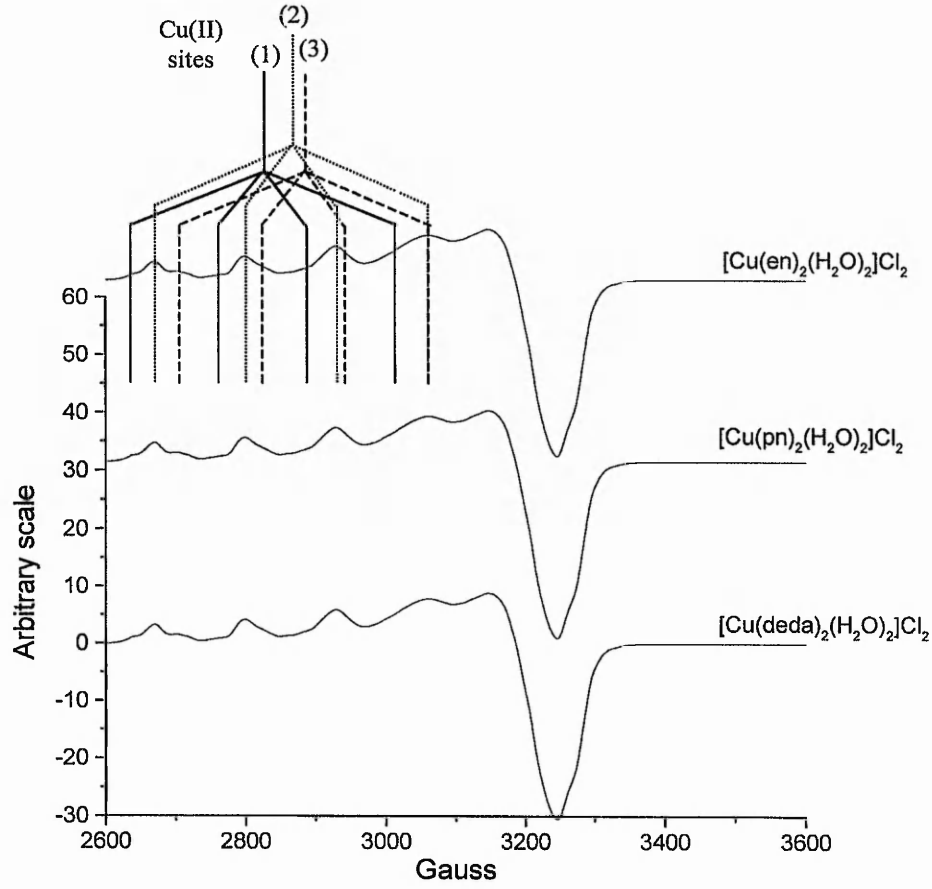

FIGURE 3.6: *X-BAND EPR SPECTRA OF GLASSY SOLUTION OF COMPLEXES IN 3M HCL AT 115K*

All the spectra are identical indicating that the copper(II) sites are identical and unaffected by the diamine/diammonium ligands.

3.4 DISCUSSION

The results show that bis(diammine)copper(II) chloride complexes are thermochromic with the type of diamine ligand significantly influencing the colour changes observed. The bis(diammine)copper(II) complexes are six co-ordinate with two chelating diammine ligands

in the x-y plane and two water molecules in the axial positions resulting in a tetragonally distorted geometry together with chloride ions in the outer sphere. Thermal dehydration of the complexes at 80°C for 1 hour resulted in loss of two water molecules from the axial positions. Dehydration of the bis(1,2-ethanediammine) and bis(1,2-propanediammine) complexes results in displacement of water by chloride ions retaining 6 co-ordinate geometry and hence only a small colour change is observed. The bulky groups on the N, N'-diethylethylenediammine ligands sterically crowd the axial positions preventing coordination of the chloride resulting in the characteristic green colouration of the square planar Cu(II) on heating.

The complexes react with acid by protonation of the ammine ligands that are then displaced from the inner coordination sphere by chloride ions. Two types of protonated complex were isolated from solutions of different Cu(II):HCl ratios. These complexes differed by the number of coordinated ammine ligands. The blue complex isolated has two coordinated ammine ligands and two ammonium groups per copper atom, although the exact structure of the complex is unknown. Increasing acidity protonated all the ammine ligands and resulted in square planar tetrachlorocuprate(II) anions and 1,2-diammoniumpropane cations. The solutions crystallise into two crystal types that differ by diammonium:Cu ratios with the green crystals being 3:1 {tri(1,2-diammoniumpropane)tetrachlorocuprate(II) hexachloride} while the yellow crystals were 1:1 ratio {(1,2-diammoniumpropane)tetrachlorocuprate(II)}. The green crystals were thermochromic when heated to 80°C for 1 hour resulting from a 2-D to 1-D crystal structure transition with loss of hydrogen bonding to the ammonium groups and small geometric and/ or electronic changes to the Cu(II) coordination environment.

Bloomquist *et al*[1] investigated a series of similar, thermochromic salts of the bis(alkylammonium)tetrachlorocuprate(II) types. These salts were prepared by mixing

stoichiometric amounts of the appropriate diammonium hydrochloride salt with copper chloride in methanol or ethanol and evaporating the solvent resulting in growth of crystals of the bis(alkylammonium)tetrachlorocuprate compounds. Spectroscopically it was shown that the colour change was associated with a relaxation of the stereochemistry from square planar, or square pyramidal, geometry towards tetrahedral geometry[2-4]. In contrast to this it was shown that $(PhCH_2NH_2CH_3)_2CuCl_4$ where the co-ordination geometry increased from square pyramidal to square bipyramidal when heated to 100°C. The crystal structure of the two phases of the diammonium salts is therefore highly dependent upon the diammonium anion involved.

3.5 Conclusions

The results have showed that diaquabis(diammine)copper(II) chloride complexes are thermochromic by a thermal dehydration mechanism with changes to ligand geometry and/ or complex symmetry being responsible for the observed colour changes dependent upon the diamine ligand type.

Acidification of solutions of bis(1,2-propanediammine)copper(II) chloride resulted in growth of two types of 1,2-diammoniumpropanetetrachlorocuprate crystals with a disproportionate ratio of diammonium cation to tetrachlorocuprate anions between crystal types. The green (1,2-diammoniumpropane)tetrachlorocuprate(II) crystals were found to be thermochromic b-1Xy a 2-D to 1-D phase change responsible for the green to yellow transition observed.

References

1. D.R. Bloomquist, R. D. Willet, *Coordination Chemistry Reveiws,* **47** (1982), 125

2. N. Dragoe, M. Andruh, A. Meghea, E. Segal, *Thermochimica Acta,* **161** (1990), 259

3. M. Andruh, *Revue Roumaine de Chimie,* **36** (1991), 101

4. N. Dragoe, M. Andruh, E. Segal, *Thermochimica Acta,* **176** (1991), 241

5. F. Cimpoesu, M. Andruh, E. Segal, *Thermochimica Acta,* **177**, (1991), 93

6. M. Brezeanu, M. Andruh, L. Patron, V. T. Popa, *Revue Roumaine de Chimie,* **30** (1985), 229

7. M. Andruh, M. Brezeanu, I. Paraschivoiu, E. Segal, *Thermochimica Acta*, **161** (1990), 247

8. C. Pariya *et al*, *J. Chem. Soc. Dalton Trans.*, **3** (1995), 337

9. A. M. Donia, H. A. El-Boraey, *Transition Met. Chem.*, **18**, (1993), 315

10. A. M., Donia, H. El-Boraey, *Thermochimica Acta,* **237**, (1994), 195

11. Y. Mori *et al*, *Bull. Chem. Soc. Jpn.*, **65**, (1992), 3358

12. D. R. Bloomquist, R. D. Willet, H. W. Dodgen, *J. Am. Chem. Soc.*, **103**, (1981), 2610

13. D. R. Willet, J. A. Haugen, J. Lebsack, J. Morrey, *Inorg. Chem.*, **13**, (1974), 2510

14. G. Marcotrigiano, L. Menabue, G. C. Pellacani, *Inorg. Chem.*, **15**, (1976), 2333

15. R. L. Harlow, W. J. Wells, G. W. Watt, S. H. Simonsen, *Inorg. Chem.*, **13**, (1974), 2106

16. D. N. Anderson, R. D. Willet, *Inorganic Chemica Acta.*, **8**, (1974), 167

CHAPTER 4 THERMOCHROMISM IN SILICA SOL-GEL

4.1 INTRODUCTION

The limiting factor in commercial application of inorganic thermochromic compounds is their poor physical characteristics as most are crystalline solids. An alternative approach is to use a carrier phase as a vehicle for the temperature sensitive dopant. The low temperature processing conditions used in the preparation of sol-gel materials[7] allows the incorporation of such high temperature intolerant compounds into a porous ceramic material which may then be used in the form of a thin film coating, monolith or powder. The composite material will have the physical and mechanical properties of a glassy ceramic and yet retain the optical properties of the thermally sensitive dopant. With potential application as infra-red recording media, temperature sensitive light filters, optical temperature sensors and self-diagnostic labels for microchips these currently valueless compounds may be of commercial value when present in a sol-gel matrix.

4.2 EXPERIMENTAL

4.2.1 Doped sol-gel preparation

0.2wt% Cu silica sol-gels were prepared by dissolving appropriate amounts of either diaquabis(1,2-ethanediammine)copper(II) chloride, diaquabis(1,2-propanediammine)copper(II) chloride) or diaquabis(N,N'-diethylethylenediamine)copper(II) chloride in 10.23ml of dry ethanol (95% ethanol dried by refluxing over magnesium) and adding this to 10ml of tetraethoxysilane (Aldrich, 99%). 3.165ml of 0.2M HCl was added and the mixture stirred for 1 hour. 5ml aliquots of the mixture were pipetted into four plastic petri-dishes (35mm diameter, 10mm deep, from BDH) and covered with Nesco™ film. Four equally spaced holes were punctured in the film using a syringe needle and the dishes placed in an oven at 40°C. The mass of the samples was monitored daily until constant.

Synthesis under neutral conditions was also made. Alkoxide silica sol-gels were pre-doped with the complex, as before, but with 0.127ml of 1M ammonium hydroxide solution added following 1 hour hydrolysis. This amount of base was sufficient to neutralise the solution as the pH was increased following hydrolysis. The sol-gel mixture was the same deep purple colour as the free complex and gelation occurred within a few minutes.

Optically transparent, colloidal silica granules were obtained from Crosfields-ICI for comparison with the alkoxide prepared gels. 1g of the silica was post-doped by immersion in a 1M aqueous solution of the complex for 1 hour, drained and left to dry on tissue paper for 30 minutes before thermal treatment. These granules were also a deep purple colour indicating the original, unprotonated complex to be present.

4.2.2 Thermal treatment of xerogels

To prevent extensive cracking, samples were initially heated from 25°C to 45°C at 0.5°C/min and held at constant temperature for 24 hours to remove excess moisture in the silica pores. The temperature was then raised rapidly to 80°C with no further cracking.

4.3 Results - xerogels prepared under acid conditions

4.3.1 Thermal treatment of xerogels

Figure 4.1 shows the effect of thermal treatment of the doped silica xerogels prepared at acidic pH conditions.

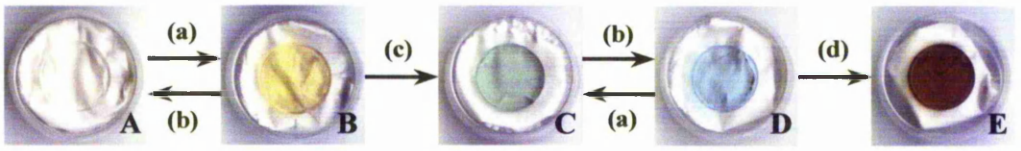

FIGURE 4.1: *THERMOCHROMIC TRANSITIONS IN 0.2WT% CU, $[Cu(PN)_2(H_2O)_2](Cl)_2$ DOPED SOL-GEL*
(a) *HEATED TO 80 °C FOR 1 HOUR,* ***(b)*** *REHYDRATED IN AIR,*
(c) *HEATED TO 80 °C FOR 24 HOURS,* ***(d)*** *HEATED TO 150 °C FOR 1 HOUR*

The unheated samples are very pale green in colour. Thermal treatment of the samples to 80°C for 1 hour results in a yellow colouration. This transition reverses upon cooling and exposure to atmosphere but may be preserved by storage in a dessicator. Prolonged thermal treatment at 80°C for 24 hours results in an irreversible thermochromic transition giving a deep green colour. Cooling and exposure of samples to atmosphere of the deep green samples results in a light blue colouration that may be preserved by storage in a dessicator. Thermal treatment of the light blue coloured samples to 80°C for 1 hour returns the deep green colour. Heating to 150°C for 1 hour causes an irreversible orange/brown colouration.

4.3.2 UV/Visible analysis

Figure 4.2 shows UV/Visible spectra of samples at different stages of thermal treatment. UV/Visible spectra of the unheated samples show a very broad absorbance with a maximum at 896nm. Thermal treatment at 80°C for 1 hour resulted in the absorption maximum shifting to 947nm. Prolonged thermal treatment at 80°C for 24 hours caused a large blue shift of the broad absorption to 701nm. Cooling and exposure of samples to atmosphere resulted in a shift of the absorption maximum to 669nm. Heating of samples to 150°C results in a spectrum with no discernible peaks but instead shows a continuous absorption across the spectrum that decreases with increasing wavelength.

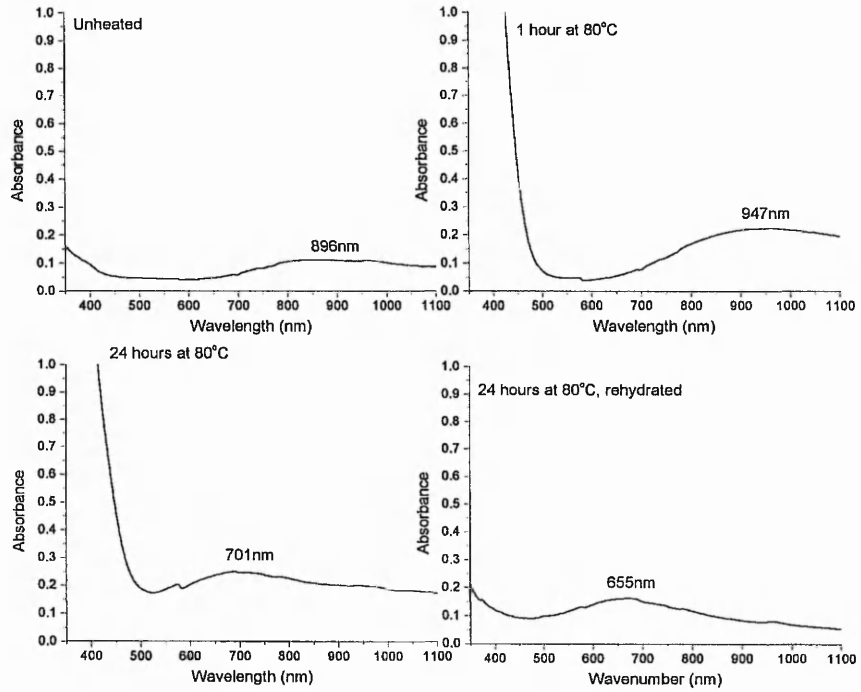

FIGURE 4.2: *UV/VISIBLE SPECTRA OF DOPED SILICA XEROGELS AT DIFFERENT STAGES OF THERMAL TREATMENT*

Figure 4.3 shows comparison of UV/Visible spectra of aqueous solutions of $[Cu(pn)_2(H_2O)_2]Cl_2$ in 1M HCl with unheated xerogels. Figure 4.3 shows a comparison of UV/Visible spectra of samples thermally treated for 24 hours at 80°C and exposed to atmosphere for 1 hour with aqueous solutions of the blue (diammoniumdiammine)copper(II) chloride complex.

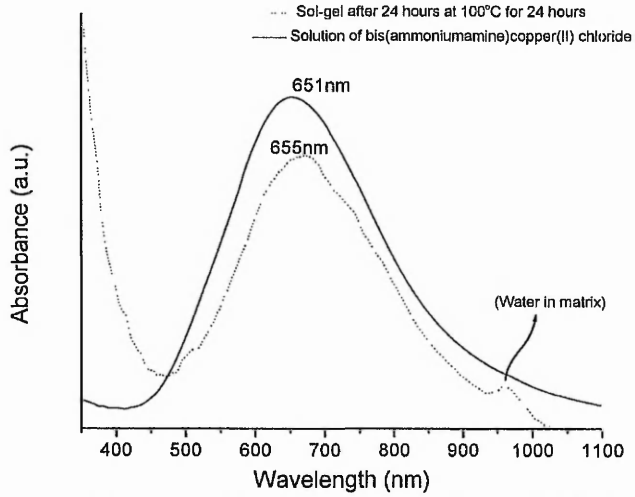

FIGURE 4.3: *COMPARISON OF UV/VISIBLE SPECTRA OF XEROGELS REHYDRATED IN AIR FOLLOWING HEATING FOR 24 HOURS AT 80 °C WITH AQUEOUS SOLUTION ON (DIAMMONIUMDIAMMINE)COPPER(II) CHLORIDE COMPLEX*

The unheated xerogels show identical spectra to that of acidified aqueous solutions of $[Cu(pn)_2(H_2O)_2]Cl_2$ in 1M HCl. Samples heated for 24 hours at 80°C show identical UV/Visible spectra to aqueous solutions of the (diammoniumdiammine)copper(II) chloride complex.

4.3.3 ESR ANALYSIS OF XEROGELS

ESR spectra of samples at any stage of thermal treatment are too complex to be interpretable due to multiple overlapping hyperfine peaks in the spectra. Unheated samples and samples heated to 80°C for 1 hour show no superhyperfine coupling. Figure 4.4 shows comparison of unheated samples with those heated to 80°C for 24 hours.

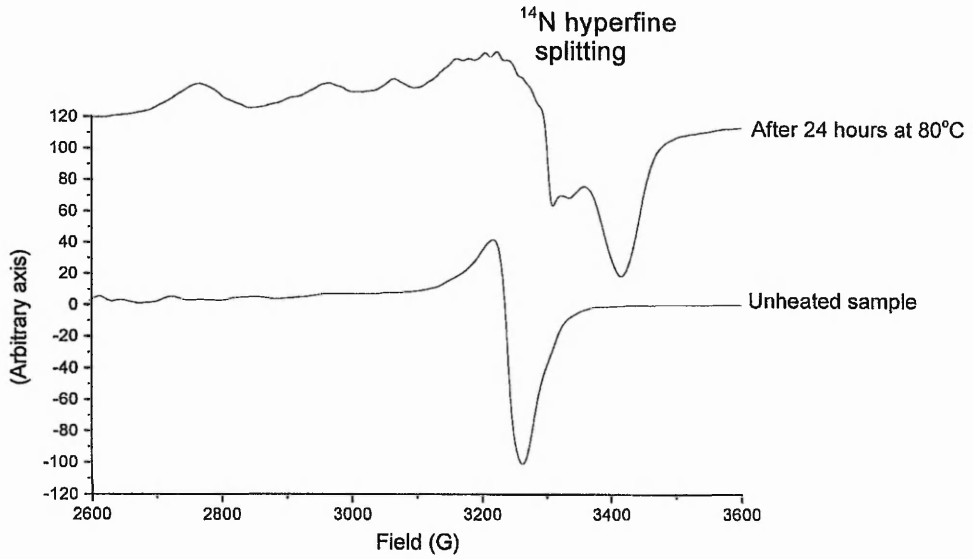

FIGURE 4.4: *EFFECT OF THERMAL TREATMENT TO 80 °C FOR 24 HOURS ON ESR SPECTRA OF XEROGELS*

Samples thermally treated to 80°C for 24 hours show nitrogen superhyperfine coupling in the $\perp$ region of the spectrum, although overlapping peaks make determination of the number of co-ordinated nitrogen ligands impossible.

4.3.4 Powder XRD analysis

Powder XRD analysis of samples show no crystalline components to be present in the xerogels at any stage of thermal treatment. Figure 4.5 shows an example diffraction pattern.

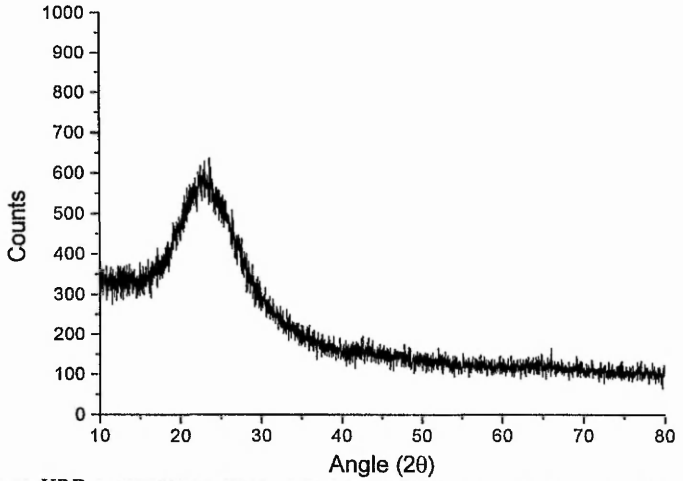

FIGURE 4.5: *POWDER XRD PATTERN OF SILICA XEROGEL FOLLOWING THERMAL TREATMENT TO 150 °C*

The broad reflection at 23.89° is due to the silica. No other diffraction peaks are found in the samples.

4.4 RESULTS - XEROGELS PREPARED UNDER NEUTRAL CONDITIONS

4.4.1 Incorporation of bis(diammine)copper(II) chloride complexes in silica xerogels

Figure 4.6 shows comparisons between UV/Visible spectra of solutions of the bis(diammine)copper(II) complexes and spectra of the complexes doped in silica prepared at neutral conditions.

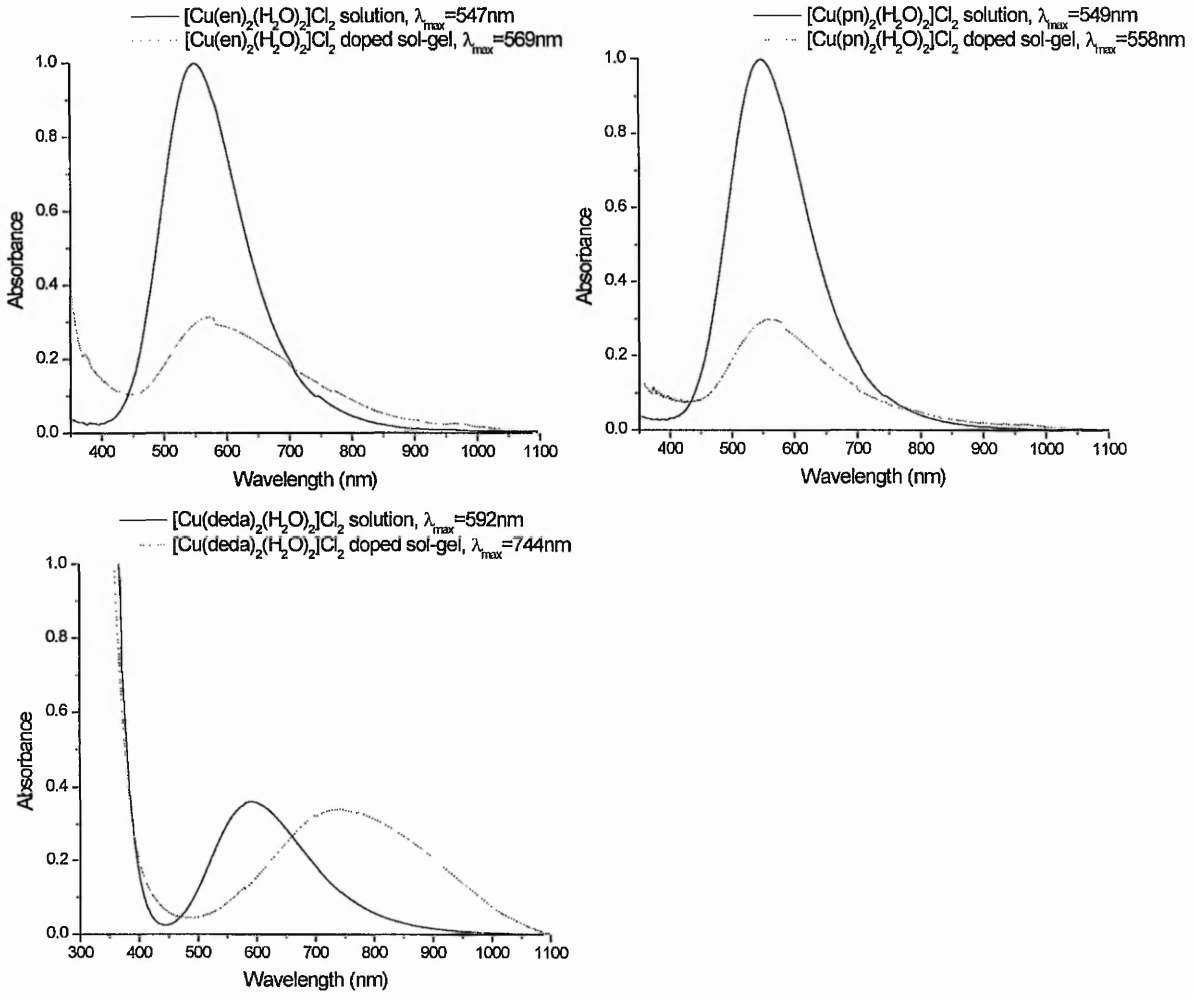

FIGURE 4.6: *COMPARISON OF UV/VISIBLE SPECTRA OF BIS(DIAMMINE)COPPER(II) SOLUTION AND DOPED SILICA XEROGELS. (A) $[Cu(en)_2(H_2O)_2]Cl_2$, (B) $[Cu(pn)_2(H_2O)_2]Cl_2$ AND (C) $[Cu(deda)_2(H_2O)_2]Cl_2$*

The absorption maximum for each complex showed a red shift when present in the silica compared to the solution alone. The magnitude of the shift depended upon diamine ligand type. $[Cu(deda)_2(H_2O)_2]Cl_2$ doped silica showed the largest shift ($\delta\lambda$ = 151nm), $[Cu(en)_2(H_2O)_2]Cl_2$ had the next largest shift ($\delta\lambda$ = 22nm) and $[Cu(pn)_2(H_2O)_2]Cl_2$ showed the smallest shift ($\delta\lambda$ = 9nm).

4.4.2) Thermal treatment of bis(diammine)copper(II) chloride doped xerogels

Figure 4.7 shows the effect of thermal treatment of silica xerogels doped with $[Cu(en)_2(H_2O)_2]Cl_2$, $[Cu(pn)_2(H_2O)_2]Cl_2$ and $[Cu(deda)_2(H_2O)_2]Cl_2$.

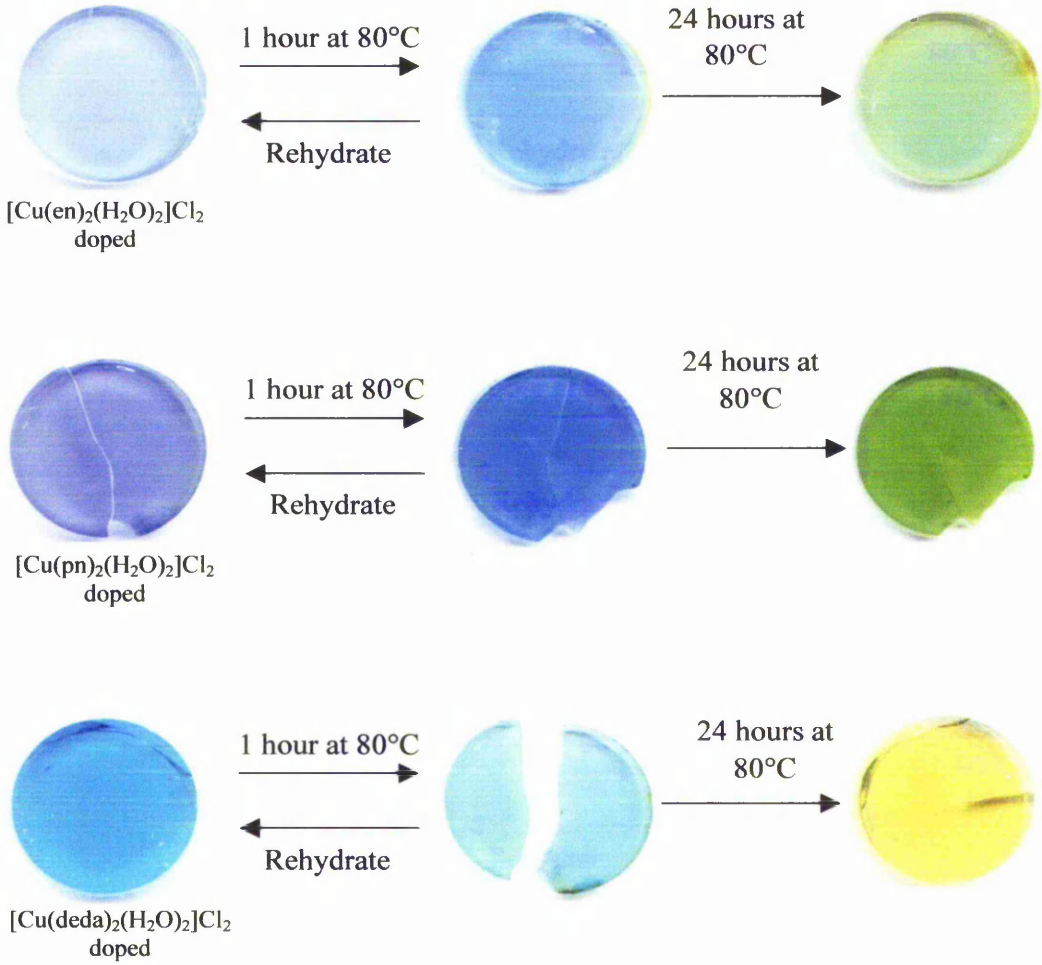

FIGURE 4.7: *THERMOCHROMIC TRANSITIONS OF SILICA XEROGELS DOPED WITH* $[Cu(en)_2(H_2O)_2]Cl_2$, $[Cu(pn)_2(H_2O)_2]Cl_2$ *AND* $[Cu(deda)_2(H_2O)_2]Cl_2$.

Xerogels doped with $[Cu(en)_2(H_2O)_2]Cl_2$ or $[Cu(pn)_2(H_2O)_2]Cl_2$ showed a similar thermochromic transition from purple to blue following thermal treatment at 80°C for 1 hour. Exposure to an ambient atmosphere reversed this colour change but the colour change may be preserved by storage in a dessicator. Prolonged thermal treatment at 80°C for 24 hours resulted in an irreversible green colouration. $[Cu(deda)_2(H_2O)_2]Cl_2$ doped xerogels were initially light blue in colour. Thermal treatment to 80°C for 1 hour resulted in a light green

colouration that reversed on exposure to ambient atmosphere and could be preserved by storage in a dessicator. Thermal treatment at 80°C for 24 hours resulted in yellow coloured samples. This transition was irreversible.

Figure 4.8 shows UV/Visible spectra of the samples at different stages of thermal treatment where the band maxima are indicated.

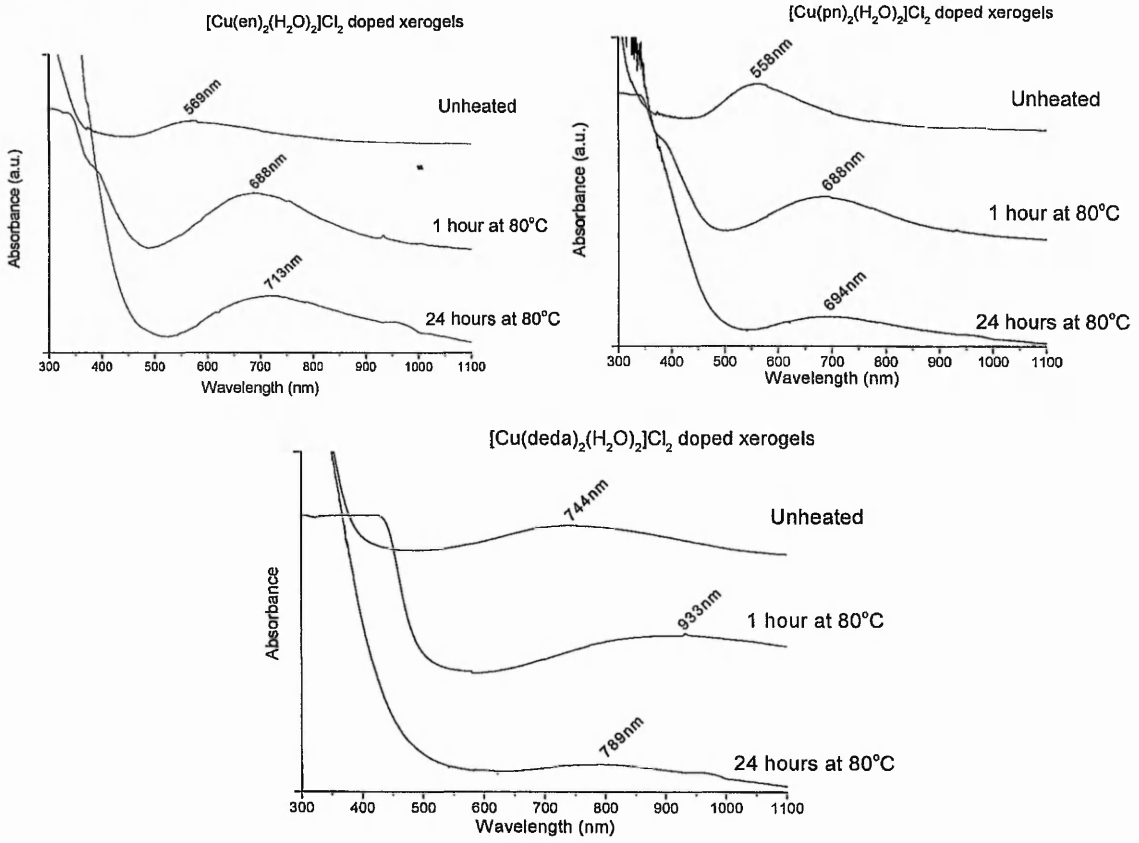

FIGURE 4.8: *UV/VISIBLE SPECTRA OF BIS(DIAMMINE)COPPER(II) CHLORIDE DOPED SILICA XEROGELS AT DIFFERENT STAGES OF THERMAL TREATMENT.*

Thermal treatment of $[Cu(en)_2(H_2O)_2]Cl_2$ doped xerogels to 80°C for 1 hour resulted in a shift of absorption maximum from 569nm to 688nm. Heating of the $[Cu(pn)_2(H_2O)_2]Cl_2$ doped xerogels at same conditions caused a peak shift from 558nm to 688nm whereas $[Cu(deda)_2(H_2O)_2]Cl_2$ doped xerogels showed a shift from 744nm to 933nm. Thermal treatment to 80°C for 24 hours resulted in a large blue shift of the maximum to 569nm for

$[Cu(en)_2(H_2O)_2]Cl_2$, 558nm for $[Cu(pn)_2(H_2O)_2]Cl_2$ and 789nm for $[Cu(deda)_2(H_2O)_2]Cl_2$. The shifts of absorption maxima are summarised in table 4.1.

	Unheated → 80°C for 1 hour	80° for 1 hour → 80°C for 24 hours
$[Cu(en)_2(H_2O)_2]Cl_2$	*-119nm*	*-25nm*
$[Cu(pn)_2(H_2O)_2]Cl_2$	*-130nm*	*-5nm*
$[Cu(deda)_2(H_2O)_2]Cl_2$	*-189nm*	*+144nm*

TABLE 4.1: *SUMMARY OF SHIFTS OF D-D ABSORPTION MAXIMA FROM UV/VISIBLE SPECTRA OF BIS(DIAMMINE)COPPER(II) CHLORIDE COMPLEXES AT DIFFERENT STAGES OF THERMAL TREATMENT*

No further colour changes were observed at higher temperatures (150°C).

4.4.3) Effect of silica type on thermochromic transitions

Figure 4.9 shows a comparison of thermochromic transitions of $[Cu(pn)_2(H_2O)_2]Cl_2$ doped silica xerogels prepared by colloidal or alkoxide methods.

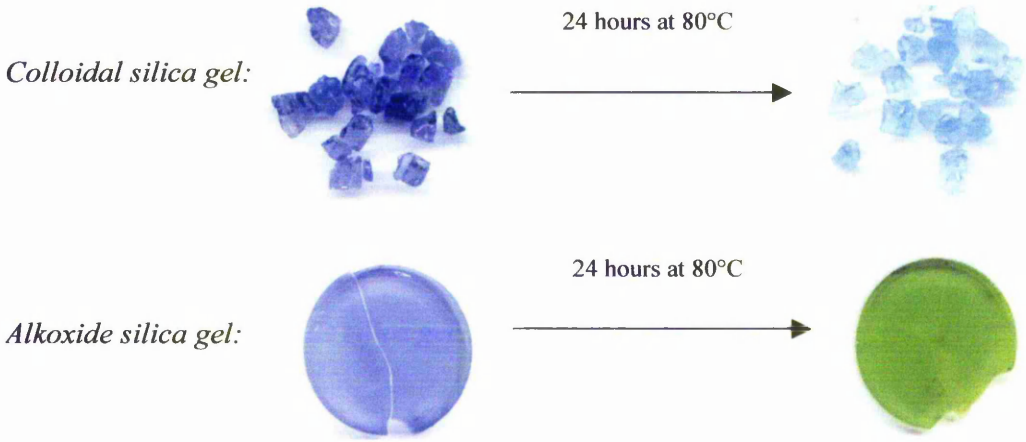

FIGURE 4.9: *THERMOCHROMIC TRANSITIONS OF $[Cu(pn)_2(H_2O)_2]Cl_2$ DOPED ALKOXIDE AND COLLOIDAL SILICA GELS*

Thermal treatment of the doped colloidal silica for 24 hours at 80°C resulted in an irreversible light blue colouration of the silica while the alkoxide silica became a light green colour when heated under the same conditions.

The differences in structure between the colloidal and alkoxide silica types is a macroscopic, not molecular property of the silica. The colloidal silica is synthesised by an aqueous route from sodium silicate with resulting particles, approximately 15nm diameter having more vicinal silanol groups on the silica surface whereas silica prepared by the alkoxide route is polymeric with few vicinal Si-OH groups.

4.4.4) ESR analysis of $[Cu(pn)_2(H_2O)_2]Cl_2$ silica xerogels

ESR analysis of the colloidal and alkoxide silica xerogels showed that all samples have two Cu(II) sites at 77K. Samples were analysed before and after thermal treatment to 80°C for 24 hours. Samples were cooled and allowed to rehydrate in order to simplify ESR spectra. This is shown in figure 4.10. The number of nitrogen ligands co-ordinated to the copper(II) cannot be determined from the spectra because of closely overlapping peaks.

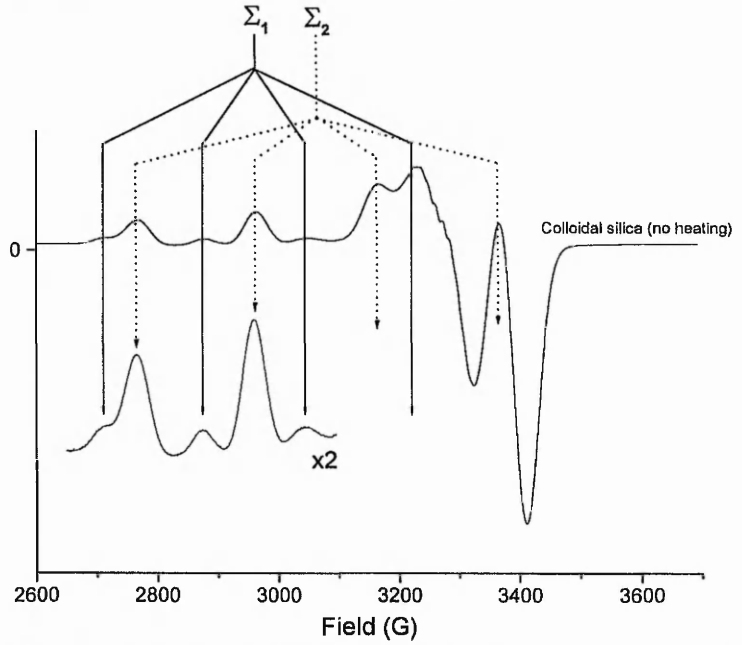

FIGURE 4.10: EXAMPLE ESR SPECTRUM OF COLLOIDAL SILICA GEL DOPED WITH $[Cu(pn)_2(H_2O)_2]Cl_2$ SHOWING TWO DIFFERENT CU(II) SITES

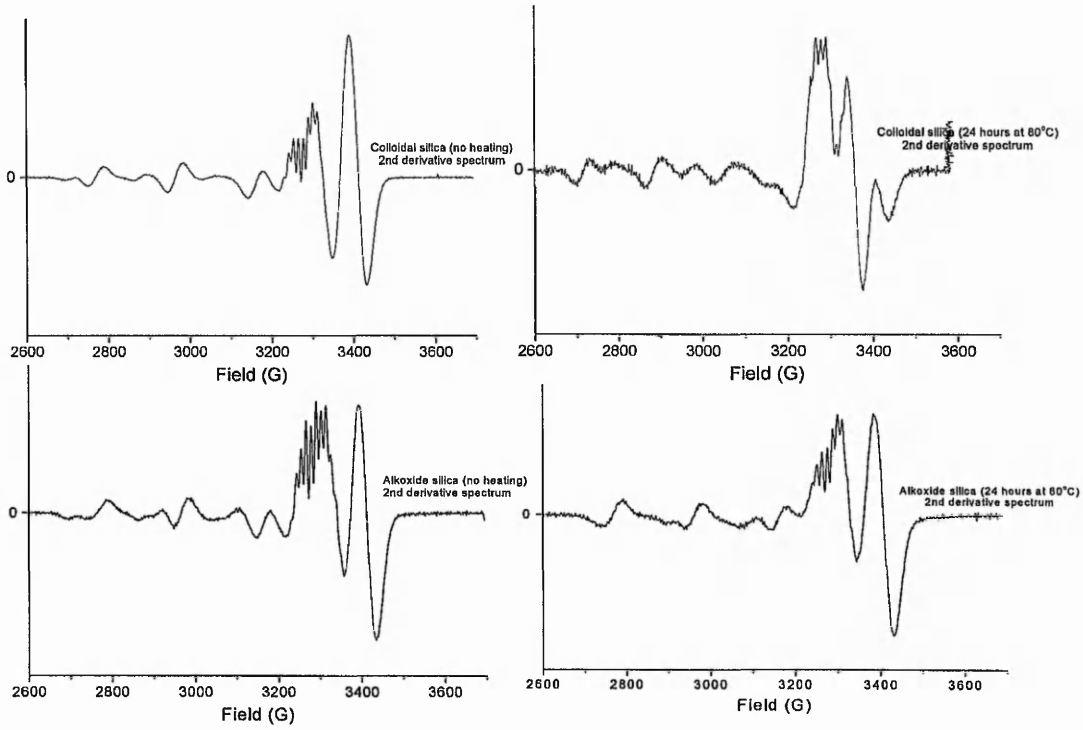

FIGURE 4.11: *SECOND DERIVATIVE OF ESR SPECTRA OF* $[Cu(PN)_2(H_2O)_2]Cl_2$ *DOPED ALKOXIDE AND COLLOIDAL SILICA XEROGELS BEFORE AND AFTER THERMAL TREATMENT TO 80 °C FOR 24 HOURS*

2nd derivative plots of the spectra (figure 4.11) revealed nitrogen superhyperfine coupling in the parallel region of the spectrum showing the nitrogen ligands to be co-ordinated in the x-y plane of the complex. The two Cu(II) sites are hereafter referred to as Σ_1 and Σ_2 sites. Table 4.2 shows the relevant g and $A_{\|}$ values for the two sites.

Silica type and thermal treatment	Σ_1	Σ_2
Alkoxide (unheated)	*75% ±10%*	*25% ±10%*
	$g_{\|\|} = 2.203$	$g_{\|\|} = 2.270$
	$g_{\perp} = 2.034$	$g_{\perp} = 2.063$
	$A_{\|\|} = 194G$	$A_{\|\|} = 170G$
Alkoxide (80°C for 24 hours)	*60% ±10%*	*40% ±10%*
	$g_{\|\|} = 2.203$	$g_{\|\|} = 2.270$
	$g_{\perp} = 2.034$	$g_{\perp} = 2.063$
	$A_{\|\|} = 194G$	$A_{\|\|} = 170G$
Colloidal (unheated)	*65% ±10%*	*35% ±10%*
	$g_{\|\|} = 2.201$	$g_{\|\|} = 2.246$
	$g_{\perp} = 2.034$	$g_{\perp} = 2.060$
	$A_{\|\|} = 202G$	$A_{\|\|} = 175G$
Colloidal (80°C for 24 hours)	*50% ±10%*	*50 ±10%*
	$g_{\|\|} = 2.201$	$g_{\|\|} = 2.246$
	$g_{\perp} = 2.034$	$g_{\perp} = 2.052$
	$A_{\|\|} = 196G$	$A_{\|\|} = 175G$

TABLE 4.2: *g AND $A_{\|\|}$ VALUES AND % ABUNDANCE FOR Σ_1 AND Σ_2 SITES IN $[Cu(pn)_2(H_2O)_2]Cl_2$ DOPED ALKOXIDE AND COLLOIDAL SILICA BEFORE AND AFTER THERMAL TREATMENT AT 80 °C FOR 24 HOURS.*

Xerogels calcined for 4 hours at 500°C had $g_{\|\|}$ and $A_{\|\|}$ values of 2.521 and 169G respectively.

Thermal treatment of the samples to 80°C for 24 hours resulted in a decrease of the relative abundance of Σ_1 and an increase of Σ_2 sites in both alkoxide and colloidal silica samples. The g and $A_{\|\|}$ values of glassy solutions of the $[Cu(pn)_2(H_2O)_2]Cl_2$ complex changed significantly depending upon whether doped in alkoxide or colloidal silica xerogels. These sites were therefore assigned as the solvated complex in the liquid in the silica pores. For greater clarity figure 4.12 shows the data plotted on a Symmons plot of $A_{\|\|}$ vs. $\Delta\delta g_{\|\|}$ showing theoretical lines of square planar and tetrahedral geometry to illustrate the co-ordination changes that occur.

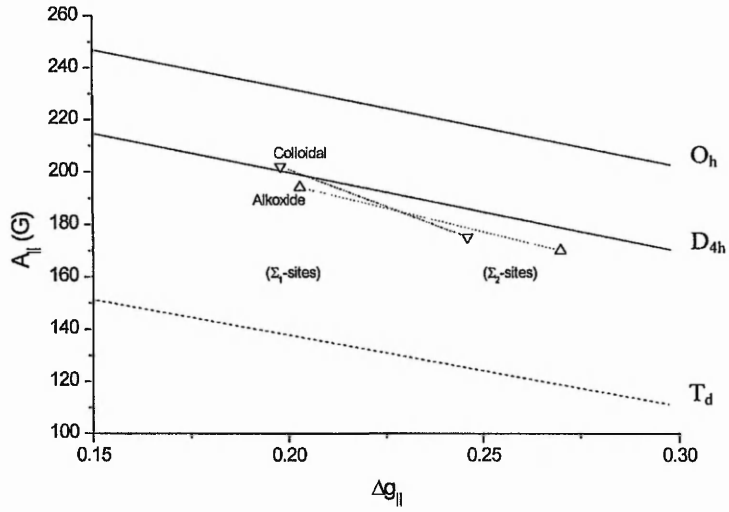

FIGURE 4.12: *SYMMONS PLOT SHOWING EFFECT OF THERMAL TREATMENT ON CO-ORDINATION GEOMETRY OF DOPED ALKOXIDE AND COLLOIDAL SILICA GELS*

The plot shows that the Σ_2 sites are distorted towards tetrahedral geometry. The degree of this distortion is slightly larger for the colloidal silica than the alkoxide derived material.

The different Cu(II) sites in the silica xerogels can be more accurately described by their metal – ligand covalency coefficients. Three parameters are required (α, β and β_1) to describe the bonding in copper(II) complexes. The square of these parameters can take values between 0 and 1, 0.5 being purely covalent while 0 and 1 is purely ionic. The α^2 coefficient describes the in-plane σ-bonding of the d_{x2-y2} orbital with ligands in the x-y plane. The β^2 coefficient describes the out of plane π-bonding of ligands with the d_{xz} orbital. For most Cu(II) complexes in a tetragonally distorted geometry the d_{xz} and d_{yz} orbitals are essentially non-bonding and β is assumed to be unity. Figure 4.13 shows how the g and $A_{\|}$ values are determined from the ESR spectrum. This is measured by computer for more accurate determination of values.

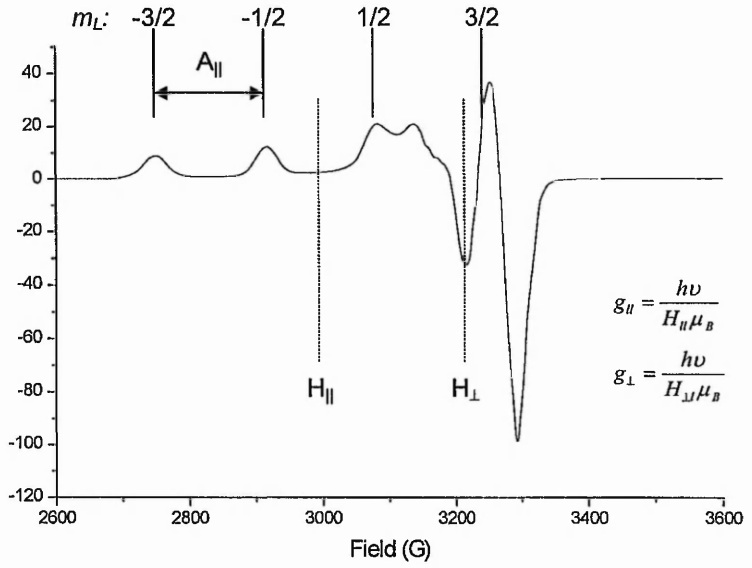

FIGURE 4.13: *DETERMINATION OF g AND $A_{||}$ VALUES FROM ESR SPECTRUM OF CU(II)*

The value of $A_{||}$ is taken directly from the spectra and conventionally has units of Gauss. The value of $A_{||}$ is dependent upon the $g_{||}$ of complex whereas the interaction between electron and Cu(II) nuclear spin is an energy. To give meaningful results these units are converted to cm^{-1} by multiplying the field values by the Bohr magneton (μ_B = 4.66964x10^{-4} cm^{-1} G^{-1}). ε is a constant proportional to the inverse square of the radius of the d_{x2-y2} orbital.

The α^2 coefficient is related to the $A_{||}$, $g_{||}$ and $g_\perp$ by equation (i).

$$A_{||} = P\left[-\alpha^2\left(0.57 + \underline{\chi_0}\right) + \delta g_{||} + 0.43\delta g_\perp + 0.03\right] \qquad \text{(i)}$$

equations (ii) and (iii) relate the β^2 and $\beta_1{}^2$ coefficients to $\delta g_{||}$ and $\delta g_\perp$.

$$\delta g_{||} = \frac{-2\varepsilon\alpha^2\beta^2}{E_{XZ}} \qquad \text{(ii)}$$

$$\delta g_\perp = \frac{-8\varepsilon\alpha^2\beta_1^2}{E_{XY}} \qquad \text{(iii)}$$

where;

$\delta g = g - g_e$

g_e is the free spin value of the electron and is equal to 2.00232, χ_0 is the Fermi contact term for the free Cu(II) ion and has a value of 0.43. P is a constant proportional to the inverse square of the radius of the d_{x2-y2} orbital ($0.93cm^{-1}$ for Cu(II)) and E_{xz} and E_{yz} are the energy transitions shown in figure 4.14.

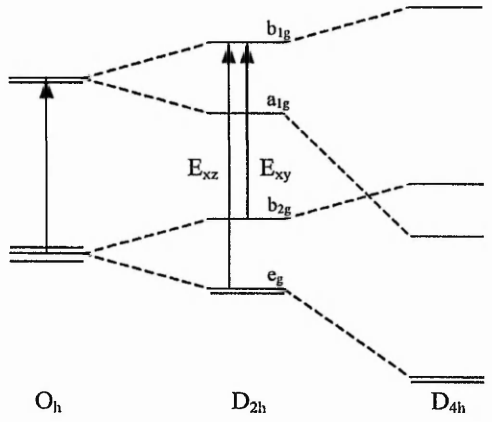

FIGURE 4.14: *SPLITTING OF ENERGY LEVELS IN AN OCTAHEDRAL CRYSTAL FIELD BY TETRAGONAL DISTORTION*

For Cu(II) ε=-828cm^{-1}. Since $(0.57+\chi_0) = 1$ and $g_\perp$ does not vary significantly ($g_\perp$~2.049) and so equation (i) simplifies to;

$$A_{\|} = P\left[-\alpha^2 + \delta g_{\|} + 0.051\right] \qquad \text{(iv)}$$

Substituting the values of $A_{\|}$ and $\delta g_\perp$ into equation (iv) the α^2 coefficients of the Σ_1 and Σ_2 sites may be calculated. The results are shown in table 4.3.

	$\alpha^2(\Sigma_1)$	$\alpha^2(\Sigma_2)$
Alkoxide	0.30	0.18
Colloidal	0.32	0.22

TABLE 4.3: *CALCULATED α^2 COEFFICIENTS FOR $[Cu(PN)_2(H_2O)_2]Cl_2$ DOPED COLLOIDAL AND ALKOXIDE SILICA*

Experimental determination of the E_{xy} and E_{xz} for the individual sites in the samples was not directly possible because of the very broad d-d absorption and relatively low sensitivity of UV/Visible spectroscopy. Some approximations must therefore be made to determine the bonding characteristics between the ligands and the d_{xy} orbital (β_1^2 coefficient).

For O_h symmetry $E_{xy} = E_0 = E_{xz}$ and the so upper limit of E_{xy} may be taken from the optical spectrum of the aqueous solution of the complex. This is shown in figure 4.14.

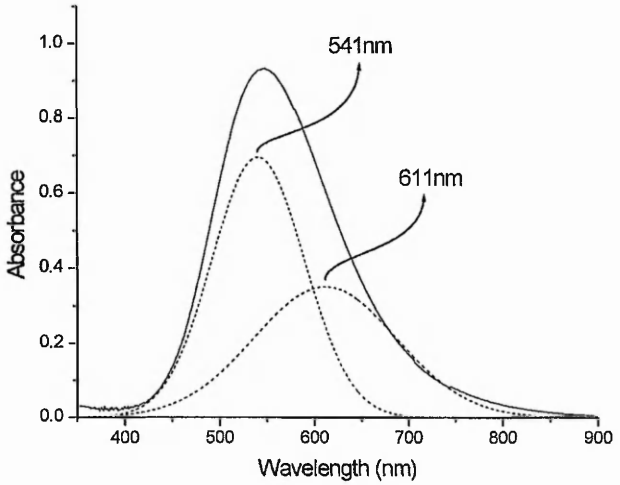

FIGURE 4.14: *CURVE FITTING ANALYSIS OF UV/VISIBLE SPECTRA OF SOLUTION OF* $[Cu(pn)_2(H_2O)_2]Cl_2$ *INTO* E_{xz} *AND* E_{xy} *PEAKS.*

Curve fitting of the optical spectrum of $[Cu(pn)_2(H_2O)_2]Cl_2$ shows that $E_{xz} = 18480cm^{-1}$ and $E_{xy} = E_0 = 16366cm^{-1}$.

For D_{4h} symmetry $E_{xy} = E_0$ must be less than E_{xz}. Using equation (iii) the value of E_{xz} may be calculated from the $\delta g_\perp$ and α^2 values assuming that β is unity. The calculated results are shown in table 4.4.

	$\lambda_{xz}(\Sigma_1)$	$\lambda_{yz}(\Sigma_2)$
Alkoxide	$14611cm^{-1}$	$4731cm^{-1}$
Colloidal	$15586cm^{-1}$	$5783cm^{-1}$

TABLE 4.4: *CALCULATED* E_{xz} *AND* E_{xy} *VALUES FOR THE* Σ_1 *AND* Σ_2 *SITES IN COLLOIDAL AND ALKOXIDE SILICA*

The degree of Jahn-Teller distortion (δ_2) can be expressed as the difference between E_{xz} and E_{yz} values.

$$\delta_2 = E_{xz} - E_{yz} \qquad \text{(v)}$$

Substituting equations (ii) and (iii) into (v) gives;

$$\delta_2 = \frac{-2\varepsilon\alpha^2}{\delta g_\perp} - \frac{-8\varepsilon\alpha^2}{\delta g_\parallel} \qquad \text{(vi)}$$

which simplifies to;

$$\beta_1^2 = \frac{\delta g_\parallel}{4}\left(\frac{1}{\delta g_\perp} - \frac{\delta_2}{2\varepsilon\alpha^2}\right) \qquad \text{(vii)}$$

The value of δ_2 must lie between zero (purely octahedral) and an upper limit set as the difference between the values obtained from the optical spectrum of the complex in solution and those calculated in table 4.4. From this the value of β_1^2 is greater than unity for both Σ_1 and Σ_2 showing that the d_{xy} orbitals on the copper in all sites in the silica are essentially non-bonding.

4.4.5) Bonding of silica to $[Cu(pn)_2(H_2O)_2]Cl_2$

Evidence for the co-ordination of silica to copper complexes is possible to obtain using infrared spectroscopy and examining the spectra for the appearance of shoulders or new vibrational bands in the Si-OH region of the spectrum ($960cm^{-1}$). Figure 4.14 shows a comparison between doped and undoped alkoxide and colloidal silica samples before and after thermal treatment to 80°C for 24 hours. DRIFTS spectra of the samples are shown to enhance the surface Si-OH bands.

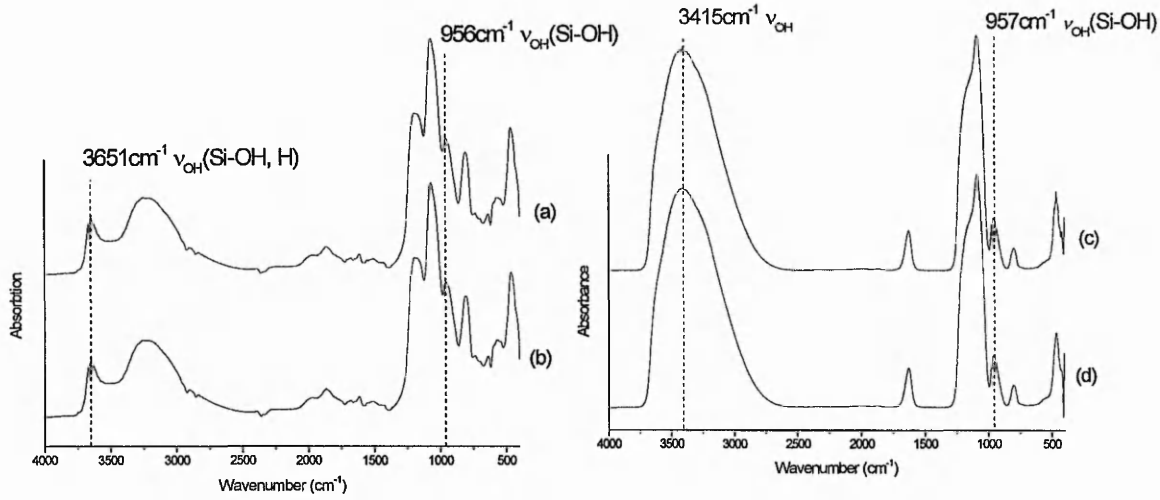

FIGURE 4.14: *DRIFTS SPECTRA OF SILICA GELS DOPED WITH* $[Cu(pn)_2(H_2O)_2]Cl_2$ *AT DIFFERENT STAGES OF THERMAL TREATMENT (A) ALKOXIDE SILICA, UNHEATED, (B) ALKOXIDE SILICA HEATED TO 80 °C FOR 24 HOURS, (C) COLLOIDAL SILICA, UNHEATED AND (D) COLLOIDAL SILICA HEATED TO 80 °C FOR 24 HOURS*

The spectra show ν_{OH}(Si-OH, H-bonded) and ν_{OH}(Si-OH) vibrational bands at 3162cm^{-1} and 953cm^{-1} respectively. No change to the Si-OH bands was found when the silica was doped with the complex before or after thermal treatment of either type of silica.

4.4.6) Bonding of silica oligomers

The aim of this experiment was to determine any influence or possible co-ordination of soluble silica species in the liquid of the pores of the silica to the complex.

Figure 4.15 shows the ESR spectrum at 77K of solutions of $[Cu(pn)_2(H_2O)_2]Cl_2$ complexes with and without silica oligomers. One type of Cu(II) site was present in the solutions. Table 4.5 shows the g and $A_{||}$ values for the complex with and without the addition of silica oligomers.

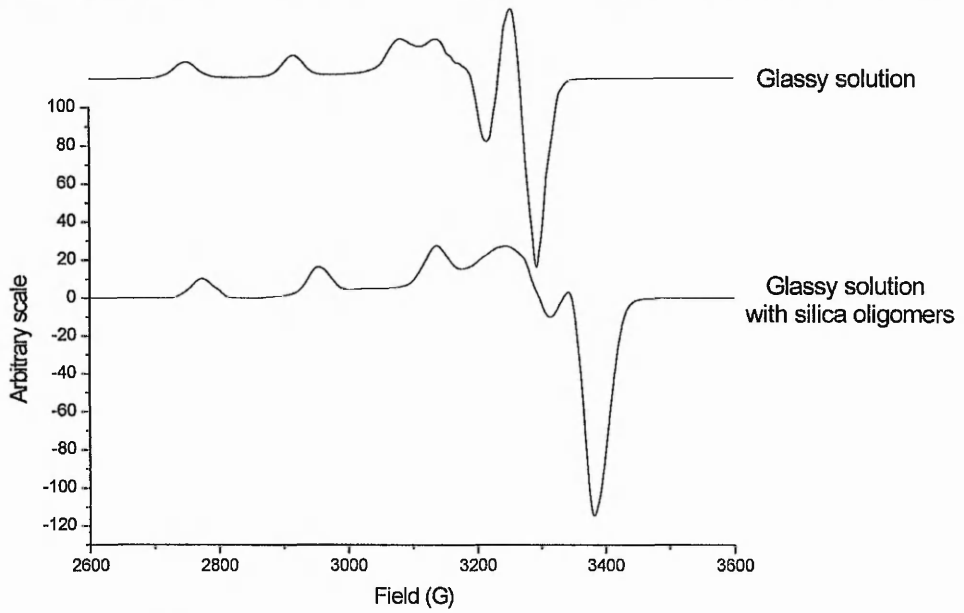

FIGURE 4.15: *EFFECT OF SILICA OLIGOMERS ON ESR SPECTRUM OF* $[Cu(pn)_2(H_2O)_2]Cl_2$

	$\delta g_{\|}$ (no silica)	$A_{\|}$ (no silica)	$\delta g_{\|}$ (with silica)	$A_{\|}$ (with silica)
$[Cu(en)_2(H_2O)_2]Cl_2$	0.209	190	0.239	193
$[Cu(pn)_2(H_2O)_2]Cl_2$	0.203	194	0.219	197
$[Cu(deda)_2(H_2O)_2]Cl_2$	0.194	194	0.215	199

TABLE 4.5: *EFFECT OF SILICA OLIGOMERS* $g_{\|}$ *AND* $A_{\|}$ *VALUES FOR BIS(DIAMMINE)COPPER(II) CHLORIDE COMPLEXES*

All three complexes showed a positive shift in $A_{\|}$ and $\delta g_{\|}$ in the solution containing silica oligomers compared to the complex alone. This effect is better illustrated using a Symmons plot (figure 4.16) of $A_{\|}$ vs. $\delta g_{\|}$ with theoretical lines for tetrahedral and square planar geometries.

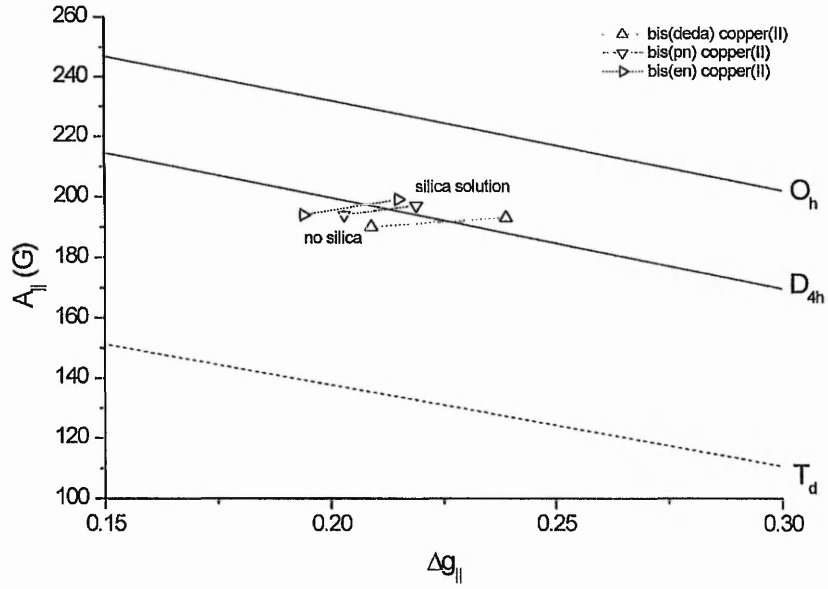

FIGURE 4.16: *SYMMONS PLOT OF $A_{||}$ VS. $\delta g_{||}$ FOR CU(II) SHOWING EFFECT OF SILICA OLIGOMERS ON ESR SPECTRA*

Solutions of the bis(diammine)copper(II) complexes in the presence of silica oligomers resulted in a small change of geometry towards square planar. These changes were not observed visually or by UV/Visible spectroscopy due to very broad absorption bands.

4.5) DISCUSSION

4.5.1 Xerogels prepared under acid conditions

The results show that incorporation of bis(diammine)copper(II) chloride complexes into silica sol-gel produced by an acid catalysed route produces a material with thermochromic properties not found in the free compounds. These silica gels contain the diammoniumtetrachlorocuprate salt as expected given the acid conditions of the process (see chapter 3).

Thermal treatment of the xerogels to 80°C for 1 hour results in a green to yellow thermochromic transition identical to the free compound and is assumed to result from the same mechanism resulting in the colour change by the formation of a layered $CuCl_4$ structure.

The difference between the doped silica and the free compounds is that storage of silica in a dessicator allowed the yellow colour to be preserved. This shows that the "high temperature phase" of the diammonium complex may be preserved at room temperature by the dry silica.

Prolonged thermal treatment at 80°C for 24 hours resulted in significant, irreversible changes to the copper(II) inner co-ordination sphere. ESR analysis showed nitrogen co-ordination takes place following thermal treatment to 80°C for 24 hours resulting in the yellow to deep green thermochromism. Comparison of the optical spectra of xerogels with aqueous solutions of the (diammoniumdiammine)copper(II) chloride complex and acidified solutions of $[Cu(pn)_2(H_2O)_2]Cl_2$ showed that thermal treatment to 80°C for 24 hours resulted in co-ordination of two nitrogen ligands to the copper(II) atoms. This co-ordination must result from loss of two protons from two ammonium groups leaving a free amine that then co-ordinated to the copper(II). This thermochromic transition is not found in the free compound so the proton must be transferred by an intermolecular route, not intramolecular, to some accepting species in the sol-gel matrix. The nature of the accepting species is not known but is likely to be surface silanol groups.

The free (diammoniumdiammine)copper(II) chloride complex is not thermochromic yet its presence in the silica xerogels resulted in a material with discontinuous, reversible thermochromic properties when heated to 80°C for 1 hour. The colouration of the samples suggested an octahedral (blue) to square planar (green) transition took place. This must result from interaction with the silica although the exact nature of the interaction remains unclear.

Heating of the xerogels to 150°C resulted in orange/ brown coloured samples. The reason for this colour transition is not clear. Given that the complex thermally decomposes at 280°C it the colouration of the sample could not be attributed to thermal decomposition of the complex to copper(II) oxide and/ or carbon. XRD analysis also showed no crystalline component was present in the silica samples. The intense colouration must arise from some structural reordering and or changes to complex co-ordination that brought about significant changes in the charge transfer characteristics of the complex.

4.5.2) Xerogels prepared under neutral conditions

The results show that incorporation of bis(diammine)copper(II) chloride complexes into silica by a two step acid-base catalysis method results in a material whose optical and thermochromic properties are significantly different to those of the free complex or solutions of the complex.

Comparison of UV/Visible spectra of complexes in solution with those of the complex in doped silica xerogels shows a red-shift of the d-d absorption maxima. The magnitude of the shift is dependant on the ligand type and is in the order of the relative conformational energy change of the N-C-C-N back-bone of the diamine ligands. 1,2-propanediamine has the highest conformational energy of the diamine compounds used due to the bulky methyl group on the N-C-C-N chain. The large ethyl groups on the N,N'-diethylethylenediamine molecule make the conformational change energy of the N-C-C-N chain higher than for ethylenediamine, although the difference in conformation energy between these two ligands would be small as no groups are actually on the N-C-C-N chain. The relative energy barrier to conformational change of the ligand is in the order of pn>deda>en. This order is the same order as the

magnitude of the shift of absorption maximum when the complexes are doped into the xerogels. The effect of incorporation into the silica is to alter the conformation of the diamine ligands. The red shift of the absorption suggests that the silica moves the ligands out of plane resulting in a lowering of the ligand field strength.

4.5.2.1) Influence of silica on optical properties of the complex

Inner sphere co-ordination of silica to Cu(II) is possible, but is not supported by the data. Doping of silica xerogels with the bis(diammine)copper(II) chloride complexes could be expected to cause deprotonation of the slightly acidic Si-OH groups by the reaction:

With this deprotonation of the silanol allowing inner sphere co-ordination of silica to Cu(II).

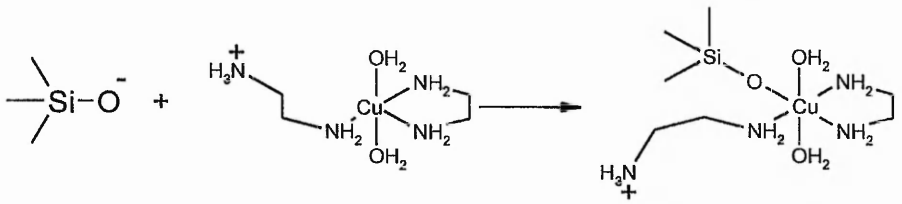

This type of silica-copper interaction has been proposed for $[Cu(Py)_4]$ doped silica xerogels[1].

The ESR ($A_{\|}$ values) data does not support this interaction between silica and the bis(diammine)copper(II) chloride complexes studied from the $A_{\|}$ values. In doped gels calcined at 500°C for 4 hours the copper ions can be assumed to have an octahedral co-ordination of network oxygens[1]. The value of $A_{\|}$ for Σ_2 Cu(II) sites in $[Cu(pn)_2(H_2O)_2]Cl_2$ doped silica gel is 188×10^{-4} cm^{-1}. The $A_{\|}$ values of the calcined Cu(II) containing silica and that of the complex in silica solution are 199×10^{-4} cm^{-1} and 180×10^{-4} cm^{-1} respectively. The fact that $A_{\|}$ in the silica gel is larger than that of the silica solution, but smaller than that of the

calcined xerogels shows no evidence of Si-O-Cu bond formation where the opposite behaviour would be expected[1].

Infrared analysis of the colloidal and alkoxide xerogels before and after thermal treatment to 80°C for 24 hours also showed no evidence of a strong silica-copper interaction. Peaks at 810 and 1100cm^{-1} are assigned as the Si-O-Si symmetric and antisymmetric vibrations while a band due to Si-OH vibrations is known to appear at 960cm^{-1} [2]. According to literature values IR peaks could arise around 960cm^{-1} from Si-O-M vibrations (e.g. Si-O-Ti at 930cm^{-1} [3], Si-O-Ni at 975cm^{-1} [3], and Si-O-Al at 1050cm^{-1} [4]). No change in the Si-OH or Si-O-Si vibrational bands, in either the alkoxide or colloidal silica gels, was found at any stage of thermal treatment compared with the undoped silica. From this it must therefore be concluded that the only silica-complex interaction is via hydrogen bonding of soluble silica species to the in-plane ammine ligands with no direct inner sphere co-ordination to the copper atoms.

From the ESR data of $[Cu(pn)_2(H_2O)_2]Cl_2$ in a solution containing soluble silica species the influence of silica oligomers appears to be to restrict conformational changes of the diammine ligands towards square planar conformation. The influence must arise from outer sphere co-ordination of the silica to the complex with no direct interaction with the copper d-orbitals. Hydrogen bonding of outer sphere ligands to hydrogen atoms on the ammine groups is most probable. Hydrogen bonding of BF_4^-, ClO_4^- and NO_3^- in a similar manner to bis(diammine)copper(II) complexes resulting in restriction of the in-plane ligand motion is known. A similar interaction between soluble silica species and bis(diammine)copper(II) complexes is proposed in the liquid in the pores of the doped silica xerogels resulting in a decrease of entropy. This is illustrated in figure 4.17.

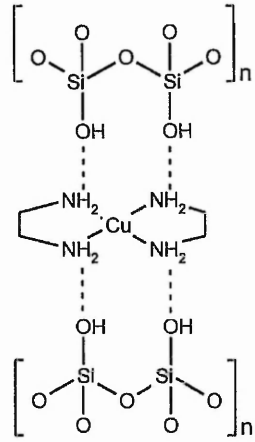

FIGURE 4.17: *SCHEMATIC DIAGRAM OF PROPOSED INTERACTION OF SOLUBLE SILICA SPECIES WITH BIS(DIAMMINE)COPPER(II) COMPLEXES*

This is not a definitive diagram of the interaction between silica and the bis(diammine)complex as the number of silica – amine hydrogen bonds formed per complex molecule is unknown.

4.5.2.2) Thermal treatment of silica gels

Thermal treatment of the doped silica xerogels for 1 hour at 80°C for 1 hour resulted in a red shift of the d-d peak maximum for the bis(diammine)copper(II) chloride doped xerogels in the order of deda>>pn>en. This is consistent with dehydration of the samples followed by co-ordination of chloride to the ethylenediamine and 1,2-propanediamine complexes while the N,N'-diethylethylenediamine complex becomes square planar due to steric crowding of the axial positions by the bulky diamine ligand preventing co-ordination of the chloride giving the green colouration of square planar copper(II) rather than the blue/purple colour expected for octahedral co-ordination.

Prolonged thermal treatment at 80°C for 24 hours resulted in irreversible, discontinuous thermochromic transitions not found in the free complexes heated under the same conditions. A red shift of the d-d absorption band for $[Cu(en)_2(H_2O)_2]Cl_2$ and $[Cu(pn)_2(H_2O)_2]Cl_2$ doped samples occurred with the magnitude of the shift in the order of pn>en. The $[Cu(deda)_2(H_2O)_2]Cl_2$ doped xerogels showed a large blue shift. ESR analysis of the gel doped with $[Cu(pn)_2(H_2O)_2]Cl_2$ showed two Cu(II) sites to be present in the silica samples. Prolonged thermal treatment resulted in a change of relative abundance of these two sites as the Σ_1 site, denoted as solvated Cu(II) sites in the liquid in the silica pores, are transformed to Σ_2 sites that are only found in the doped silica. ESR analysis shows these Σ_2 sites to be Cu(II) sites with the in-plane ligands twisted out of plane towards tetrahedral geometry relative to the Σ_1 sites. Some association and or influence of the silica must therefore be responsible for this thermochromic transition. Direct coordination of the silica to the Cu(II) has been shown not to occur while soluble silica species act to restrict ligand motion therefore some other property of the silica must be responsible for this transition.

The thermochromic transition is dependant on the structure of the silica with colloidal silica gels showing differences in colour compared to alkoxide silica gels. The principle difference between silica gels prepared by the alkoxide and aqueous (colloidal) route is the type of Si-OH groups on the material surface. Colloidal silica gels possess a higher number of *vic*-OH groups while alkoxide gels possess very few. Further to this, strong surface forces exist up to 40Å from the silica surface sufficient to hold water in a glassy state when frozen. Domains of strong electronic influence in the micropores of diameter equal to twice this distance are found in the silica structure that can "trap" dopant species. It is proposed that loss of water from the silica pores by thermal dehydration of the silica results in migration of the complex

into the micropores. Following rehydration the complex cannot escape the micropores due to the strong forces therein and so a decrease in the relative amount of "free" Σ_1 sites in the liquid of the pores occurs while an increase in the "trapped" Σ_2 sites results. The difference in the colours observed for the different silica types is a result of the difference in surface chemistry of the micropores of the two silicas resulting in a greater distortion of the complex geometry towards tetrahedral in the alkoxide silica relative to the colloidal silica.

4.6) Conclusions

Incorporation of bis(diammine)copper(II) complexes into silica matrices results in a highly variable range of thermochromic transitions not encountered in the free compounds. The explanation of these transitions and differences in optical properties between solution and doped silica is due to their interaction with the silica matrix.

Incorporation of diammononium tetrachlorocuprate complexes into silica results in a material with thermochromic properties identical to that of the free compound when heated to 80°C for 1 hour by conversion between low and high temperature phases of the compound. In contrast to the complex alone, the colour of the high temperature form of the compound may be preserved at low temperatures by desiccation of the doped silica. Thermal treatment of the material for longer periods results in intermolecular proton transfer from two ammonium groups, one from each ligand, of the diammonium molecules to an unidentified acceptor in the matrix. The resulting amine group co-ordinates to the copper giving a square planar complex assumed to possess two nitrogen and two chloride ligands. Rehydration of the silica results in the [bis(ammineammoniumalkyl)copper(II)] complex as was isolated and characterised from acidified solutions of bis(diammine)copper(II) complexes as described in chapter 3. This blue

complex itself is not thermochromic yet thermal treatment of the silica results in a blue to green transition from a complex-silica interaction.

Doping of silica gels with bis(diammine)copper(II) complexes at neutral conditions results in outer sphere co-ordination of silica oligomers by hydrogen bonding to the amine ligands and restriction of their motion resulting in different optical properties to solutions of the complex. Thermal treatment of the doped xerogels to 80°C dehydrates the complexes removing water from the axial positions resulting in co-ordination of chloride with the exception of the N,N'-diethylethylenediamine complex where steric hindrance of the axial positions prevents co-ordination, as for the free compounds. The process can be reversed by rehydration of the silica by exposure to humidity. Thermal treatment for prolonged periods results in irreversible thermochromic transitions not found in the free complexes. These transitions arise from a twisting of the amine ligands out of the x-y plane lowering orbital overlap and resulting in the observed colour change. As the silica is dehydrated the complex migrates into the micropores where it becomes trapped by strong electronic forces. The difference in silica surface characteristics, and hence surface forces, can be used to explain the differences in colour between the different silica types.

These thermochromic transitions show that combination of thermochromic complexes with silica sol-gel matrices results in a materials with unique thermochromic and optical properties not found in the free compounds with a variety of matrix-dopant interactions being responsible for the new transitions.

References

1. J. Yan, A. M. Buckley, M. Greenblatt, *J. Non-cryst. Solids*, **180**(1995), 180

2. R. Reisfeld, *J. Non-cryst. Solids,* **121**(1990), 245

3. A. Makishima, T. Tani, *J. Am. Chem. Soc.,* **69**(1986), C-72

4. A. Emmerling, J. Gross, R. Gerlach, G. Reichenhaur, J. Fricke, H-G. Haubold, *J. Non-cryst. Solids*, **69**(1986), C-72

5. D.R.Bloomquist, R.D.Willet, "Thermochromic phase-transtitions in transition metal salts", Coordination Chemistry Reviews, **47**, 125-164, 1982

6. K. Sone, Y. Fukuda, *Inorganic Thermochromism*, Springer-Verlag, Berlin, 1987

7. C. J. Brinker, G. W. Scherer, *Sol-Gel Science: the physics and chemistry of sol-gel processing*, Academic Press, 1990

CHAPTER 5 CONDENSATION IN AQUEOUS 0.1M ZINC(II) ACETATE SOLUTIONS

5.1 INTRODUCTION

Condensation of divalent cations

Divalent metal ions are often found in an octahedral co-ordination. Condensation of divalent metal ions begins when h=1 (h=hydrolysis ratio, see pg.7), forming dimeric species $[M_2(OH)_2(OH_2)_8]^{2+}$. The μ^2-OH bridges remain negatively charged allowing further condensation changing the μ^2-OH into μ^3-OH bridges by addition of two edge sharing dimers giving a compact and symmetrical tetramer.

Formation of such tetramers was found by kinetic measurements in Ni(II)[4] systems and x-ray crystallographic measurements in Pb(II)[5] systems. The formation of tetramers allows metal-metal interactions as found by magnetic coupling in Ni(II)[4] and Co(II)[6] systems. The Jahn-Teller distortion of Cu(II) results in the formation of linear chains[7]. The solvated Cu(II) ions hydrolyse in the equatorial plane resulting in a corner sharing dimer leading to edge sharing polymeric chains.

Co-ordinated ligands also significantly influence the formation of condensed phases in aqueous solution. Matijevic[8] showed that the counter ion significantly affects particle morphology of α-Fe_2O_3 particles while Livage[9] showed that acetate has the unique ability to form organic/ inorganic polymeric structures.

This chapter investigates condensation in aqueous zinc acetate systems and the ability of acetate to form polymeric zinc hydroxide-acetate compounds.

5.2 EXPERIMENTAL

Hydrous zinc oxide precipitates were synthesised by the addition of 25ml of ammonia or potassium hydroxide solution of varying concentration (0 to 1.44M) to 250ml of 0.1M zinc acetate solution. The initial pH of the solution was measured using a glass electrode (accurate to ±0.05pH). This was stirred for 2 hours and the resulting precipitates filtered under suction, washed with 2 x 100ml aliquots of distilled, deionised water and dried at 40°C overnight.

Precipitates were characterised by transmission electron microscopy (TEM) using a JEOL 2010 electron microscope. Holey carbon grids were prepared for TEM analysis by grinding 6mg of sample in 10ml of acetone and placing a drop of the suspension onto the grid. X-ray diffraction patterns were obtained using a modified Hiltonbrooks diffractometer operating with Cu-Kα radiation (1.54051Å). Thermogravimetric analysis (TGA) were recorded at a heating rate of 2°C/min in air using a Stanton-Redcroft thermobalance. Fourier transform infrared spectra were recorded using a Nicolet Magna-IR spectrometer as KBr disks at a resolution of $2cm^{-1}$ and averaging 64 scans.

5.3 RESULTS

5.3.1 Precipitation

Table 1 shows mass of precipitates obtained from the reaction after 2 hours at different pH levels at or below pH10.6. The mass increases sharply at pH is raised above 8.0. The mass of precipitates obtained above pH9.5 shows only small variations.

pH	Mass ppt. (g)	Standard deviation
8.0	*0.488*	*0.023*
8.5	*3.335*	*0.035*
9.0	*5.002*	*0.034*
9.5	*5.493*	*0.012*
10.0	*5.551*	*0.045*
10.5	*5.670*	*0.020*

TABLE 5.1: *EFFECT OF PH ON MASS OF PRECIPITATE OBTAINED FROM CONDENSATION USING AMMONIA*

5.3.2 X-ray diffraction

The x-ray diffraction patterns were used to identify different crystalline phases present in the materials prepared at various pH conditions (figure 5.1). Differences in XRD patterns were observed only when the synthesis pH was carried out at pH10.7 or higher.

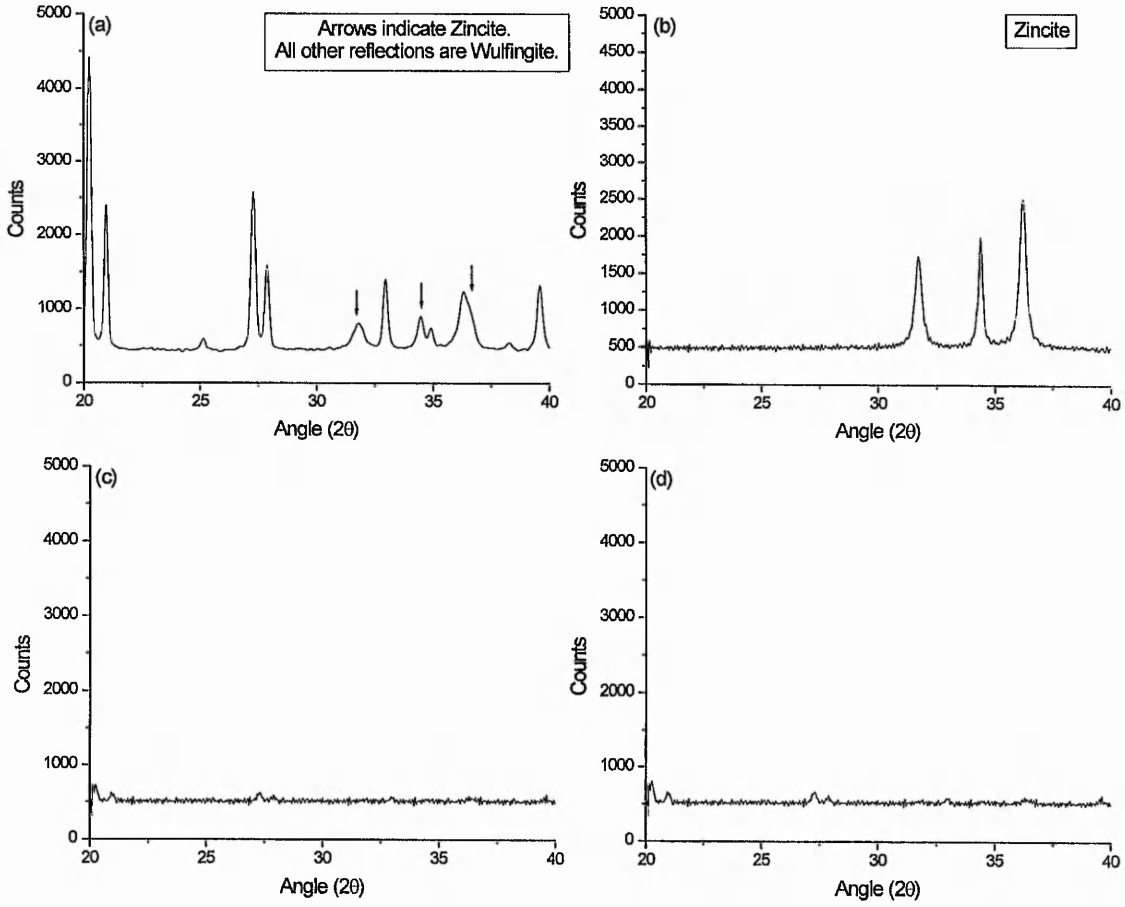

FIGURE 5.1: *POWDER XRD PATTERNS OF PRECIPITATES (a) >pH10.6, NH_3 (b)>pH10.6, KOH (c)<pH10.6, NH_3, (d) <pH10.6, KOH (50WT% α-AL_2O_3, 50WT% SAMPLE)*

Precipitation at pH10.7 or above using ammonia resulted in the formation of Wulfingite {ε-$Zn(OH)_2$} with a small amount of zincite (ZnO). Precipitation at the same pH using potassium hydroxide results in zincite formation only. Precipitates synthesised at pH10.6 or lower using either ammonia or potassium hydroxide were largely amorphous.

5.3.3 Thermal analysis

The relative amounts of different phases present may be deduced from thermogravimetric analysis. X-ray diffraction analysis was performed on samples heated to different temperatures where a mass loss was observed (figure 5.2). The TGA curve of precipitates synthesised above pH10.6 using ammonia showed a 13% mass loss at 145°C. This corresponded to the thermal decomposition of Wulfingite to zinc oxide.

$$\varepsilon\text{-}Zn(OH)_2 \longrightarrow ZnO_{(s)} + H_2O\uparrow \qquad (T=145°C)$$

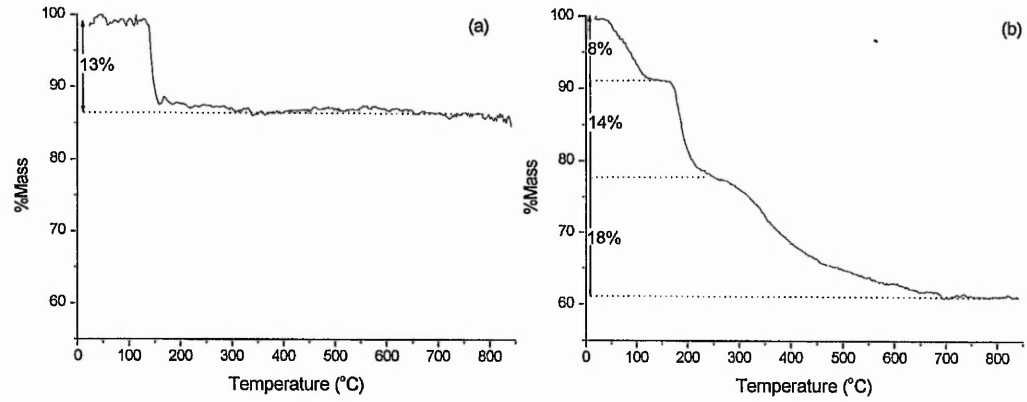

FIGURE 5.2: *TGA CURVES OF (a) >pH10.6, NH_3 AND (b) <pH10.6, KOH OR NH_3*

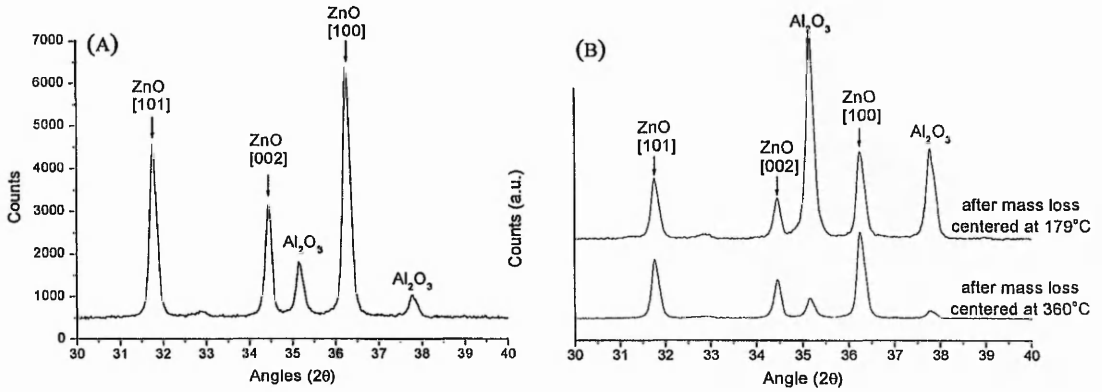

FIGURE 5.3*: XRD PATTERNS AT DIFFERENT STAGES OF THERMAL TREATMENT (A) >PH10.6, NH_3 AFTER HEATING TO 145 ℃ AND (B) <PH10.6, NH_3 OR KOH AFTER HEATING TO 179 ℃ AND 360 ℃*

Precipitates prepared using potassium hydroxide at or above pH10.6 showed no mass loss on heating. Precipitates prepared using either ammonia or potassium hydroxide at pH10.6 or lower show virtually identical TGA curves with mass losses of 8% (centred at 82°C), 14% (centred at 179°C) and 18% (at 300°C to 700°C). The mass loss at 82°C had no effect on the XRD patterns. Given the low temperature of the mass loss this is attributed to dehydration of the sample. Heating to 179°C resulted in zinc oxide formation. Given the temperature and %mass loss of this step it was attributed to the decomposition of amorphous zinc hydroxide to zinc oxide.

$$Zn(OH)_2 \longrightarrow ZnO_{(s)} + H_2O\uparrow \qquad (T=179°C)$$

XRD analysis of samples before and after heating to 360°C showed the formation of zinc oxide while infrared analysis after thermal treatment showed no acetate to be present. This step is therefore attributed to the thermal decomposition of the acetate/ hydroxide polymer.

The Coats-Redfern and Flynn-Wall methods, described by Segal *et al*, were applied to determine the non-isothermal kinetic parameters for the decompositions. These two methods are based upon equations (I) and (II) respectivly.

$$\ln\frac{F(\alpha)}{T^2} = \ln\frac{AR}{\beta E_a}\left(1-\frac{2RT}{E_a}\right) - \frac{E_a}{RT} \qquad \text{(I)}$$

$$\log F(\alpha) = \log\frac{AE_a}{T^2} - \log\beta - 2.315 - 0.457\frac{E_a}{RT} \qquad \text{(II)}$$

where for n≠1,

$$F(\alpha) = \frac{1-(1-\alpha)^{1-n}}{1-n}$$

and for n=1,

$$F(\alpha) = -\ln(1-\alpha)$$

where α = degree of conversion, β = heating rate (2°C min^{-1}), A = pre-exponential factor (s^{-1}), T = temperature (°C), E_a = activation energy for thermal decomposition (J mol^{-1}), R = the universal gas constant and n = reaction order. n is solved by iteration until the best R^2 value for the function fit to the data is found. The calculated results are shown in figure 5.3.

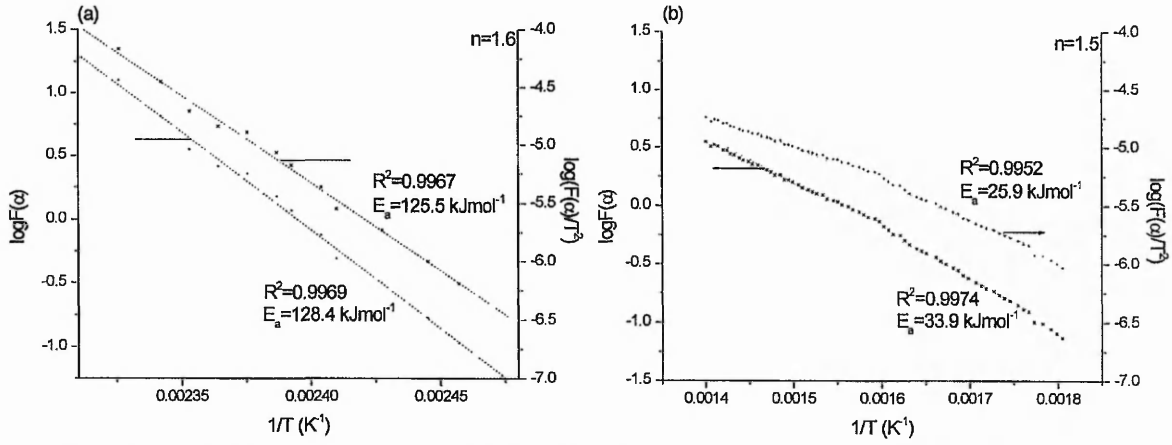

FIGURE 5.3: *EVALUATION OF ACTIVATION ENERGIES FOR THERMAL DECOMPOSITION OF PRECIPITATES. (a) >pH10.6, NH_3 (b) COMPONENT WITH DECOMPOSITION CENTERED AT 360 °C AT pH<10.6, NH_3 OR KOH*

The non-isothermal kinetic parameters for the thermal decomposition by both methods are in close agreement with each other. The activation energy for Wulfingite was determined to be approximately 126 $kJmol^{-1}$ with a reaction order of 1.5. Decomposition of the zinc

hydroxyacetate polymer has an activation energy of approximately 28kJmol^{-1} and a reaction order of 1.6.

5.3.4 Infrared analysis

The effect of increasing synthesis pH on the infrared spectra of the resulting precipitate is shown in figure 5.4. Precipitation at pH10.6 or lower resulted in a material with identical infrared spectra irrespective of base strength with several overlapping hydroxyl bands. The presence of carbonyl bands at ~1500cm^{-1} showed the acetate ligands to be incorporated into the structure at this pH. Previous studies on the infrared spectra and structure of acetates has shown that the spacing between the ν_s(COO) at 1395cm^{-1} and ν_{as}(COO) at 1554cm^{-1} bands is useful in determination of acetate co-ordination mode.

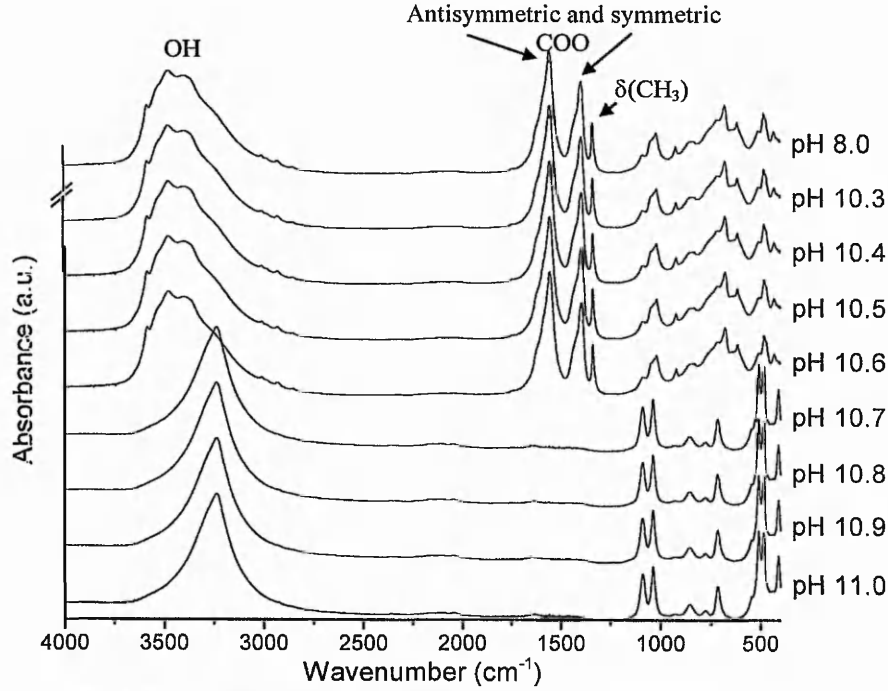

FIGURE 5.4: *EFFECT OF INCREASING SYNTHESIS PH ON INFRARED SPECTRUM OF PRECIPITATE USING AMMONIA*

A difference of ~150cm^{-1} represents bridging co-ordination while 114cm^{-1} represents chelation. Precipitates prepared at pH10.6 or lower have a ν_{as}(COO)-ν_s(COO) of 159cm^{-1} showing the acetate to be co-ordinated in the μ^2 bridging mode. This value is very close to

that of free acetate and so the acetate ligands in the polymer have minimum O-C-O bond strain.

5.3.5 TEM ANALYSIS

Figure 5.5 shows TEM micrographs and associated diffraction patterns of the different precipitates prepared.

Precipitates prepared at or above pH10.7 showed crystalline particle morphologies dependent upon base strength. Synthesis using ammonia resulted in rhombohedral plate-like particles identified as Wulfingite from the electron diffraction measuring approximately 4.7μm. Synthesis using KOH formed elongated hexagonal shaped particles of zincite measuring 0.35μm). Precipitation at or below pH10.6, using either ammonia or KOH, produced an amorphous material with irregular morphology.

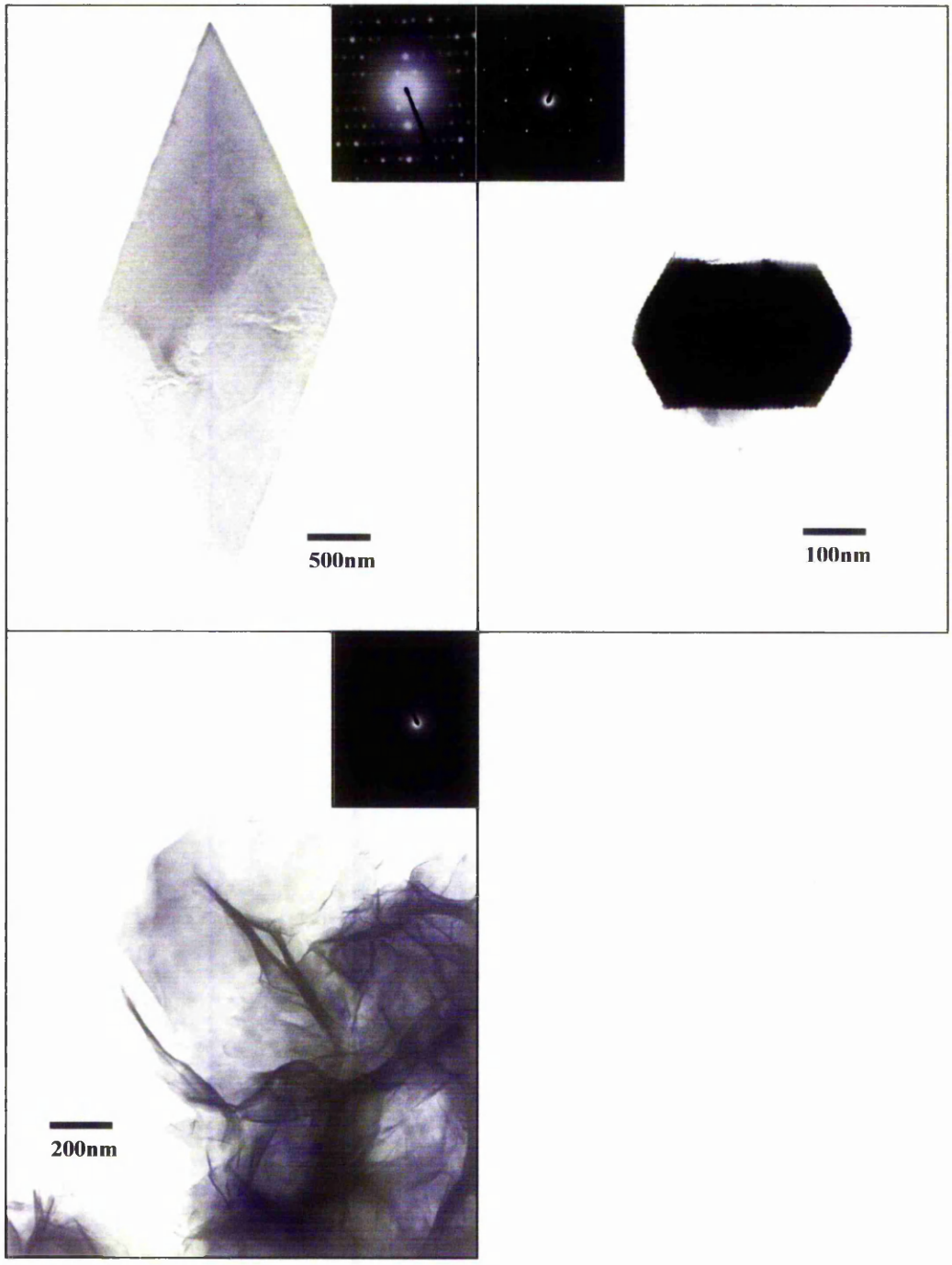

FIGURE 5.5: *TEM MICROGRAPHS AND DIFFRACTION PATTERNS OF PRECIPITATES PREPARED AT (a) >pH10.6 WITH NH_3, (b) >pH10.6 WITH KOH AND (c) FEATURELESS MATERIAL OBTAINED AT <pH10.6 USING EITHER NH_3 OR KOH*

5.4 DISCUSSION

The results show that formation of condensed phases in aqueous 0.1M zinc acetate solution is highly dependent upon pH and alkaline base strength.

A critical pH of ~10.5-10.7 was found where precipitation above or below this pH resulted in significant changes to the material formed.

Precipitates formed at pH10.7 or above are crystalline. Precipitation using ammonia resulted in the formation of ε-$Zn(OH)_2$ (Wulfingite) with rhombohedral plate-like particles. Infrared analysis showed that acetate was completely removed by washing suggesting the acetate was not chemically associated with the zinc ions, thus allowing the formation of highly compact polycations. Condensation would initially result in the formation of $[Zn_2(OH)_4(OH_2)_6]^0$ dimers. Growth to give the polymers would then proceeded by addition of dimers[3] forming compact $[Zn_4(OH)_8(OH_2)_6]^0$ tetramers with μ^3 bridging hydroxyl groups. Further condensation would then proceed bi-dimensionally resulting in the rhombohedral shaped sheet structure observed with stacking of sheets forming a layered structure held together by hydrogen bonding between layers typical of the Brucite-type crystal structure. This process is illustrated in figure 5.6.

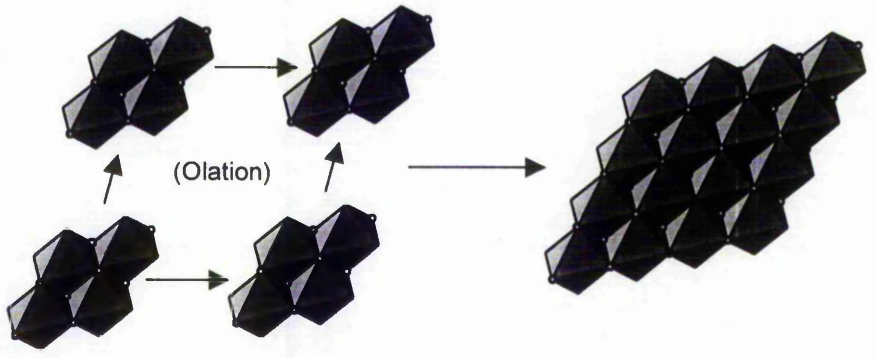

FIGURE 5.6: *CONDENSATION PATHWAY RESULTING IN RHOMBOHEDRAL ε-$Zn(OH)_2$ PARTICLES*

Increasing base strength of the alkali (e.g. KOH or NaOH) resulted in the exclusive formation of zinc oxide (zincite). Condensation of aqueous Zn(II) precursors only proceeds via the olation mechanism resulting in hydroxides. The formation of oxo-bridges is therefore most likely via the deprotonation of relatively acidic μ^3 hydroxyl groups. It is probable that this deprotonation would begin with the formation of the first μ^3 hydroxyl in the compact tetramers while continued olation would result in the production of more μ^3 hydroxyl groups, and subsequently oxo bridges, with the oxo bridges altering the precursor structure and hence forming different particle morphologies to those found for the hydroxide.

Precipitation at or below pH10.6 resulted in an amorphous material with no regular morphology. Infrared analysis showed the material to be a hybrid organic/ inorganic polymer based upon bridging acetate/ hydroxyl ligands. This material with bridging acetate ligands will hereafter be referred to as zinc hydroxyacetate. The difference between the symmetric and antisymmetric COO absorption band positions was close to that of free acetate showing the acetate ligands in the material to have bond angles close to that of free acetate with minimum O-C-O bond strain. The material structure is also independent of pH with no variation in the infrared spectrum at different pH levels.

A theoretical speciation diagram can be derived using equilibrium constants for monomeric $[Zn(OH)_n]^{2-n}$ species using literature values.

Hydrolysis of a heterogeneous solution of Zn^{2+} results in formation of various hydroxide species whose type and relative abundance depend upon pH and, if polymeric species exist,

concentration. Hydrolysis of Zn^{2+} proceeds according to the reaction scheme (H_2O ligands excluded for clarity and six co-ordination assumed)

$$Zn^{2+} \longleftrightarrow Zn(OH)^{+} \longleftrightarrow Zn(OH)_2 \longleftrightarrow Zn(OH)_3^{-} \longleftrightarrow Zn(OH)_4^{2-}$$

Using the stability constants for hydrolysis of aqueous Zn^{2+} by water to each of the species (equations iii to vi) a mathematical relationship between pH and the relative proportions of each species may be calculated.

$$Zn^{2+} + H_2O \longrightarrow Zn(OH)^{+} + H^{+} \qquad \text{(iii)}$$

$$Zn^{2+} + 2H_2O \longrightarrow Zn(OH)_2 + 2H^{+} \qquad \text{(iv)}$$

$$Zn^{2+} + 3H_2O \longrightarrow Zn(OH)_3^{-} \qquad \text{(v)}$$

$$Zn^{2+} + 4H_2O \longrightarrow Zn(OH)_4^{2-} \qquad \text{(vi)}$$

In a homogenous system the concentration condition (equation vii) must be fulfilled.

$$Zn_T = \left[Zn^{2+}\right] + \left[Zn(OH)^{+}\right] + \left[Zn(OH)_2\right] + \left[Zn(OH)_3^{-}\right] + \left[Zn(OH)_4^{2-}\right] \qquad \text{(vii)}$$

Where Zn_T is the total amount of zinc atoms in solution. Substituting equations iii to vi into equation v gives equation viii;

$$Zn_T = Zn^{2+}\left(1 + \frac{{}^{*}K_1}{\left[H^{+}\right]} + \frac{{}^{*}\beta_1}{\left[H^{+}\right]^2} + \frac{{}^{*}\beta_2}{\left[H^{+}\right]^3} + \frac{{}^{*}\beta_3}{\left[H^{+}\right]^4}\right) \qquad \text{(viii)}$$

where ${}^{*}K_1$, ${}^{*}\beta_1$, ${}^{*}\beta_2$ and ${}^{*}\beta_3$ are stability constants for the different hydrolysis ratios of individual species.

Successive distribution coefficients that describe the fraction of each species in solution can now be defined as equations ix to xiii.

$$\alpha_0 = \left[Zn^{2+}\right] / Zn_T \qquad \text{(ix)} \qquad \alpha_1 = \left[Zn(OH)^{+}\right] / Zn_T \qquad \text{(x)}$$

$$\alpha_2 = \left[Zn(OH)_2\right] / Zn_T \qquad \text{(xi)} \qquad \alpha_3 = \left[Zn(OH)_3^{-}\right] / Zn_T \qquad \text{(xii)}$$

$$\alpha_4 = \left[Zn(OH)_4^{2-}\right] / Zn_T \qquad \text{(xiii)}$$

Equations ix and viii then help to define the fraction of unhydrolysed zinc ions in solution (equation xiv).

$$\alpha_0 = \left(1 + \frac{^*K_1}{[H^+]} + \frac{^*\beta_1}{[H^+]^2} + \frac{^*\beta_2}{[H^+]^3} + \frac{^*\beta_3}{[H^+]^4}\right)^{-1} \quad \text{(xiv)}$$

Subsequently, fractions of the other species in solution may be given by combining equations iii to vi and x to xiii in terms of the fraction of unhydrolysed Zn^{2+}, α_0, with equation xiv. These are shown in equations xv to xviii.

$$\alpha_1 = \frac{\alpha_0 {}^*K_1}{[H^+]} \quad \text{(xv)} \qquad \alpha_2 = \frac{\alpha_0 {}^*\beta_1}{[H^+]} \quad \text{(xvi)} \qquad \alpha_3 = \frac{\alpha_0 {}^*\beta_2}{[H^+]^2} \quad \text{(xvii)} \qquad \alpha_4 = \frac{\alpha_0 {}^*\beta_3}{[H^+]^4} \quad \text{(xviii)}$$

where α_n are fractions of hydrolysed species of hydrolysis ratio n.

Equations XII to XVI can then be plotted as a function of pH. This is shown in figure 5.7.

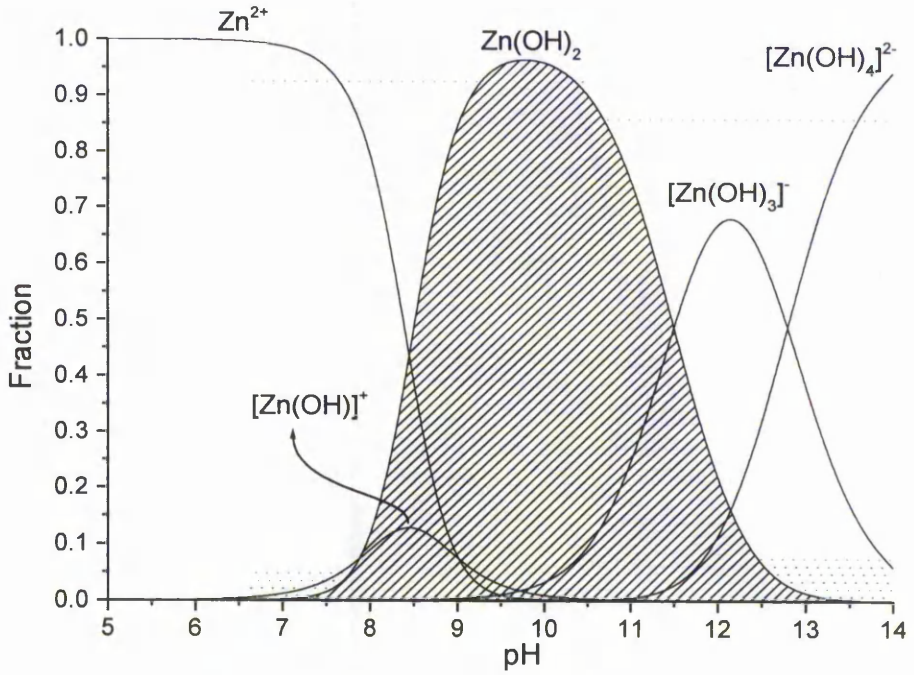

FIGURE 5.7: *SPECIATION OF AQUEOUS Zn^{2+} FROM EQUATIONS XII TO XVI*

The mass of zinc hydroxyacetate precipitated after 2 hours reaction appears to follow the calculated fraction of $Zn(OH)_2$ (figure 5.8) within experimental error and errors of stability constants.

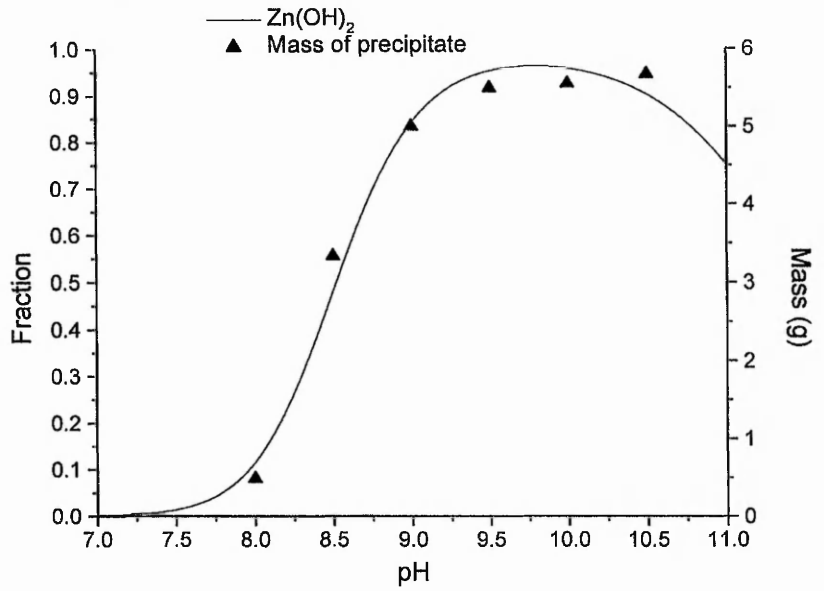

FIGURE 5.8: *PLOT OF MASS OF PRECIPITATES AT PH<10.6 AGAINST THE SPECIATION CURVE FOR ZN(OH)₂*

The formation of the solid phase must result only from condensation of h=2 precursors. Condensation of other precursors (h=1, h=3) may take place but a solid phase does not result from these reactions.

A qualitative description of the co-ordination of acetate to Zn(II) in aqueous solution is possible by application of the partial charge model. Here we calculate the critical pH above which the ionic dissociation of acetate from Zn(II) takes place. This is described by equations XVII and XVIII.

$$pH_q^* = \left\{ \left[\frac{\chi_q(\Delta + 5.732\alpha + 2.064) - 4.061(3.507\alpha + 2.064q)}{\Delta + (1.408\alpha + 0.507q) - (3.507\alpha + 2.064q)} \right] \Big/ 2.732 \right\} - 0.035 \qquad \text{(xix)}$$

$$\Delta = z - 2.225N - \left(4.071 - \chi_m^0\right) \Big/ \left(1.36\sqrt{\chi_m^0}\right) \qquad \text{(xx)}$$

where z is the valency of the metal ion, N is the co-ordination number of the metal ion, $\chi_m{}^0$ is the Allred-Rochow electronegativity of the metal ion, χ_q is the mean electronegativity of the ligand at protonation of q, α is the co-ordination mode of the ligand and $pH_q{}^*$ is the critical pH

for the dissociation of the ligand from the metal ion. The ligand may dissociate by hydrolysis or ionic dissociation. This is accounted for by substituting $q=1$ or $q=0$ respectively.

For zinc (II) acetate N is assumed to be 6 as is common for divalent metal ions. χ_{Zn2+} is 1.66, χ_{OAc-} is 2.28, q=0, acetate ligands are bridging as shown by the infrared spectra (α=2). From this it is calculated that pH_0^* is 10.6. This provides a quantitative theoretical account of the observed loss of acetate from the material when synthesised at pH10.7 or higher.

Thermal analysis of the zinc hydroxyacetate shows that some amorphous zinc hydroxide is formed during condensation although EDX analysis using TEM did not detect any discrete regions in the material that were free of carbon. This suggests that formation of distinctly separate phases of hydroxide and hydroxyacetate does not occur but instead small regions of amorphous hydroxide are present in the polymeric hydroxyacetate structure.

5.5 Conclusions

It has been shown that condensation in aqueous zinc acetate solutions producing solid phases results only from h=2 precursors. pH of the condensation controls the speciation distribution of the precursors, and hence the fraction of the h=2 precursor, and also the co-ordination of the acetate ligand. A theoretical explanation of the pH dependent behaviour of the acetate accounts for the observed ionic dissociation of acetate from Zn^{2+} result in crystalline hydroxide or oxide phases. The zinc hydroxyacetate structure formed from condensation of precursors with co-ordinated acetate ligands is a hybrid organic/ inorganic polymer with μ^2 bridging acetate ligands and O-C-O bond angles with minimum bond strain. Condensation above pH10.6 is dependant upon base strength. Weak bases result in the formation of

Wulfingite (ε-$Zn(OH)_2$) while strong bases are able to deprotonate the acidic μ^3 hydroxyl groups resulting in oxo bridges and zinc oxide formation.

References

1. M. Ardon, A. Bino, Structure and Bonding **65**, 1, (1987)

2. R. H. Tytko, O. Glemser, *Adv. Inorg. Chem. Radiochem.*, **19**, 239, (1976)

3. M. Henry, J. P. Jolivet, J. Livage, *Structure and Bonding 77*, 153, (1992)

4. G. B. Kolski, N. W. Kildahl, D. W. Margerum, *Inorg. Chem,* **8**, 1211, (1969)

5. G. Johansson, A. Olin, *Acta. Chem. Scand.*, **A38**, 3197, (1968)

6. C. F. Baes, R. E. Mesmer, *Hydrolysis of cations*, (1976), J. Wiley & Sons, New York

7. D. D. Perrin, *J. Chem. Soc.*, 3189, (1960)

8. E. Matijevic, R. S. Sapieszko, J. B. Melville, *J. Colloid Interface Sci.*, **50**, 567, (1975)

9. J. Livage, C. Bonhomme, M. Henry, *J. Sol-Gel Sci. Tech.*, **6**, 155, (1996)

CHAPTER 6 PREPARATION AND CHARACTERISATION OF ZINC HYDROXYACETATE GELS

The aim of this chapter was to produce a sol suitable for producing thin film coatings of zinc oxide from aqueous zinc acetate solutions and investigate the chemistry of the process at various stages of preparation. The effect of small amounts of sulphate ions on the chemistry of the process was also investigated. The factors to be investigated are shown in table 6.1.

Factor	**Variables**
Zn/NH_3 ratio	1.271 to 0.477
Ageing of gel	Time of ageing (0-1 hour)
Dispersal of gel	Time of dispersal (0-1 hour)
Separation method	Filtration, centrifugation
Freezing of samples in liquid N_2 for analysis	Volume frozen (1-5ml), freeze drying vs. thermal drying, freezing time (1min-1hour)
Ultrasonication of dispersion	Ultrasonication time
Warming of final dispersion	25-100°C, 0-3 hours
Addition of sulphate	Effect of addition at different stages of preparation, 1ml of 0-0.5M concentration

TABLE 6.1: *FACTORS TO BE INVESTIGATED IN PREPARATION OF SOLS*

Analysis of samples was made by FTIR (transmission and DRIFTS), powder XRD and TEM to examine acetate/ hydroxyl polymer structure, crystallinity and morphology respectively.

6.1 Definition of terms

A *gel* will hereafter be used to refer to the product formed immediately upon addition of ammonia to a saturated solution of zinc acetate or after filtration/ centrifugation following dispersion into larger volumes of water. *Sol* will be referred to as the *gel* dispersed into larger volumes of water.

6.2 EXPERIMENTAL

Zinc hydroxyacetate gels were prepared by addition of 35% ammonia to aqueous, saturated zinc acetate (1.38M) (see appendix I for determination of concentration) doped with different

amounts of sulphate ions followed by a washing and re-dispersal process to remove contaminating ions and produce a sol suitable for coating substrates with thin films.

1ml of potassium or sodium sulphate (0-0.5M) was added to 25ml of saturated zinc acetate with continuous stirring. 3ml of ammonia solution of varying concentration was added and the mixture stirred vigorously to ensure homogenous mixing. Mixtures of Zn/NH_3 ratio greater than 0.477 were very viscous and could not be stirred homogeneously. The effect of ageing the mixture was examined by pipetting 1ml of the mixture into a 1.5ml volume Eppendorf sample tube with a 2mm hole punctured in the lid using tweezers and freezing the sample in liquid nitrogen. This was repeated every minute for the first 10 minutes of stirring and then every 10 minutes for 1 hour. The mixture was then stirred for 1 week before a final sample was taken. Samples were freeze dried at -52°C and 0.5mBar for 12 hours. Repeat experiments studied the effect of immersion of samples in liquid nitrogen for different periods of time.

The gel was dispersed into 500ml of water with stirring for 30 minutes. The dispersion was ultrasonicated for 15 minutes. Repeat experiments to study the effect of ultrasonication were made by freezing four 1ml aliquots at 5 minute intervals during ultrasonication for up to 1 hour.

The gel was separated from the liquid by filtration under suction and then washed with three 100ml aliquots of distilled, deionised water (approx. 1 hour) until washings were free of acetate, zinc(II) and ammonium ions (see Appendix I for tests for ions). Repeat experiments used centrifugation at 2500rpm for 15 minutes and pouring off the supernatant solution and

repeating the washing and dispersion process once more. 1ml samples of the gel separated by filtration or centrifugation were freeze dried and compared.

Determination of the presence of tetrahedrally co-ordinated zinc(II) was made by far-infrared spectroscopic analysis. Far-infrared spectra were prepared by grinding 0.0066g of sample with 0.1100g of CsI. 0.0770g of this was evenly spread in a pellet die and pressed to 10 tonnes for 6 minutes. Spectra were recorded from 200 to 600cm^{-1} at a resolution of 2cm^{-1}. This was repeated 5 times for each sample measuring the peak area of the $\nu(ZnO_4)$ absorption bands and analysing the results statistically at the 95% confidence level using Origin32 software.

6.2.1 ZINC HYDROXYACETATE GEL PREPARATION PROCEDURE

The general synthesis method is shown in the flow chart below.

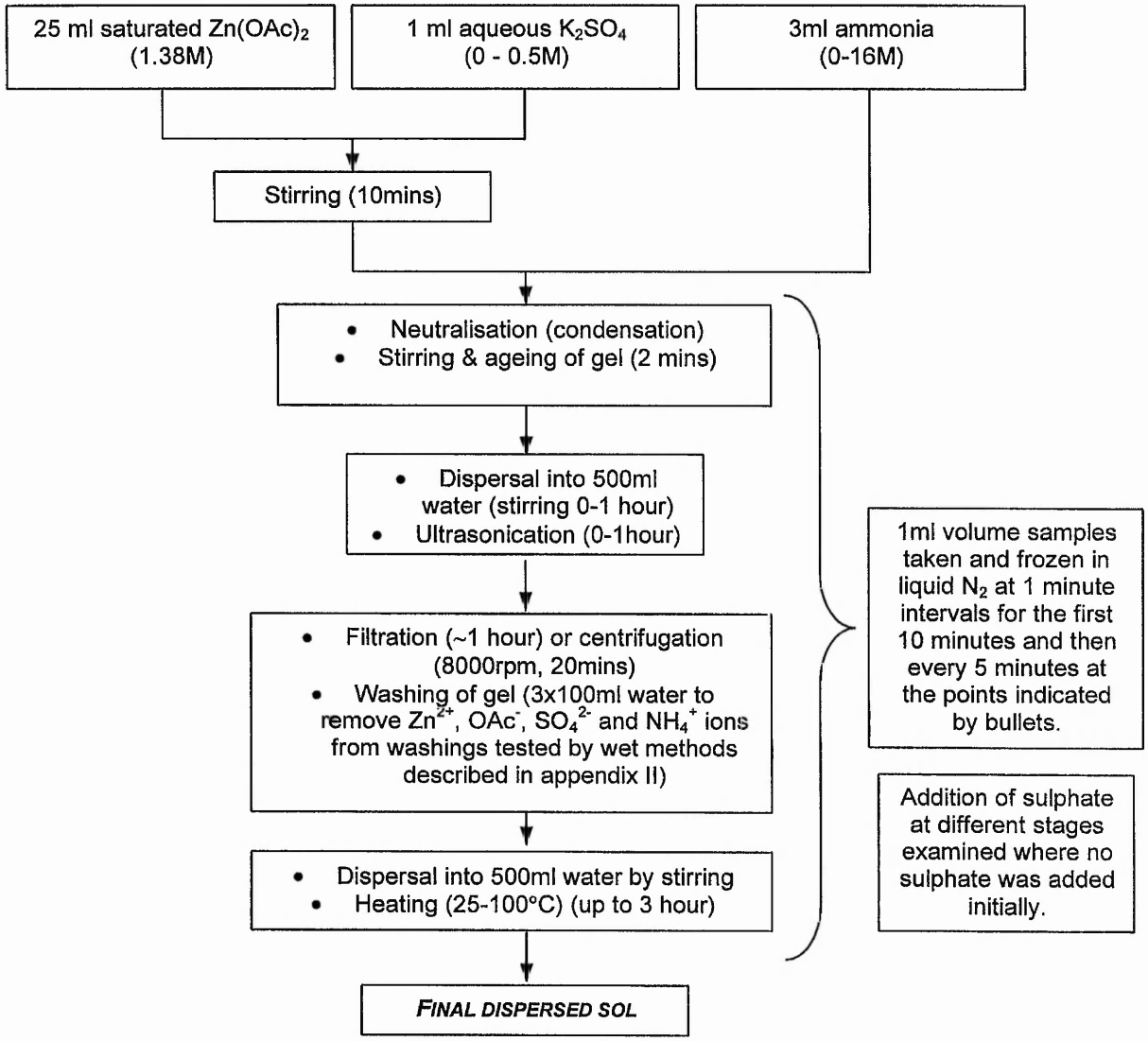

6.3 RESULTS

Table 6.2 shows which stages of processing result in changes to the material detectable by either Mid-IR, Far-IR, powder x-ray diffraction or transmission electron microscopy.

Variable	**Effect**			
	Mid-IR spectrum	*Far-IR spectrum*	*XRD pattern*	*TEM*
Zn/NH_3 ratio	✓	✓	✓	✓
Ageing of gel	✗	✗	✗	✓
Freeze drying vs. Thermal drying	✗	✗	✗	✗
Immersion time in liquid N_2	✗	✗	✗	✗
Ultrasonication	✗	✗	✗	✗
Filtration vs. Centrifugation	✗	✗	✗	✗
Warming of final dispersion	✓	✓	✓	✓

TABLE 6.2: *EVALUATION OF PROCESSING PROCEDURE*
(✓=CHANGE OBSERVED, ✗ =NO CHANGE OBSERVED)

The critical factors influencing the chemistry of the process were found to be variations of the Zn/NH_3 ratio during synthesis, ageing of the gel and warming of the final dispersion resulting in changes to the polymer structure, crystallinity and/or morphology of the solid phases formed.

Other processing factors of drying method (freeze drying versus thermal drying), freezing time of samples, ultrasonication and solid-liquid separation methods had no influence on the material formed. For convenience the experimental procedure adopted was freeze drying of samples as opposed to thermal drying and the gel was filtered rather than centrifuged.

6.3.1 Effect of Zn/NH_3 ratio on synthesis

Figure 6.1 shows the mid-IR transmission spectra of zinc hydroxyacetate gels synthesised with varying Zn/NH_3 ratios immediately (within first 5 seconds) following addition of ammonia to the saturated zinc acetate. The ν(C-C) band of zinc acetate at 953cm^{-1} decreased in intensity with increasing Zn/NH_3 ratio to a ratio of 0.762. This indicates that hydrolysis of zinc acetate is complete at Zn/NH_3 ratios equal to or less than 0.762. The π(COO) in the fingerprint region

of the spectrum (~600-800cm^{-1}) did not show significant variation of absorption intensities with variation of Zn/NH_3 ratio. The appearance of shoulder $\delta(CH_3)$ absorption bands at 1100-1300cm^{-1} was found as the Zn/NH_3 ratio decreased. The symmetric and antisymmetric carboxylate peaks at 1300-1700cm^{-1} showed significant changes to the overlapping peaks as the Zn/NH_3 ratio was varied.

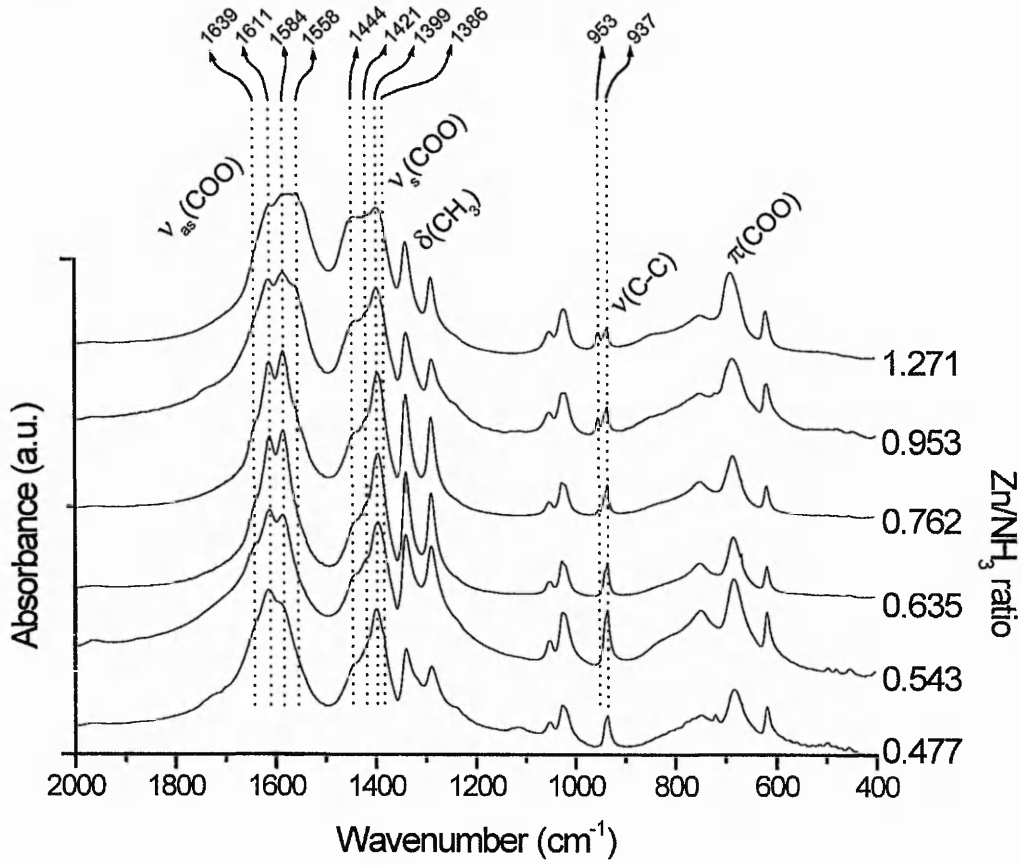

FIGURE 6.1: *EFFECT OF VARIATION OF Zn/NH_3 RATIO ON MID-IR SPECTRA*

The symmetric and antisymmetric regions of the spectra of gels synthesised at Zn/NH_3 ratio less than 0.762 were curve fitted using GRAMS32 software to an R^2 of >0.998 using Gaussian line shapes. Samples of higher Zn/NH_3 ratio than 0.762 could not be curve fitted satisfactorily because of the presence of overlapping carbonyl peaks from unhydrolysed zinc acetate. The results of the curve fitting are shown in figure 6.2.

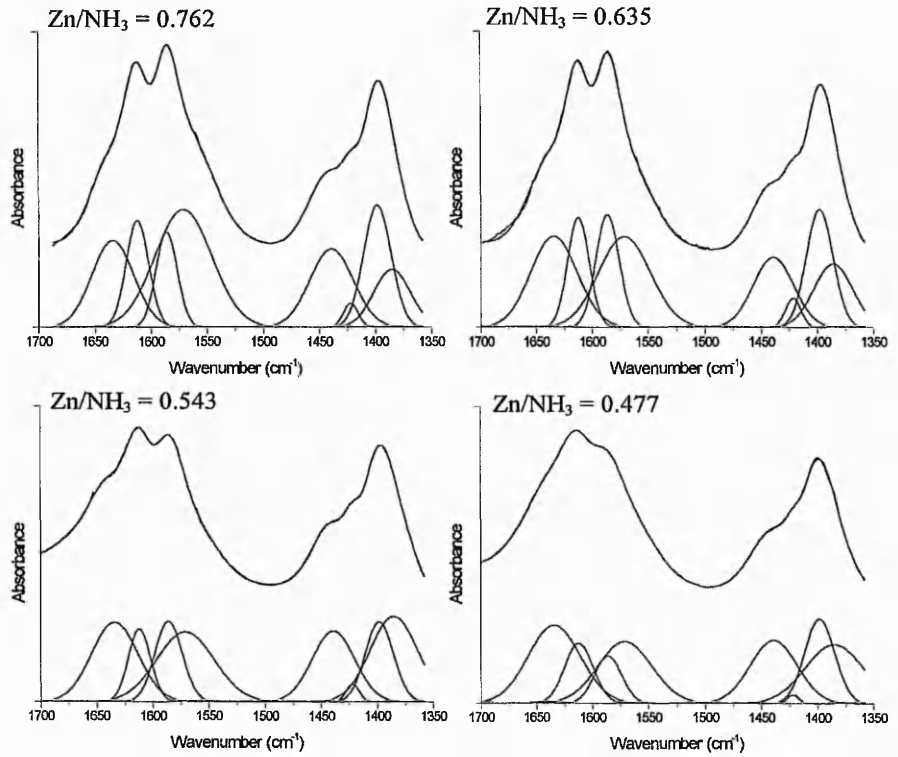

FIGURE 6.2: *CURVE FITTING OF COO REGION OF SPECTRA OF GELS PREPARED AT Zn/NH_3 RATIOS ≤0.762*

The peak fitting shows four pairs of carboxylate peaks (four overlapping symmetric, four overlapping antisymmetric). The positions of the peaks obtained as a result of curve fitting from higher to lower wavenumbers is summarised in table 6.3.

	Peak position (cm^{-1})
ν_{as}(COO)	*1639*
	1611
	1584
	1558
ν_s(COO)	*1444*
	1421
	1399
	1386

TABLE 6.3: *PEAK POSITIONS OF CARBONYL BANDS FROM CURVE FITTING OF SPECTRA*

Figure 6.3 shows the comparison between transmission and DRIFTS measurements for gels synthesised at a Zn/NH_3 ratio of 0.635 performed to obtain information on absorption bands due to surface groups.

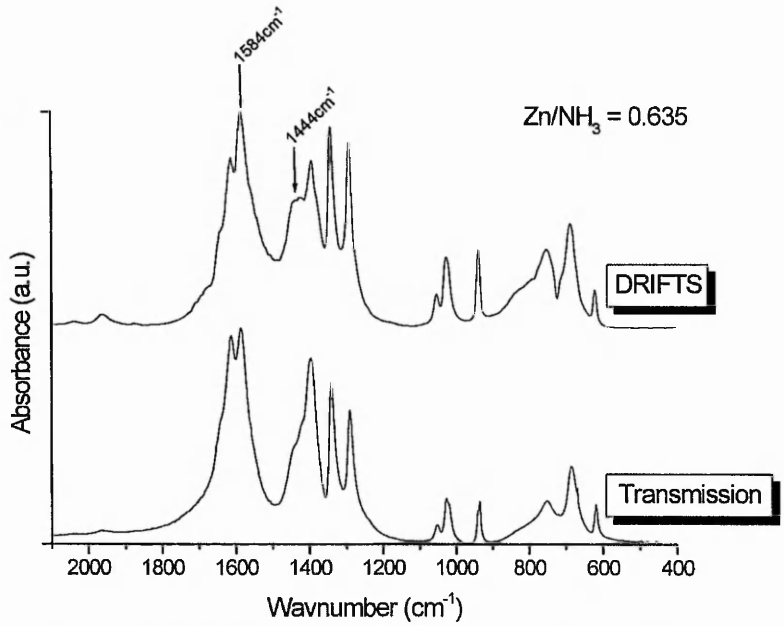

FIGURE 6.3: *COMPARISON OF INFRARED SPECTRA OBTAINED BY TRANSMISSION AND DRIFTS TECHNIQUES*

Antisymmetric and symmetric peaks at 1584cm^{-1} and 1444cm^{-1} show increased intensity in the DRIFTS spectrum compared with the transmission spectrum. These ligands are therefore assigned as surface acetate sites.

The results of far-IR analysis of the samples to detect zinc(II) tetrahedrally co-ordinated by oxygen atoms is shown in figure 6.4. Figure 6.5 shows variation of total $\nu(ZnO)_4$ peak area with Zn/NH_3 ratio. Statistical analysis of the samples shows that all fall within the 95% confidence limits validating reproducibility of the method (see appendix II for results).

Five principal absorption bands are present in the far-IR spectra of the zinc hydroxyacetate gels. The most intense, broad absorption at ca. 290cm^{-1} corresponds to Zn(II) tetrahedrally co-ordinated by acetate ligands. The absorption is broad with several overlapping peaks present suggesting several different types of co-ordinated acetate ligands as found from analysis of the carbonyl region of the spectrum. Four other, weaker absorption bands are found at 398cm^{-1},

457cm^{-1}, 483cm^{-1} and 499cm^{-1} relative to the 300cm^{-1} peak. As the Zn/NH_3 ratio of the synthesis is decreased the intensity of the absorption bands at higher wavenumbers increases.

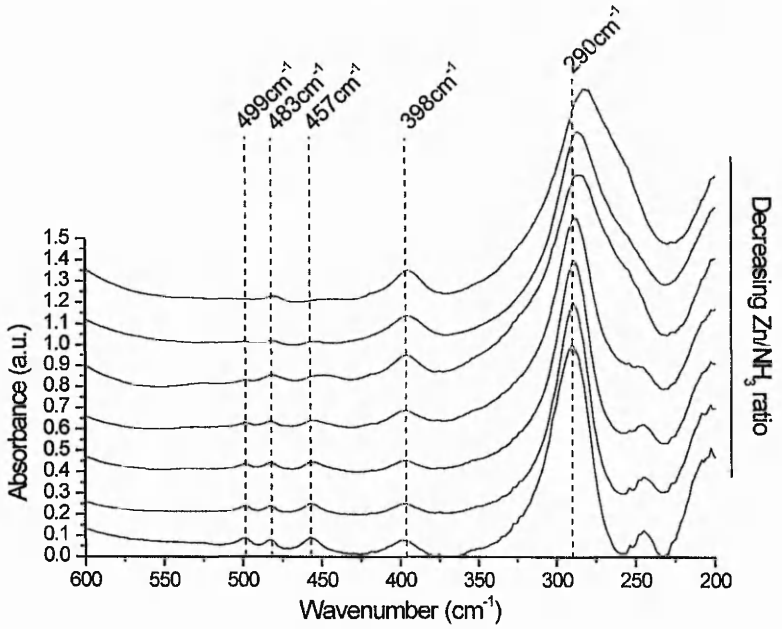

FIGURE 6.4: *EFFECT OF DECREASING ZN/NH$_3$ RATIO ON FAR-IR SPECTRA*

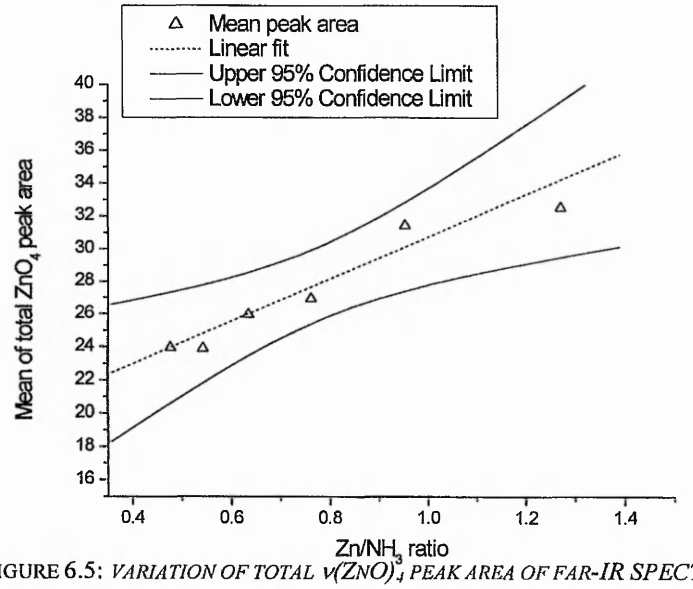

FIGURE 6.5: *VARIATION OF TOTAL ν(ZNO)$_4$ PEAK AREA OF FAR-IR SPECTRA*

6.3.2 Effects of ageing of gel

Figure 6.6 shows TEM micrographs and associated diffraction patterns for zinc hydroxyacetate gel at 0, 5, 30 and 60 minutes ageing following addition of ammonia to the saturated zinc acetate solution.

At t = 0 minutes (figure 6.6a) amorphous, spherical particles and misshapen particles ranging in size from ~20 to 200nm are formed. After 5 minutes (figure 6.6b) the particles become more irregularly shaped and begin to aggregate. As the particles coalesce "necking" occurs as condensation and/or dissolution/ re-precipitation (Otswald ripening) takes place resulting in particles growing together (t = 30 minutes, figure 6.6c). This process continues until a continuous gel structure develops (t = 60 minutes, figure 6.6d) corresponding with a visually observed increase in viscosity.

6.3.3 Effects of dispersion and heating

Figure 6.7 shows the effect of dispersion by rapid stirring and ultrasonication of the washed gel into warm water on the infrared spectra of the material to temperatures above 40°C for 1 hour compared with samples taken prior to dispersal.

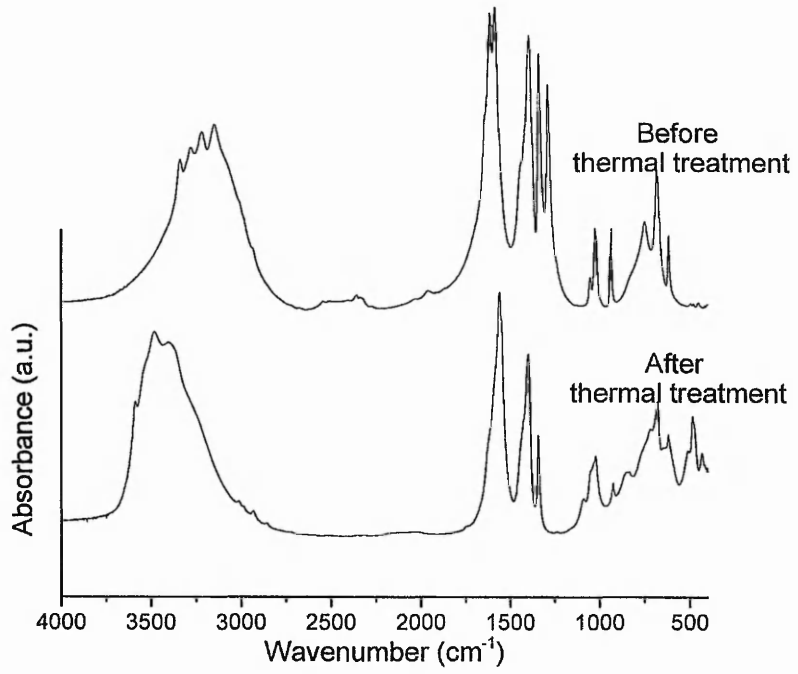

FIGURE 6.7: *EFFECT ON IR SPECTRUM OF WARMING GEL DISPERSION TO TEMPERATURES ABOVE 40 ℃*

Changes in the OH (~3400cm^{-1}) and carboxylate (~1500cm^{-1}) absorption bands following warming of the dispersion indicate significant structural alteration to the hydroxyacetate polymer. The infrared spectrum is indistinguishable from precipitates obtained at lower Zn(II) concentrations with acetate ligands having OCO bond angles equivalent to that of free acetate as assessed by the Δ values measured from the spectra.

6.3.4 The effect of sulphate addition on final dispersion and warming of solution

Addition of sulphate in small amounts (Zn/SO_4^- = 3451 to 69) to the saturated zinc acetate solution prior to addition of ammonia resulted in zinc oxide formation when the solution was warmed to temperatures above 40°C. Addition of sulphate to any other stage in the process in any amount does not result in zinc oxide formation. A plot of zinc oxide content (normalised against 50wt% α-Al_2O_3) against time at various temperatures is shown in figure 6.8.

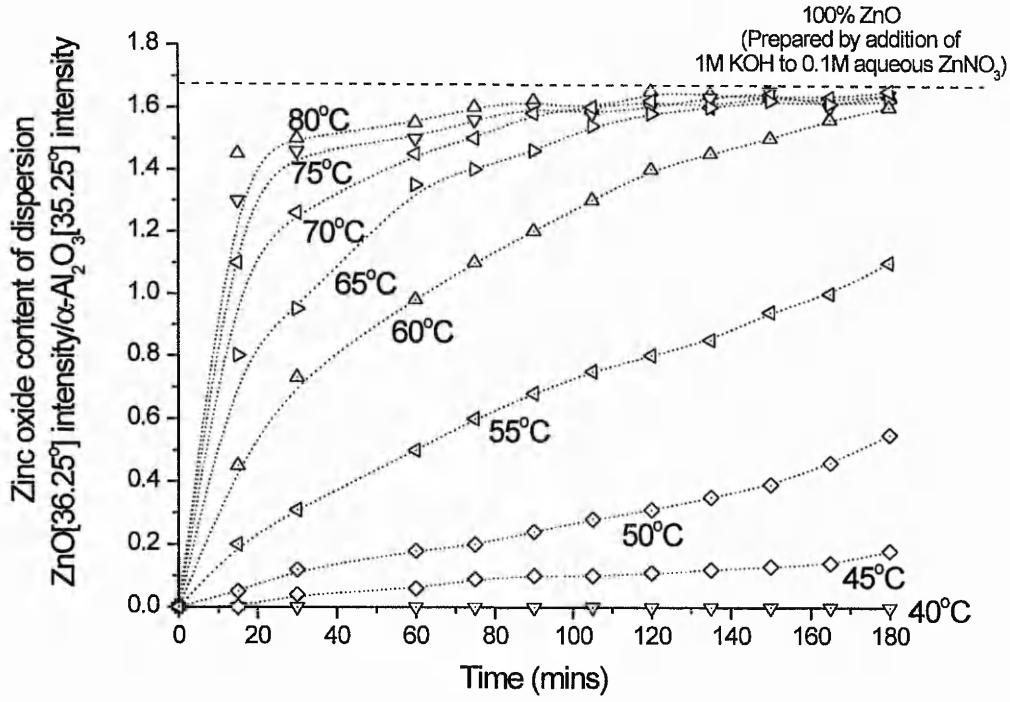

FIGURE 6.8: *THE EFFECT OF VARIATION OF TEMPERATURE AND TIME ON ZINC OXIDE CONTENT OF THE DISPERSION MEASURED FROM ZNO[002] AND α-AL$_2$O$_3$ [002] REFLECTIONS (RESULTS UP TO 80 °C SHOWN FOR CLARITY)*

Zinc oxide formation was found at temperatures above 40°C up to 100°C where the reaction is almost complete after 15 minutes. Figure 6.9 shows a plot of zinc oxide content after 30 minutes versus temperature.

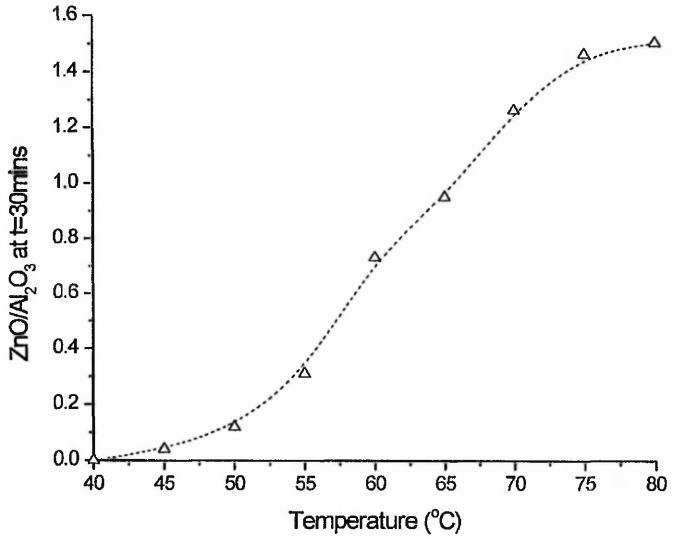

FIGURE 6.9: *VARIATION OF ZINC OXIDE CONTENT AFTER 30 MINUTES AT VARIOUS TEMPERATURES*

As the temperature is raised above 40°C an almost exponential increase in reaction rate is observed. At temperatures above 65°C the increase in reaction rate is diminished reaching a maximum at 80°C.

6.3.5 The effect of variations in amount of sulphate during warming of dispersion

Figure 6.10 shows the effect of variation of sulphate concentration when added prior to addition of ammonia during heating of the final dispersion after 30 minutes. Increasing the amount of sulphate resulted in a sharp increase of zinc oxide content of the dispersion when heated to 70°C up to a concentration of 0.0025M sulphate. Further increases in sulphate concentration did not result in any significant change to zinc oxide content at a specific time.

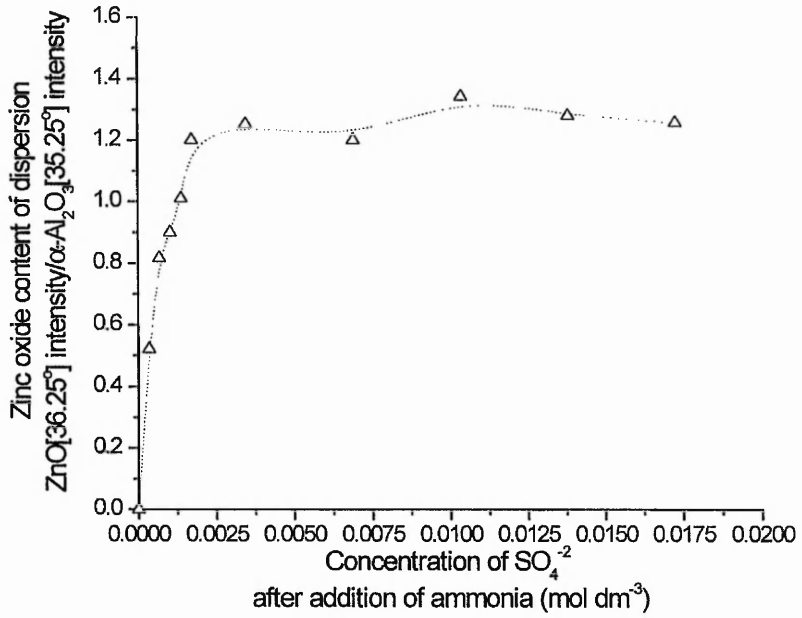

FIGURE 6.10: *EFFECT OF VARIATION OF SULPHATE CONCENTRATION WHEN ADDED BEFORE AMMONIA*

6.3.6 The effect of pH changes during dispersion

Figure 6.11 shows the effect of addition of sulphate ions (Zn/SO_4^{2-} = 69 shown) to the saturated zinc acetate solution prior to initiation of condensation by addition of ammonia on pH variations during warming at 80°C.

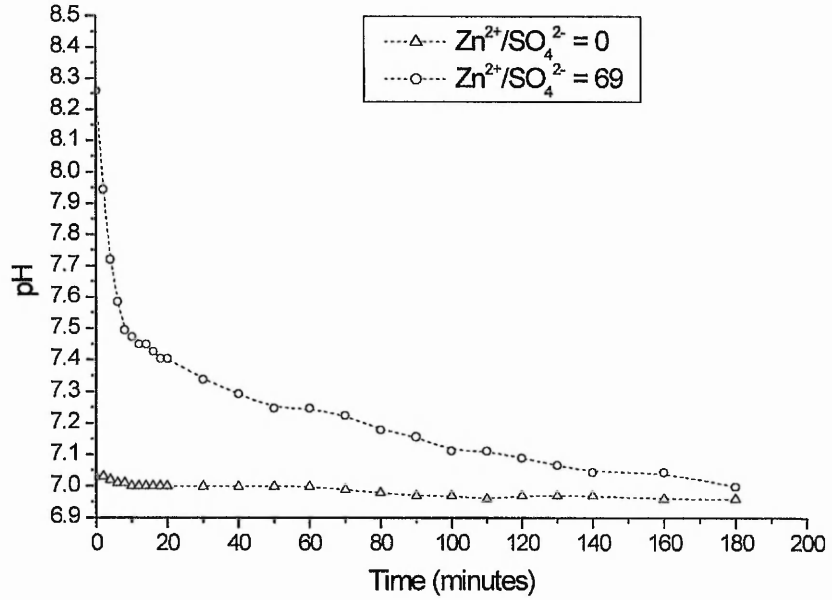

FIGURE 6.11: *EFFECT OF SULPHATE ADDITION TO THE GEL ON pH DURING WARMING OF FINAL DISPERSION*

Dispersions of gels prepared without sulphate show no variation of pH with time. Dispersions of gels prepared with sulphate are initially slightly alkaline but gradually become more acidic over the warming period. While the exact pH curves with added sulphate could not be very accurately reproduced, gels with sulphate *always* show exponential-like pH decreases while gels without sulphate remain neutral.

6.3.7 Ageing of final dispersion

Table 6.4 shows variation in crystalline sizes for zinc oxide formed during the warming of the final dispersion prepared with sulphate. A plot of Debye-Scherrer crystallite size for the [100], [002] and [101] reflections is shown in figure 6.12.

Ageing time (days)	**[100]**	**[002]**	**[101]**
0	*40.43 Å*	*44.42 Å*	*40.12 Å*
1	*39.27 Å*	*40.72 Å*	*37.92 Å*
2	*32.16 Å*	*25.86 Å*	*33.33 Å*
3	*0 Å*	*0 Å*	*0 Å*

TABLE 6.4: *EFFECT OF AGEING OF ZINC OXIDE SOL ON CRYSTALLITE SIZES*

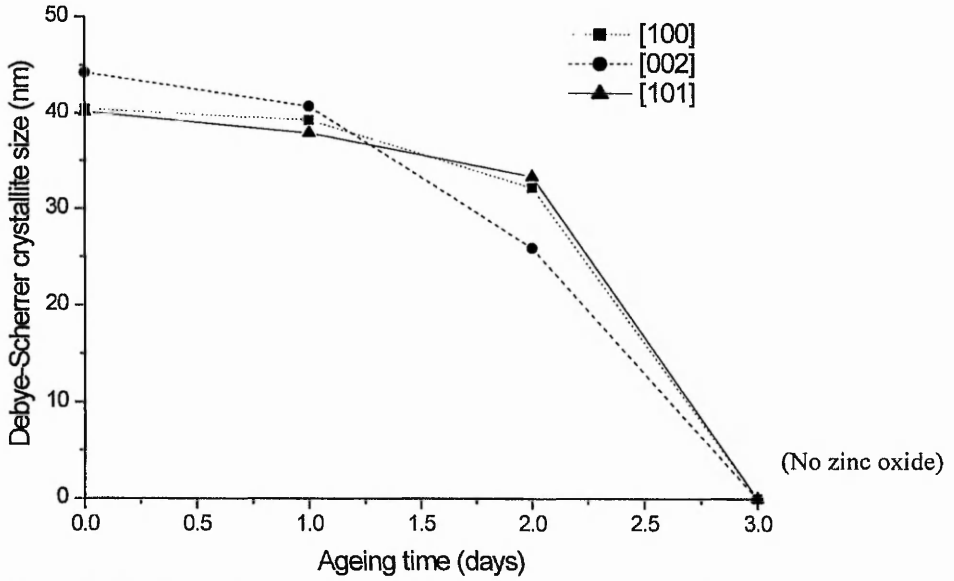

FIGURE 6.12: *PLOT OF CRYSTALLITE SIZE WITH AGEING TIME OF ZINC OXIDE SOL*

The Debye-Scherrer crystallite sizes shows a decrease over an ageing period of 3 days.

Figure 6.13 shows the infrared spectrum of the final dispersed sol with and without sulphate added prior to condensation warmed to 80°C for 15 minutes. The spectrum shows that the washed, dispersed sol prepared without sulphate has an infrared absorption spectrum identical to that found by precipitation at lower zinc acetate concentrations (chapter 5). Dispersed sols prepared with small amounts of sulphate ions under the same conditions show differences in carboxylate, hydroxyl and fingerprint regions of the infrared spectra.

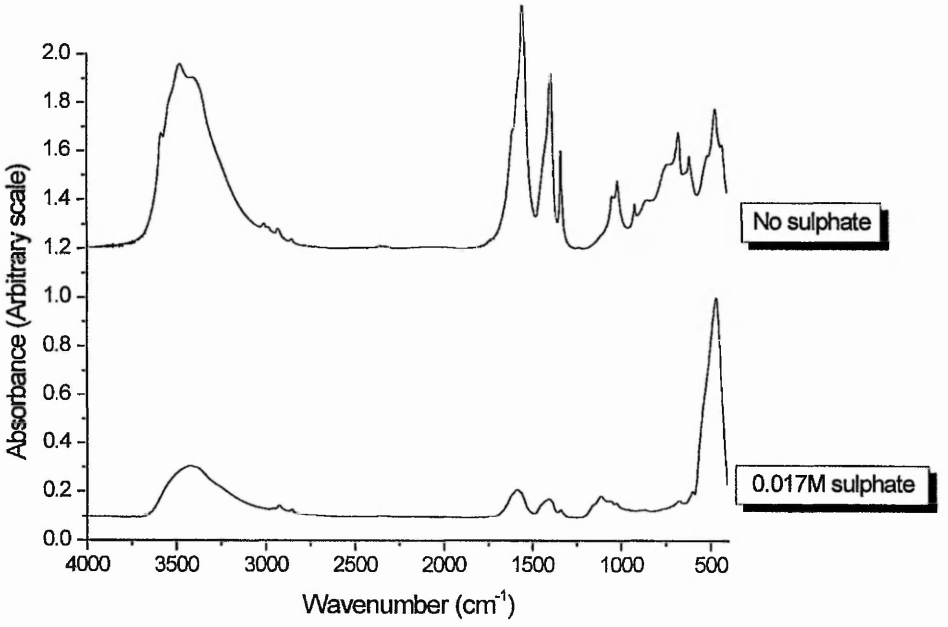

FIGURE 6.13: *COMPARISON OF INFRARED SPECTRUM OF WASHED, DISPERSED SOLS PREPARED WITH AND WITHOUT SULPHATE*

Ageing of the sols results in precipitation after 3-4 days for sols prepared without sulphate. Sols prepared with sulphate were more stable with precipitation observed after 7-8 days. Figure 6.14 shows that ageing of sols results in an increase of carboxylate and hydroxyl bands over a period of 4 days.

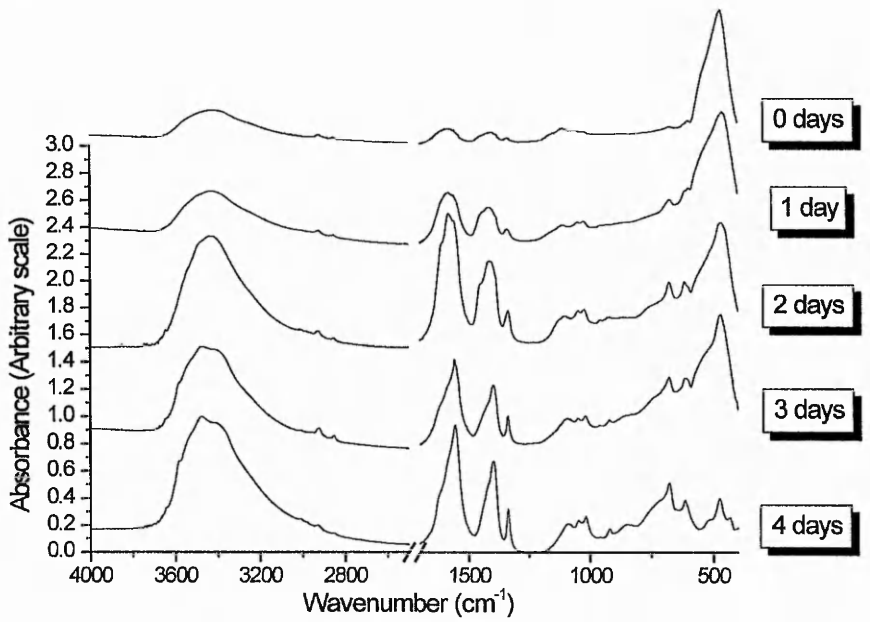

FIGURE 6.14: EFFECT OF AGEING OF SOLS PREPARED WITH SULPHATE ON INFRARED SPECTRUM OF MATERIAL WASHED AND FREEZE DRIED FOR ANALYSIS

The increase in intensity of carboxylate and development of hydroxyl structure is accompanied by a decrease of intensity of the ZnO absorption band at 493cm^{-1}. Sols prepared without sulphate showed no change to the infrared spectra or XRD patterns.

6.4 DISCUSSION

6.4.1 Effect of Zn/NH_3 ratio on material

Neutralisation of an aqueous solution of saturated zinc acetate with ammonia results in rapid nucleation and growth of an inorganic/ organic hybrid polymer based upon bridging acetate and hydroxyl ligands. Analysis of the carbonyl absorption peaks in the infrared spectra by curve fitting reveals four principle acetate ligand sites. Assignment of these peaks to individual acetate ligands is made by the following argument.

Peaks at 1584cm^{-1} and 1444cm^{-1} show an increased absorption intensity in the DRIFTS spectrum compared with the transmission spectrum. Acetate ligands of this type are assigned

as surface sites with Δ=140cm^{-1} and are hereafter referred to as ϕ-sites. Given the low Δ value of these ligands it is possible that the ϕ-sites are chelated or μ^2-bridging with a small O···O distance but this is not clear from the spectra. Decreasing the Zn/NH_3 ratio of the synthesis results in a relative decrease of ϕ-sites.

Comparing the infrared spectra of gels prepared using saturated zinc acetate with the spectra of condensation products at lower concentrations (chapter 5) reveals a second acetate ligand type. The structurally relaxed material prepared at low concentration shows a pair of antisymmetric and symmetric carbonyl peaks at 1558 and 1393cm^{-1} respectively. These peaks are also present in the saturated Zn(II) system albeit in relatively low abundance. This difference in intensity of the 1558 and 1393cm^{-1} peaks between the two concentrations is because of the fast condensation rates involved in the saturated system preventing the slow structural relaxation found at lower Zn(II) concentrations. These acetate ligands have Δ=159cm^{-1} close to that of free acetate showing these ligand types to be most stable with minimum O-C-O bond strain. These ligands are hereafter referred to as γ-sites. Decreasing the Zn/NH_3 ratio of the synthesis procedure results in a relative decrease of γ-sites as found by curve fitting in figure 6.2.

Assignment of the remaining carbonyl peaks to the remaining acetate ligands is made by comparing the relative variation of the intensity of the unassigned symmetric and antisymmetric peaks as the Zn/NH_3 ratio changes. Decreasing the Zn/NH_3 ratio results in a relative increase of intensity of the antisymmetric COO peak at 1639cm^{-1} compared with the 1611cm^{-1} peak. The symmetric COO peak intensity at 1386cm^{-1} increases relative to the peak at 1421cm^{-1} as the Zn/NH_3 ratio decreases. The 1639 and 1386cm^{-1} peaks are therefore

assigned to an acetate ligand site, hereafter termed η-sites (Δ=253cm^{-1}), while the 1611 and 1421cm^{-1} peaks are assigned to the second acetate ligand site hereafter termed ι-sites (Δ=190cm^{-1}).

An estimate of the O-C-O bond angle is possible using the empirical equation developed by Nara *et al*[1] using a molecular orbital approach to calculate the vibrational frequencies for carboxylate compounds. This is a quantitative equation relating the bond angle and difference in C-O bond length to Δ (equation 1).

$$\Delta = 1818.1\delta r + 16.47(\theta_{OCO}-120) + 66.8 \qquad (1)$$

where δr is the difference between the two C-O bond lengths (Å) and θ_{OCO} is the O-C-O bond angle (°). The value of δr for the different acetate sites cannot be measured but is instead taken to vary from a minimum (δr = 0Å) to twice the maximum known C-O bond length difference in zinc acetate systems (δr = 0.02Å) allowing a large estimated error. The defines the range of θ_{OCO} values for the individual acetate sites defined. The calculated and experimental data for the acetate sites is summarised in table 4.

Site	ν_{as}(COO) (cm^{-1})	ν_s(COO) (cm^{-1})	Δ (cm^{-1})	Min. θ_{OCO}	Max. θ_{OCO}
ϕ	1584	1444	140	122.2	124.0
γ	1558	1399	159	123.4	125.6
η	1639	1386	253	129.1	131.3
ι	1611	1421	190	125.3	127.5

TABLE 6.5: *SUMMARISED DATA FOR PRINCIPLE ACETATE SITES FOUND IN ZINC HYDROXYACETATE GEL*

Variation of the Zn/NH_3 ratio of the synthesis results in variation of the *ratio* of the ϕ, γ, η and ι-sites but not in the *type* of ligands that form the acetate/hydroxyl polymer network. Decreasing the Zn/NH_3 ratio favours the formation of acetate ligands with higher O-C-O bond strain (η and ι-sites).

6.4.2 Far-IR analysis

Five $\nu(ZnO_4)$ absorption bands are present in the spectra. The most intense absorption at ca. 290cm^{-1} corresponds to Zn(II) tetrahedrally co-ordinated by acetate ligands. Five possible tetrahedral Zn(II) co-ordination sites in the hydroxyacetate structure are possible by varying the hydroxyl/acetate ratios of ligands (figure 6.15).

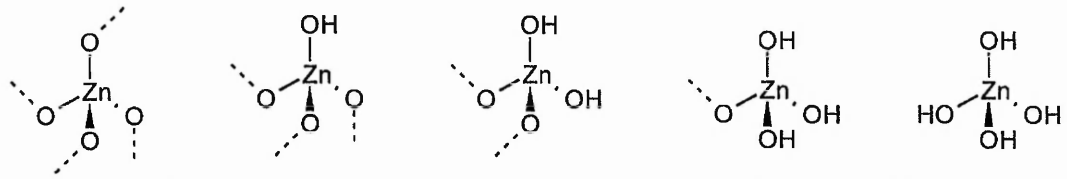

FIGURE 6.15: *FIVE POSSIBLE TETRAHEDRAL ZN(II) SITES WITH VARYING ACETATE/HYDROXYL LIGAND RATIOS (ACETATE LIGANDS REPRESENTED BY DOTTED LINES)*

As the Zn/NH_3 ratio decreases the hydroxyl content of the gel increases favouring formation of sites with higher hydroxyl/acetate ratios. Tetrahedral complexes of zinc(II) hydroxide are not stable and prefer either square planar geometry (as in aqueous $[Zn(OH)_4]^{2-}$ at high pH) or octahedral geometry (as in solid phases of $Zn(OH)_2$).

As the Zn/NH_3 ratio of the synthesis is decreased the relative intensity of the absorption bands at higher wavenumbers increases although these still remain relatively small with an overall relative decrease in the number of tetrahedral Zn(II) sites. This data fits with the hypothesis that increasing the hydroxyl level of the synthesis results in Zn(II) sites in the structure with higher OH/Ac ligand ratios. These are unstable so forming a greater number of octahedral and/or square planar sites. However some tetrahedral sites with hydroxyl ligands do remain in the zinc hydroxyacetate polymer with higher OH/Ac ratios and are probably stabilised by their incorporation in the polymer matrix.

6.4.3 Ageing

Ageing of the zinc hydroxyacetate gel does not result in any polymer structure changes shown by infrared spectra and x-ray diffraction analysis. The rapid condensation rate results in the organic/inorganic polymer structure being established immediately following addition of ammonia and is dependent only upon the Zn/NH_3 ratio of the synthesis. Establishment of the initial, spherical polydisperse sized particles is rapid although the liquid remains saturated with hydrolysed precursors. Condensation continues resulting in particles becoming misshapen and assists "ripening" of coagulated particles. Washing of the gel to remove contaminating ions and unreacted precursor must therefore be *rapid* immediately following addition of ammonia to the zinc acetate solution to produce a more stable suspension and minimise aggregation of particles.

6.4.4 The effect of sulphate on products

Addition of sulphate in any amount had no effect on the infrared spectra, XRD pattern or TEM analysis of the gel on the material formed immediately following addition of ammonia to the saturated zinc acetate solution. The normally intense absorption bands of sulphate could not be detected in the infrared spectra presumably because of the small amounts involved. Addition of sulphate ions at any other stage of the process had no effect on the material produced.

However, addition of sulphate at the initial stage of precursor mixing before addition of ammonia altered the chemical nature of the Zn(II) containing material produced if heated to temperatures above 40°C during the final stages of dispersal.

6.4.5 The effect of final dispersion and warming

The results show that warming of the dispersed zinc hydroxyacetate gel to temperatures greater than 40°C significantly alters the hydroxyacetate polymer structure of the final material. The infrared spectra show that the relative abundance of the η and ι-acetate sites is decreased while the more stable γ-sites significantly increases resulting in an infrared absorbance spectrum identical to that of synthesis of similar materials at lower Zn(II) concentrations (chapter 5). Warming of the solution therefore promotes structural relaxation of the polymeric network. Warming of the material formed immediately following addition of ammonia to the saturated zinc acetate solution did not result in any change to the infrared spectrum showing that dispersal of the gel into water is required to bring about this change. The mechanism of relaxation must therefore proceed via a dissolution/re-precipitation mechanism to form the stable phase of the zinc hydroxyacetate polymer.

Addition of small amounts of sulphate ions before addition of ammonia to the saturated zinc acetate solution results in zinc oxide formation, rather than zinc hydroxyacetate, when the solution is warmed to temperatures above 40°C. Addition of sulphate ions, in any amount, at any other stage of the processing up to the final dispersion stage does not result in oxide formation at any temperature. Zinc oxide formation at the final dispersion stage requires incorporation in the zinc hydroxyacetate polymer structure while addition at any other stage after the initial formation of the solid phase has no effect.

The small amounts of sulphate that may be used to bring about almost complete (~96%) zinc oxide formation (ca. 1 SO_4^{2-} : 3400Zn^{2+}) shows the role of sulphate to be catalytic. A process

resulting in regeneration of some intermediate species resulting in the formation of zinc oxide must therefore be included in any proposed mechanism.

Gels synthesised without sulphate added prior to gelation remain at neutral pH during the second dispersal. Addition of sulphate prior to condensation results in a slightly alkaline dispersion that becomes neutral over time. The consequence of sulphate ions incorporated in the early stages of condensation is an increase of H^+ when the solution is warmed.

Oxide formation in aqueous solution proceeds via the oxolation mechanism with a 1,3-proton transfer between adjacent hydroxyl groups resulting in the formation of "oxo" bridges and elimination of a water molecule. Condensation in aqueous Zn(II) solution only results in hydroxide formation via the olation mechanism as found experimentally and explained theoretically by the partial charge model. Addition of sulphate ions to the system must therefore provide a different chemical mechanism to olation and oxolation to form zinc oxide. If loss of the proton from the hydroxyl forming the oxo-bridge were simply transferred to solution the amount of ZnO produced by the reaction would be expected to be proportional to the sulphate concentration and this is not what the data shows.

The partial charge model may be used to describe the pH conditions where sulphate can co-ordinate to Zn(II), as described in chapter 5. Considering a maximum co-ordination mode for the sulphate of $\alpha=3$ (i.e. a sulphate ion bridging 3 Zn(II) ions) gives a lower limit for the ionic dissociation of sulphate to zinc of pH>9.6. This predicts co-ordination of sulphate over the pH ranges measured during the final dispersion and warming step.

6.4.6 Influence of sulphate co-ordination on charge distribution of OH bond

The partial charge model may be used to calculate the electron density distribution in a molecule. Equation (2) shows how the mean electronegativity is calculated from the constituent atoms.

$$\chi = \frac{\sum_i \sqrt{\chi_i^0} - 1.36z}{\sum_i 1/\sqrt{\chi_i^0}} \qquad (2)$$

χ is the mean electronegativity of the molecule, χ_i^0 is the Allred-Rochow electronegativity of the *i*th atom and z is the overall charge on the molecule. The partial charges on individual atoms are then calculated by equation (3).

$$\delta_i = \left(\chi - \chi_i^0\right) / \left(1.36\sqrt{\chi_i^0}\right) \qquad (3)$$

where δ_i is the partial charge on the *i*th atom.

Here we consider two similar structures of zinc hydroxide and examine the theoretical effect of sulphate co-ordination on the partial charges of the hydroxyl group. The actual structure of any given species in the zinc hydroxyacetate structure is unknown but this evaluation may be used to show the difference on partial charges of a bridging OH induced by co-ordination of sulphate to the structure. The empirical formulae for the hypothetical structures considered is $[Zn_2(H_2O)_6(OH)_2\mu(OH)_2]^0$ and $[Zn_2(H_2O)_5(OH)_2(SO_4)\mu(OH)_2]^{2-}$. To simplify calculation the various ligands are treated as individual groups using their mean electronegativities for calculation and the partial charges on the individual atoms of the ligands is neglected. This allows simpler calculation of the partial charges on the oxygen and hydrogen atoms of the bridging OH ligand. Given that the calculated mean electronegativities of H_2O, SO_4^{2-} and OH^-

are 2.49, 2.28 and 1.61 respectively the calculated partial charges on the μ(OH) bond for both situations is shown in table 6.6.

	δ(O)	**δ(H)**
$[Zn_2(H_2O)_6(OH)_2\mu(OH)_2]^0$	*-0.487*	*+0.082*
$[Zn_2(H_2O)_5(OH)_2(SO_4)\mu(OH)_2]^{2-}$	*-0.606*	*-0.072*

TABLE 6.6: *EFFECT OF CO-ORDINATION OF SULPHATE ON Zn-O-H PARTIAL CHARGES IN A HYPOTHETICAL COMPLEX*

The calculations predict that co-ordination of sulphate to zinc with a local hydroxyl ligand results in the proton on the local hydroxyl becoming more electronegative and so promotes acid dissociation of the proton. Following dissociation the proton could either be transferred to another ligand or go into solution.

Transfer of a proton from the hydroxyl to a sulphate ligand is a possible route resulting in the formation of a HSO_4^- ligand. PCM calculations show that the maximum upper pH limit for ionic dissociation of HSO_4^- from Zn(II) ($\alpha_{minimum}$ =0.5) is pH>4.7. The result of proton transfer from an hydroxide ligand to a sulphate ligand would therefore be the formation of a Zn-O-Zn bridge and ionic dissociation of HSO_4^-. This mechanism is similar to the oxolation mechanism except the leaving group is HSO_4^- in place of H_2O.

The equilibrium constant for the acid dissociation of HSO_4^-;

$HSO_4^- \rightleftharpoons H^+ + SO_4^{2-}$

is 1.2×10^{-6} mol dm^{-3}. At neutral pH it is calculated that dissociation of HSO_4^- is greater than 99.99% complete. This dissociation results in an increase of H^+ ions, lowering solution pH as observed, and regenerating SO_4^{2-}. The pH conditions of the dispersion results in co-ordination of sulphate to Zn(II) completing the catalytic cycle of zinc oxide formation. This is summarised in figure 6.16.

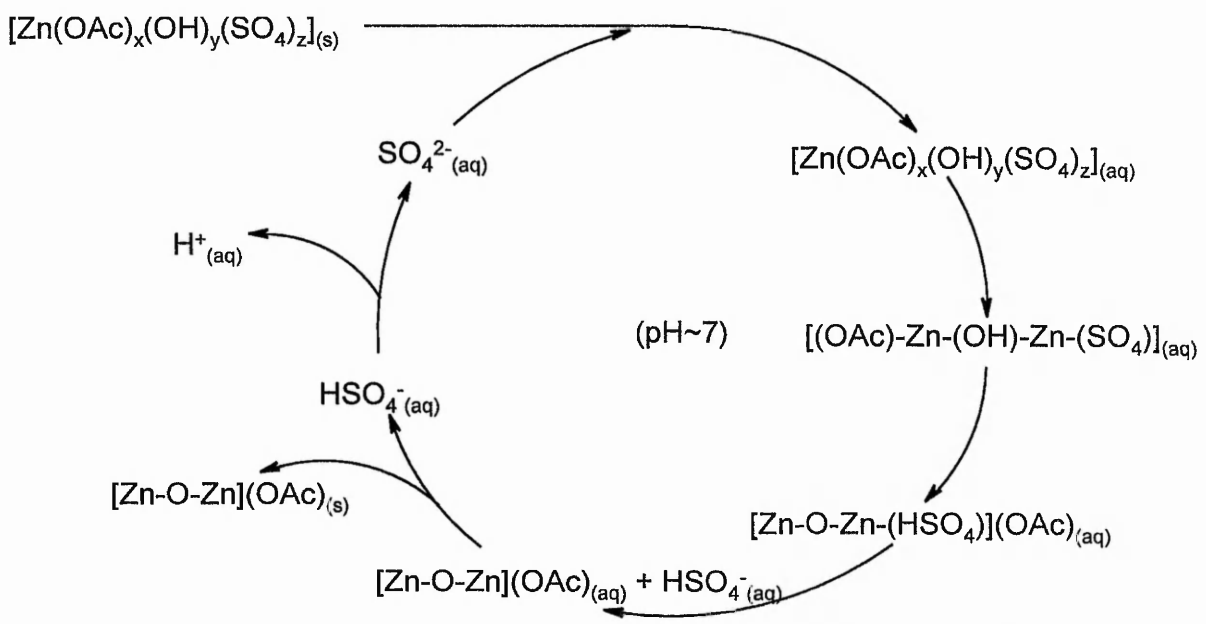

FIGURE 6.16: *PROPOSED SULPHATE CATALYSED CYCLE IN THE FORMATION OF ZINC OXIDE*

A plot of variation of zinc oxide content of the sol at a specific time against temperature of the dispersion shows an s-shaped type of curve. As reaction temperature is raised about 40°C the rate of zinc oxide production increases but becomes limited above 65°C to a maximum at 80°C. A limiting step resulting in the reduction of zinc oxide must become significant at higher temperatures. The results obtained following the ageing of the zinc oxide sol at room temperature show that dissolution of zinc oxide takes place with co-ordination of acetate to Zn(II) and formation of the "relaxed" hydroxyacetate polymer with stable γ-acetate ligands. This dissolution/ re-precipitation, process is thought to be responsible for the limitation at higher temperatures as solubility of zinc oxide increases. At higher temperatures the solubility of zinc oxide is higher and so the rate of formation of hydroxyacetate is increased resulting in a limiting reverse reaction to zinc oxide formation. This is summarised in figure 6.17.

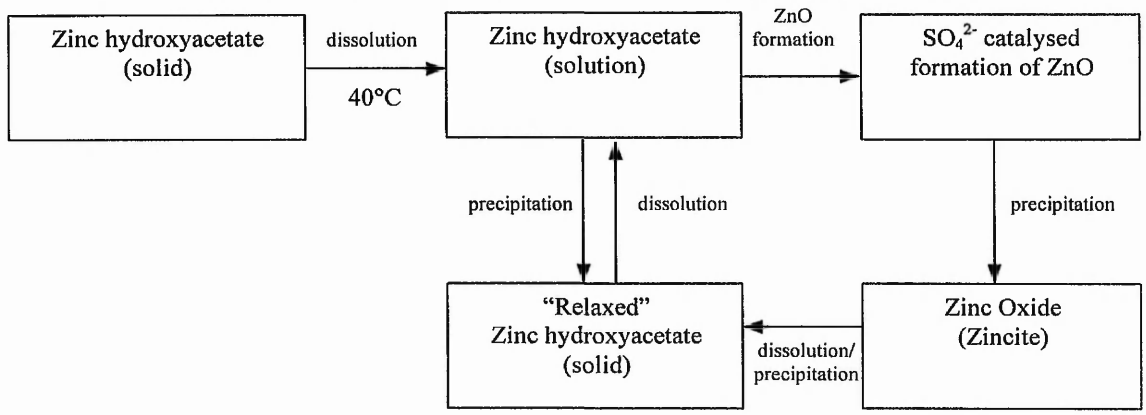

FIGURE 6.17: *PROPOSED CYCLE DURING WARMING OF ZINC HYDROXYACETATE SUSPENSION*

This cycle accounts for the observed results. In the absence of sulphate ions the dissolution and reprecipitation of the zinc hydroxyacetate polymer results in production of the stable hydroxyacetate polymer while addition of small amounts of sulphate ions results in the catalytic production and precipitation of zinc oxide in the form of zincite.

6.5 CONCLUSIONS

Addition of ammonia to saturated solutions of zinc acetate results in the rapid formation of an amorphous material made of bridging acetate/hydroxyl polymer. Analysis of the acetate ligand environments shows them to have different OCO bond angles. Increasing the pH of the condensation results in a change of relative proportion of these ligands favouring acetate sites with higher bond strains. As the mixture is aged no change of the zinc hydroxyacetate structure or crystallinity is found. The amorphous spherical particles aggregate and grow together while addition of small amounts of sulphate ions had no effect on the processing up to warming of the final dispersion.

Warming of the washed, dispersed gel to temperatures above 40° results in a structural relaxation of the gel by a dissolution precipitation process forming a material composed of stable acetate ligands with OCO bond angles close to that of free acetate.

Incorporation of small amounts of sulphate ions (1 SO_4^{2-}:3400 Zn^{2+}) prior to condensation results in zinc oxide formation. A mechanism has been proposed to account for the formation of the oxide based upon theoretical calculations from the partial charge model on the ligand co-ordination/ ionic dissociation and the effect of sulphate on local O-H partial charges. The mechanism is similar to the oxolation mechanism but with transfer of a proton from a hydroxyl group to an adjacent sulphate ligand and subsequent dissociation of HSO_4^-. This process does not occur with zinc salts other than acetate (e.g. nitrate, chloride) but the role of acetate is not yet understood in the mechanism.

References

1. M. Nara, H. Torii, M. Tasumi, *J. Phys. Chem.*, **100**, 19812, (1996)

CHAPTER 7: ZINC OXIDE THIN FILM AND ACOUSTIC WAVE DEVICE FABRICATION

7.1 Introduction

Acoustic wave devices are simple sensors that consist of a piezoelectric material (such as quartz, lithium niobate or zinc oxide) overlaid by two interdigital transducers to launch and detect acoustic waves.

The electrodes consist of many pairs of fingers produced by photolithography with each finger being only a few micrometers wide. In chemical sensing applications a piezoelectric substrate is coated with a sensing layer[1-3], such as a polymer or phthalocyanines, to selectively adsorb molecules. As the acoustic wave travels from one interdigital transducer to the other the presence of adsorbed molecules on the surface alters the velocity of the wave. The devices are highly sensitive to changes in adsorbed mass (~100 picogrammes/cm^2) making them particularly suitable in gas sensing applications and they have been used as nitrogen dioxide sensors[1,2], sulphur dioxide sensors[3], mercury vapour sensors[4] and oxygen sensors[5] as well as electronic "noses".[6]

As an example figure 7.1 shows a schematic diagram of a surface acoustic wave device.

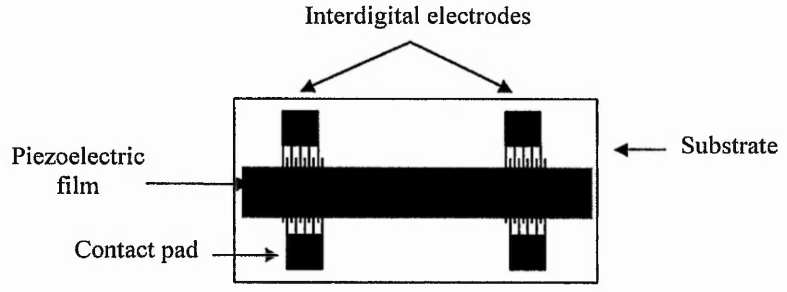

FIGURE 7.1 - *SCHEMATIC REPRESENTATION OF CONSTRUCTION OF A SAW DEVICE*

The actual design and construction of the device significantly affects the acoustic wave device properties with variation of type of substrate, electrode design, piezoelectric material type and

frequency of operation influencing the acoustic wave characteristics. Typically the substrate is formed from the piezoelectric material although inert substrates and piezoelectric thin films is another design possibility.

7.1.1) Zinc oxide thin film preparation methods

Apart from the "conventional" methods of zinc oxide thin film preparation, such as sputter coating[9, 10] using zinc oxide targets and argon oxygen gas mixtures, sol-gel based methods are also known. These largely derive from the alkoxide route via a zinc salt, usually zinc acetate or nitrate, in an organic solvent such as methoxyethanol[11, 12]. The details of the chemistry of the alkoxide process are largely unknown although $Zn(NO_3)(OCH_2CH_2OCH_3)$ precursors have been identified by infrared spectroscopy[12]. The crystal orientation of zinc oxide thin films prepared by the alkoxide process has been found to be dependant upon the coating method[13, 17], thermal treatment of repeat coatings prior to thermal curing[13], withdrawal speed of substrate when dip-coating and film thickness[11]. Zinc acetate has low solubility in organic solvents but addition of alkanolamines (monoethanolamine and diethanolamine) to the solution improves solubility[14]. Zinc oxide thin films prepared from these solutions showed highly preferred [002] orientation when thermally cured at 500°C. It was proposed that the ligand chelates to zinc to increase the zinc acetate solubility although the way it co-ordinates (chelate or bridging) was not clear. It was also proposed that the high boiling point of the alkonamine assists [002] preferred thin film orientation whereas films prepared using lower boiling point solvents, such as water[15], 2-propanol[15] or 2-methoxyethanol[16], hinder strongly preferred orientation.

Aqueous routes to zinc oxide thin films are less well known. Thin films with [002] preferred orientation have been prepared by spray pyrolysis from aqueous zinc acetate solutions when

annealed at 400°C[18]. Substrate temperature, optimum at 490°C, was also found to influence the [002] orientation preference of the film[19]. Chemical deposition methods have also been used to prepare zinc oxide films from solutions of zinc acetate and sodium hydroxide with varying amounts of 1,2-ethanediamine[20], although these films showed no preferential film orientation while the effect of ethanediamine was to alter film morphology.

It is the purpose of this chapter to produce zinc oxide thin films from suspensions prepared by the aqueous sol-gel routes investigated in chapter 6.

7.2 Experimental

Zinc oxide thin films were prepared on amorphous silica glass microscope slides from dispersions of zinc hydroxyacetate, prepared as described in Chapter 6, with no heating of the dispersion.

7.2.1 Coating methods

Different methods of thin film preparation, as described in Chapter 2, were examined to determine the most appropriate preparation route from aqueous sols.

7.2.2 Spin coating

Glass substrates were cut to 2cm x 2cm. The sol was applied to the substrate by either flooding the surface with excess amounts before spinning or adding the sol drop-wise to the centre of the substrate using a teat pipette during spinning. Substrates were spun to 4000rpm for 30 seconds before drying in air.

7.2.3 Dip coating

Substrates were immersed in 50ml of the sol suspension in a beaker measuring 38mm internal diameter. The sol was drained from the beaker using a peristaltic pump at a rate of 3ml per minute. This gave a withdrawal rate of 0.11 cm/min. Substrates were then dried in air at room temperature for 30 minutes. Thicker coatings were prepared by repeat coating of substrates. Thicker coatings were prepared by modification of the sol preparation process described in Chapter 6 by dispersal of the washed gel into 100ml of water instead of 500ml.

7.2.4 Acoustic wave device fabrication

Pairs of gold on titanium interdigital electrodes on amorphous silica glass substrates were fabricated by photolithography by Mr. Fabrice Martin of the Department of Chemistry and Physics, The Nottingham Trent University and were designed for operation at 20-25MHz frequencies.

Thin film coatings on top of the interdigital electrodes were made by masking the area to be coated with a 5mm wide strip of adhesive paper (post-it^{TM}). A fine brush to coat the exposed area and contact pads with Maskol^{TM} in order to prevent coating of the electrical contact pads. The adhesive was removed and the Maskol^{TM} dried at 40°C for 10 minutes. Substrates were then dip coated with the zinc hydroxyacetate suspension and air dried for 30 minutes.. The Maskol^{TM} coating was then peeled off the substrate. Coated acoustic wave device substrates were thermally treated by gradually increasing the temperature at 2°/min per minute up to 360°C holding the temperature at the maximum for 12 hours.

7.3 Results

7.3.1 Coating method

Spin coating of substrates resulted in opaque coatings that were visibly uneven regardless of technique. Dip coated substrates were initially slightly opaque but became visibly transparent after drying in air.

Dip coating results in thin films of high quality and uniformity and is a simple method and so was adopted for thin film preparation hereafter.

7.3.2 SEM analysis

Figure 7.1 shows SEM micrographs of coated acoustic wave device following thermal treatment at 360°C for 12 hours.

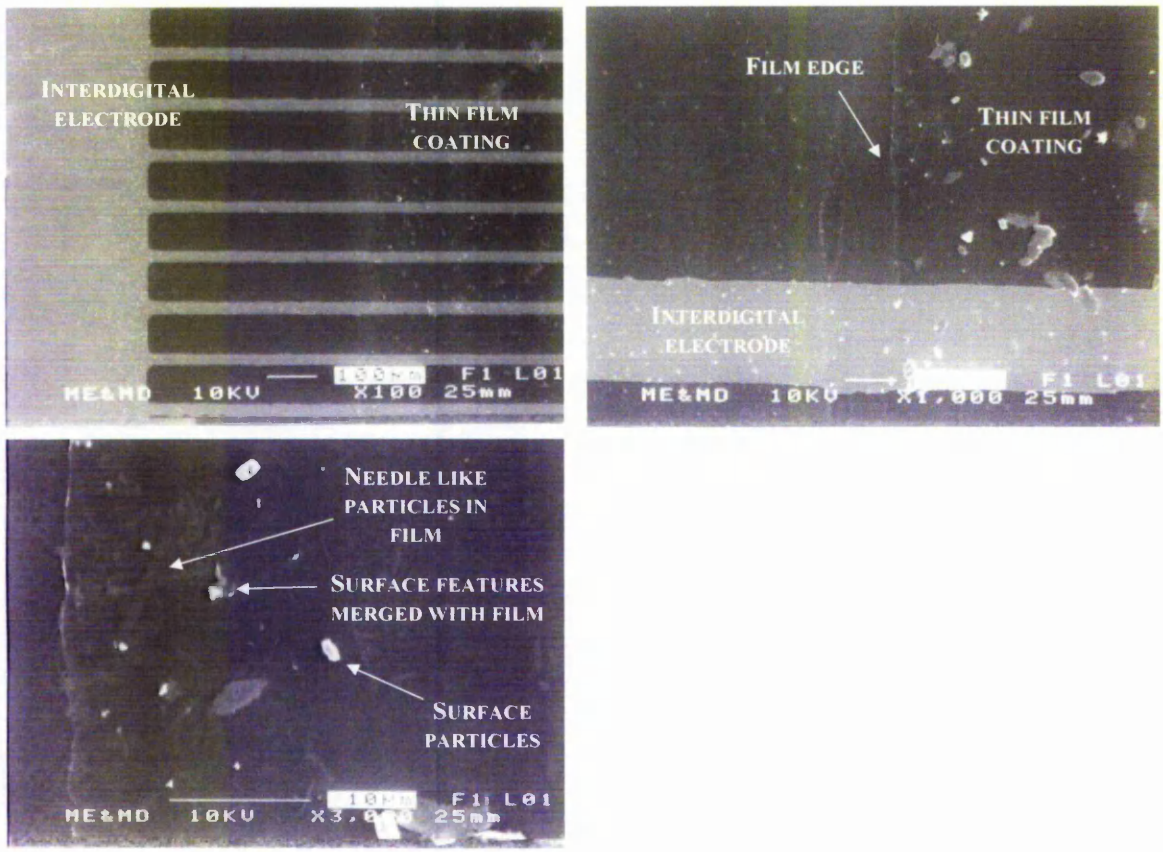

FIGURE 7.1: *SEM MICROGRAPHS OF COATED ACOUSTIC WAVE DEVICE AT X100, X1000 AND X3000 MAGNIFICATIONS.*

SEM analysis showed that a continuous thin film coating was produced by the fabrication process that covers and adheres to the interdigital electrodes. The film has three morphological features. Randomly oriented needle shaped particles of varying sizes from <1μm to approx. 10μm in length were found across the film. Figure 7.2 shows EDX analysis of these particles.

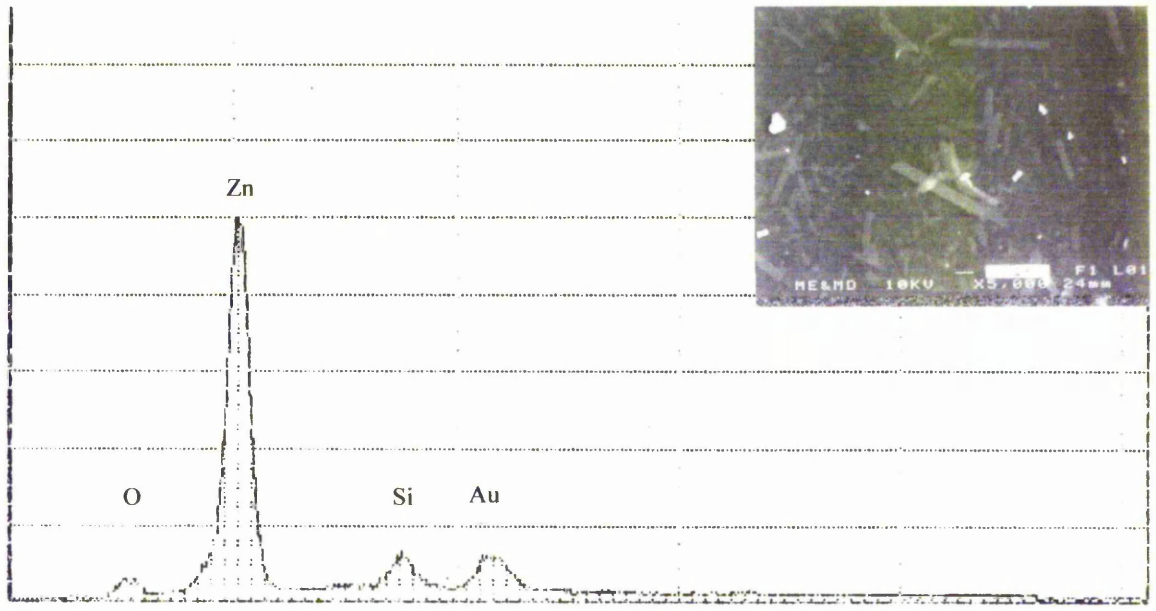

FIGURE 7.2: *EDX ANALYSIS OF NEEDLE SHAPED PARTICLES OF THE INSET MICROGRAPH*

EDX analysis showed that zinc is present in the particles while no carbon was found showing the particles to be free of acetate. Quantified analysis of relative amounts of zinc and oxygen could not be made due to the silica substrate.

Figure 7.3 shows an example SEM micrograph of a misshapen surface feature on the film.

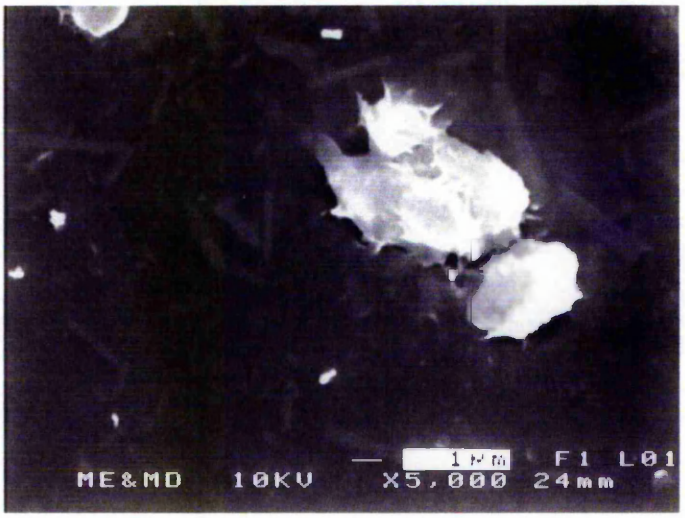

FIGURE 7.3: *SEM MICROGRAPH AT X5000 MAGNIFICATION OF MISSHAPEN SURFACE FEATURE*

The feature had no regular morphology and appeared to be physically merged with the film at the edges. EDX analysis of the feature showed no carbon to be present. Given the irregular shape of the feature this is most probably zinc hydroxyacetate that has thermally decomposed but retained the disordered morphology.

Figure 7.5 shows SEM micrographs of regular shaped particles found on the film surface.

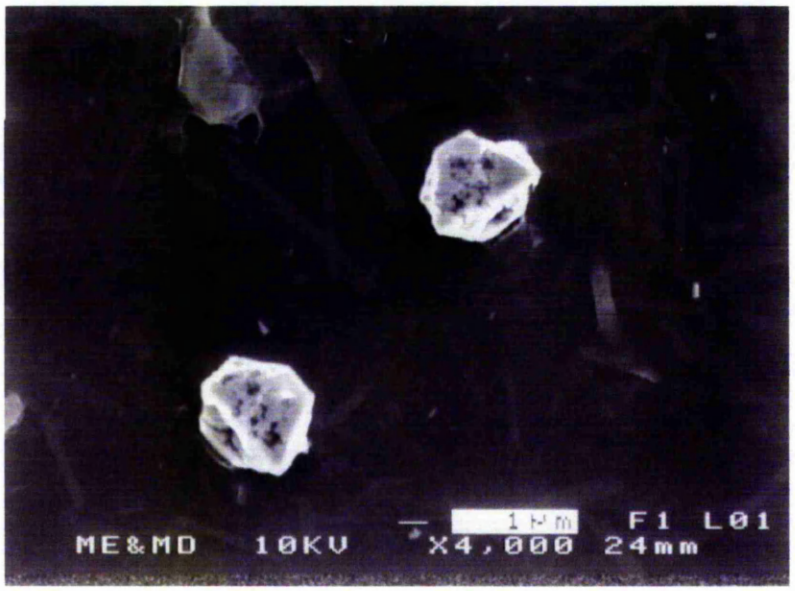

FIGURE 7.5: *SEM MICROGRAPHS OF REGULAR SHAPED PARTICLES FOUND ON THE FILM SURFACE*

The particles are of the same morphology as the zinc hydroxide particles found in the unheated films except for apparent damage to the structure. These particles are suggested to be zinc hydroxide that has decomposed to zinc oxide.

7.3.3 Acoustic device performance

The acoustic wave device was tested for acoustic wave carrier capability by pulsing the first electrode with a frequency of 25MHz. The receiving electrode output was monitored. The result is shown in figure 7.7.

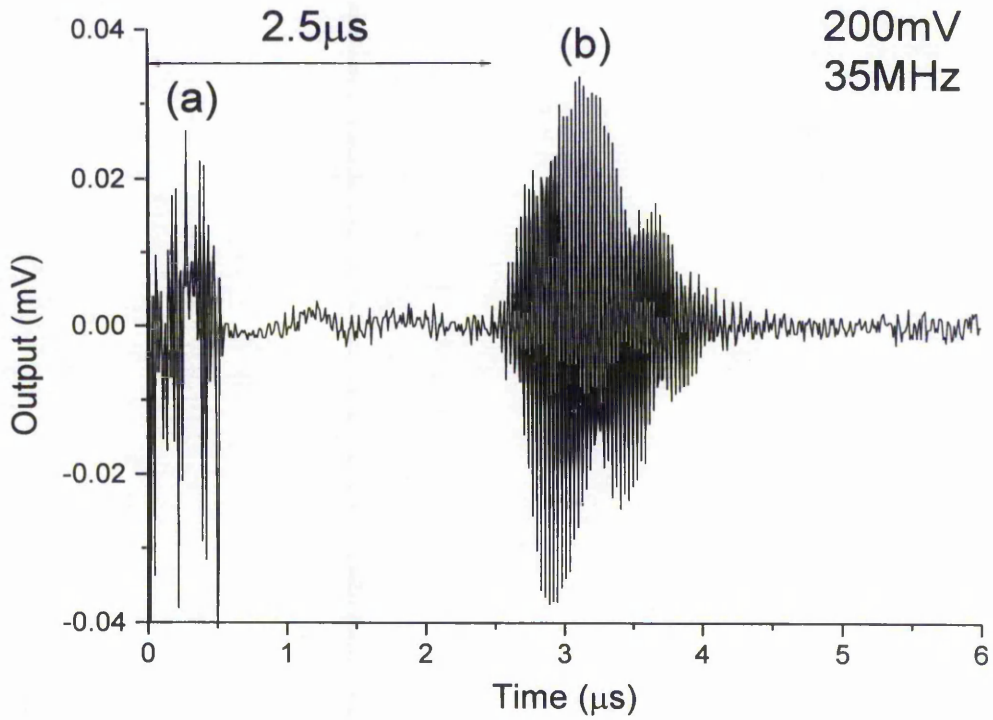

FIGURE 7.7: *OUTPUT OF THE ACOUSTIC WAVE DEVICE PREPARED BY THE AQUEOUS SOL-GEL ROUTE (A) INPUT SIGNAL OF SENDING ELECTRODE, (B) SIGNAL AT RECEIVING ELECTRODE*

The input signal of the sending interdigital electrode was followed by a 2.5μs delay before a signal was received by the second interdigital electrode. The path length of the film was approximately 1cm and so the velocity of the wave was approximately 4000ms^{-1}

corresponding to the order of magnitude appropriate for sound waves. Figure 7.8 shows the output of the device when a drop of water was placed across the film surface.

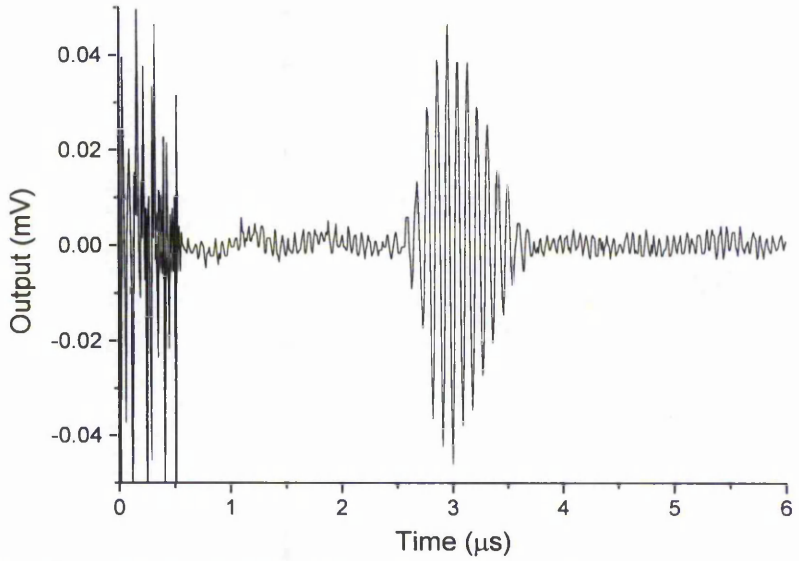

FIGURE 7.8: *OUTPUT OF THE DEVICE WITH DROP OF WATER ACROSS THE SURFACE OF THE FILM*

The output of the device was not damped by the presence of water. The signal is therefore due to bulk acoustic waves and not surface acoustic waves.

Figure 7.9 shows the effect of variation of frequency of the input signal on the peak height of the received signal.

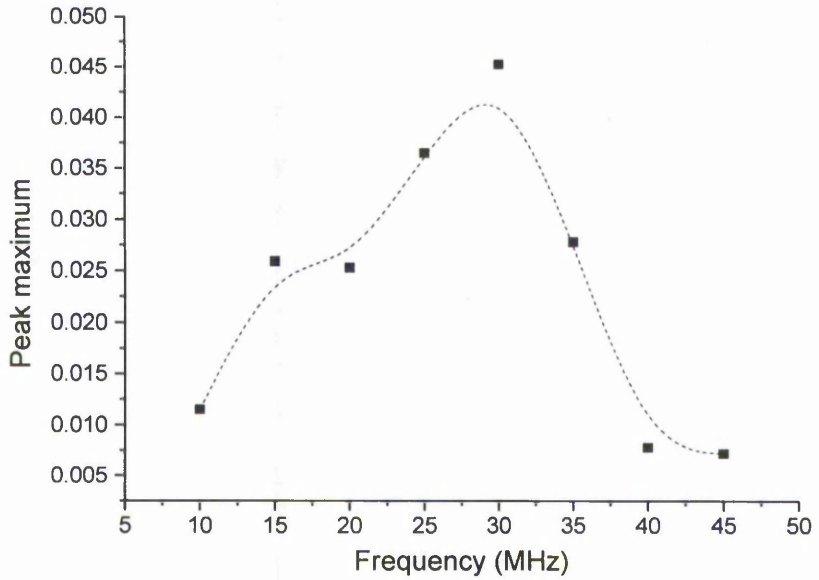

FIGURE 7.9: *EFFECT OF VARIATION OF INPUT SIGNAL FREQUENCY ON OUTPUT SIGNAL INTENSITY*

7.4 Discussion

Thin films prepared by zinc acetate derived aqueous sol-gel methods had three different morphologies of zinc oxide in their structure. The film predominantly consisted of randomly oriented needle shaped zinc oxide particles. Some irregularly shaped zinc oxide features merged into the film were probably from decomposed zinc hydroxyacetate that had not structurally reordered to the needle shaped morphology. The regularly shaped particles appeared to be thermally destroyed and most likely occur from thermal decomposition of a small amount of crystalline zinc hydroxide present in the films.

The zinc oxide films were capable of transmitting bulk acoustic waves rather than surface acoustic waves. This could be because of the thickness of the films although given the random orientation of the zinc oxide particles in the film it is more likely that surface acoustic waves could not be generated because of no preferential crystalline axis for the waves to travel along. An optimum operating frequency of 25MHz was found to give the largest output signal of the device.

7.5 Conclusions

It has been shown that zinc acetate derived, aqueous sol-gel routes to zinc hydroxyacetate suspensions is a viable method in the fabrication of zinc oxide thin film based acoustic wave devices.

This initial investigation did not result in a film carrying surface acoustic waves but instead gave a zinc oxide film that transmitted bulk acoustic waves. Further work to refine the thin film fabrication method from zinc hydroxyacetate suspensions is required in order to optimise the performance and properties of such a device.

References

1. A. Rugemer, S. Reiss, A. Geyer, M. von Schickfus, S. Hunklinger, *Sensor Actuat B-Chem,* **56** (1-2), 1999, 45

2. C. Muller, T. Nirmaier, A. Rugemer, M. von Schickfus M, *Sensor Actuat B-Chem,* **68** (1-3), 2000, 69

3. S.J. Qin, Z. J. Wu, Z. Y. Tang, Y. L. Song, F. Z. Zeng, D. Zhao, *Sensor Actuat B-Chem,* **66** (1-3), 2000, 240

4. J. J. Caron, R. B. Haskell, P. Benoit, J. F. Vetelino, *IEEE T Ultrason Ferr,* **45** (5), 1998, 1393

5. D. M. Oglesby, B.T. Upchurch, , B. D. Leighty, J. P. Collman, X. M. Zhang, P. C. Herrmann, *Anal. Chem,* **66** (17), 1994, 2745

6. R. Allan, *Electron. Des.,* **48**(15), 2000, 30

7. Y. M. Yang, P. Y. Yang, X. R. Wang, *Sensor Actuat B-Chem,* **66** (1-3), 2000, 167

8. R. A. McGill, V. K. Nguyen, R. Chung, R. E. Shaffer, D. DiLella, J. L. Stepnowski, T. E. Mlsna, D. L. Venezky, D. Dominguez, *Sensors Actuat B-Chem,* **65** (1-3), 2000, 10

9. H. K. Kim, W. Kleemeier, Y. B. Li, D. W. Langer, D. T. Cassidy, D. M. Bruce, *J. Vac. Sci. Technol. B,* **12** (3), 1328, (1994)

10. H. H. P. T. Bekman, K. W. Benoist, J. L. Joppe, *Appl. Surf. Sci.,* **70-1**, 347, (1993)

11. M. Ohyama, H. Kozuka, T. Yoko, *Thin Solid Films,* **306**, 78, (1997)

12. M. Toyoda, J. Watanabe, T. Matsumiya, *J. Sol Gel Sci. Techn.,* **16**, 93, (1999)

13. M. Ohyama, H. Kozuka, T. Yoko, S. Sakka, *J. Ceram. Soc. Jpn.,* **104**, 296, (1996)

14. M. Ohyama, H. Kozuka, T. Yoko, S. Sakka, *J. Ceram. Soc. Jpn.,* **104**, 296, (1996)

15. S. Major, A. Banjeree, K. L. Chopra, *Thin Solid films,* **108**, 333, (1983)

16. Y. Takahashi, M. Kanamori, A. Kondoh, H. Minoura, Y. Ohya, *Jpn. J. Appl. Phys. Pt. 1,* **33**, 6611, (1994)

17. T. J. Bukowski, K. McCarthy, F. McCarthy, G. Teowee, T. P. Alexander, D. R. Uhlmann, J. T. Dawley, B. J. J. Zelinski, *Integr. Ferroelectr.*, **17**, 339, (1997)

18. S. Oktik, G. J. Russell, A. W. Brinkman, *J. Cryst. Growth,* **159**, 195, (1996)

19. H. H. Afify, S. A. Nasser, S. E. Demian, *J. Mater. Sci-Mater. El. 2*, **2**, 152, (1991)

20. P. O'Brien, T. Saees, J. Knowles, *J. Mater. Chem.*, **6**, 1135, (1996)

CHAPTER 8 CONCLUSIONS AND FUTURE WORK

8.1 Conclusions

This thesis was concerned with two areas of sol-gel chemistry – the thermochromic behaviour of copper(II) complexes in alkoxide derived silica sol-gel gels and condensation in aqueous zinc acetate solutions for the production of acoustic wave devices. Incorporation of bis(diammine)copper(II) chloride complexes into silica sol-gel was examined and the influence of the matrix on the optical and thermochromic properties explored. Investigations were made into different methods of obtaining different phases of hydrous zinc oxides at low temperatures in aqueous solution and into sol preparation for thin film fabrication.

8.1.1 Thermochromism in silica sol-gel

Several new thermochromic transitions have been discovered unique to doped silica sol-gel materials that require both thermochromic dopant and silica matrix to be present. The behaviour of the complex in the silica matrix was found to be dependant upon both the nature of the complex and the structure of the silica. Incorporation of 1,2-diammoniumpropanetetrachlorocuprate salts into silica sol-gel results in a pale green material characteristic of the "low temperature phase" of the complex. When thermally treated at 80°C for 1 hour the silica became a yellow colour characteristic of the "high temperature phase" of the free complex. Unlike the free complex, the high temperature phase colour may be preserved at room temperature by storing the silica in a dry atmosphere. This is a property not found in the free complex. Rehydration of the silica in ambient conditions causes the colour to revert to pale green. Prolonged thermal treatment at 80°C for 24 hours resulted in an irreversible deep green colour from thermal intermolecular proton transfer from two ammonium groups to an acceptor in the matrix with the free amine groups consequently co-

ordinating to the Cu(II). This colouration could be preserved by storage in a dessicator whereas exposure of the silica to ambient conditions gave a light blue colour identical to that of the bis(ammineammonium)copper(II) complex. Dehydration of the blue coloured silica at 80°C for 1 hour returned the deep green colour. The bis(ammineammonium)copper(II) complex is not itself thermochromic yet when in the silica matrix thermochromic behaviour is observed.

Bis(diammine)copper(II) chloride doped sol-gels showed a different thermochromic behaviour to the 1,2-diammoniumpropanetetrachlorocuprate doped sol-gels. ESR analysis showed that incorporation into silica gel resulted in outer sphere co-ordination of oligomeric silica species to hydrogen atoms on the in-plane diammine ligands restricting ligand motion resulting in a change in optical properties of the doped silica compared with solutions of the complexes. Dehydration of the silica resulted in thermochromic transitions identical to the free complexes as water was displaced from the inner co-ordination sphere by chloride ligands. Prolonged thermal treatment resulted in irreversible thermochromic transitions not found in the free compounds as the complex molecules migrate into the micropores in the matrix and are held by the strong surface forces therein together with an out of plane twisting of the diammine ligands. Different silica structures have different micropore chemistry and hence different thermochromic transitions resulted as the degree of complex geometry distortion varies between alkoxide and colloidal silica types.

These transitions are unique to the dopant-matrix combinations studied and represent new thermochromic phenomenon for silica sol-gel materials.

8.1.2 The aqueous chemistry of zinc acetate

Experiments investigating the chemistry of zinc acetate at low Zn(II) concentrations (<0.1M) have qualitatively described the formation of condensed phases from aqueous solutions. A critical pH of 10.6 was found experimentally and explained theoretically by the partial charge model to account for significant differences in products obtained above or below this pH. This was because of the pH dependent complexation of acetate ligands. When the acetate ligands are co-ordinated to the zinc a regular, pH independent type of polymeric structure of bridging acetate and hydroxyls formed from h=2 precursors giving an amorphous material. When the acetate was not co-ordinated to the zinc (pH10.7 or above) highly compact, crystalline zinc hydroxide (Wulfingite) was formed. Under these conditions it was possible to form zinc oxide by increasing base strength causing deprotonation of the acidic μ^3 OH groups of the hydroxide.

Condensation in saturated zinc acetate solutions resulted in rapid growth of the hydroxy/acetate polymer forming amorphous, spherical particles with four principle acetate ligand types, of varying OCO bond strain, the ratio of which is controlled by the Zn/NH_3 ratio of the reaction medium. Washing of this material to remove contaminating ions and dispersion into water at temperatures above 40°C resulted in the structural relaxation of the polymer to a type identical to that produced at lower Zn(II) concentrations with acetate ligands of minimal OCO bond strain. Addition of small amounts of sulphate ions to the gel prior to condensation resulted in the formation of zinc oxide when the washed dispersal was heated to temperatures above 40°C. A catalytic mechanism to account for zinc oxide production from aqueous solution, similar to the oxolation mechanism, where proton transfer from a hydroxyl ligand to an adjacent sulphate, and liberation of HSO_4^-, resulting in formation of "oxo" bridges

has been proposed. This mechanism is supported by theoretical calculations using the partial charge model predicting the effect of sulphate co-ordination on changes to O-H bond charge distribution is one of increasing the difference in charge between oxygen and hydrogen atoms so encouraging acid dissociation of the hydroxyl. Calculations on the pH dependant complexing ability of HSO_4^- and SO_4^{2-} at the conditions of the experiment also supports the proposed mechanism. This mechanism does not account for some factors as yet (e.g. acetate requirement in the reaction or experimental evidence of HSO_4^-) but has proposed a new, low temperature route to metal oxides in aqueous solution.

8.1.3 Acoustic wave device fabrication

Zinc oxide thin films on silica prepared by thermal decomposition of thin film coatings of zinc hydroxyacetate produced a device with bulk acoustic wave carrier properties. The thin film coating did not result in surface acoustic waves, as was hoped. This was most likely because of random orientation of crystallites in the zinc oxide thin film but shows the technique of aqueous sol-gel chemistry in zinc oxide thin film production is a possible route to acoustic wave device fabrication.

8.2 Further work

Many areas of expansion exist for further work from those areas presented in this thesis in development and/ or expansion of specific areas and refinement of understanding of ideas.

8.2.1 Thermochromism in silica sol-gel

The proposed mechanism of thermochromism in diammonium tetrachlorocuprate doped silica xerogels of thermal intermolecular proton transfer from ammonium groups to the matrix presents several areas to further examine the mechanism.

The generality, or otherwise, of the mechanism of proton transfer could be examined by extension of the range of complex types to different transition metal ions and different anions (e.g. F^-, Br^-, NO_3^-, SO_4^-). The proton transfer may not be restricted to transition metal complexes. Doping of the silica with diammonium salts themselves may result in proton transfer when thermally treated but lack of any chromophore would not make such a transition immediately apparent. A solid state ^{14}N and/ or ^{1}H NMR study would be capable of determining if the Cu(II) is required for the transfer or whether it simply acts as a chromophore. This transfer was found to be very slow at room temperature (a few months) and could result in shelf-life restrictions to devices fabricated using silica sol-gel with ammonium groups in the dopant molecules.

Further to this the fate of the transferred proton is unknown. To provide complete knowledge of the mechanism a more detailed examination of samples by infrared spectroscopy, TG-MS and solid state NMR spectroscopy would be made to study protons in the matrix. This would determine whether they are transferred to Si-OH, H_2O, Si-O-Si, species in the silica pores or even to outer sphere anions such as Cl^- and are lost as HCl.

Gels prepared at neutral conditions result in limitation on the number of Cu(II) sites in the matrix. This appears to be a function of the ligand complexation limited by the chelating nature of the diammines in comparison with the large range of Cu(II) sites found in $CuCl_2$ doped xerogels. EPR analysis of the dependency of the number of Cu(II) sites and characteristics of the sites with different numbers of chelated ligands and/ or ligand types could prove interesting and perhaps give more detailed insight into the irreversible mechanism found when xerogels are dehydrated for 24 hours at 80°C.

As shown in chapter 4 the structure of the silica matrix influences the thermochromic behaviour of the material resulting in different optical properties for the different silica types attributed to differences in micropore structure. The experiments could therefore be extended to doped silica xerogels with chemically modified surfaces by covalent addition of organic functionalities to the silica sol prior to gelation. It is conceptually possible, by careful manipulation of the silica surface by slight variations of surface functional groups, to attain fine control of the degree of complex geometry distortion in the micropores so allowing subtle chemical control of the optical absorption maximum of the material using a single dopant bis(diammine) complex.

8.2.2 Aqueous chemistry of zinc acetate

The mechanism of the catalytic formation of zinc oxide by sulphate ions requires refinement and quantification of the proposed cycle. The presence of HSO_4^- is proposed to exist and so analytical confirmation of this species is required. The use of ^{17}O labelled sulphate to detect this probably transient species would provide strong support for the mechanism while also giving invaluable information of the behaviour of sulphate throughout zinc oxide formation.

A kinetic study establishing a quantitative relationship between the variation of zinc oxide content of the dispersal during warming and the pH changes observed through dissociation of HSO_4^- would be useful as a future experiment. The poor reproducibility of the variations of pH with time during warming of the dispersion is probably due to practical experimental difficulties of achieving homogenous dispersion of the sol quickly into the warm water of appropriate temperature and starting the pH measurements. Errors in time taken to achieve homogenous dispersion of the zinc hydroxyacetate and true measurement of t=0 and hence the

poor reproducibility of the pH curves. A possible, slightly more complex, solution to this problem could be made taking advantage of the fact that zinc oxide formation does not begin until above 40°C. Homogenous dispersions can therefore be reached at room temperature. Instead of thermostating the reaction at a specific temperature a third dimension could be introduced into the experiment by using specific, controlled rates of temperature increase and measuring pH (with a temperature compensation probe) and zinc oxide content over time. By comparing data from two or more experiments with variations in rate of increase of temperature between experiments it would be possible to provide a quantitative relationship between pH and percentage zinc oxide of the dispersion.

Acetate ligands have an important role in the zinc oxide formation mechanism yet their role in the reaction is unknown. It is possible that they increase solubility of the material but this is unclear. Further investigations utilising the infrared spectroscopy of the carboxylates to gain information, possibly using FTIR-HATR or Raman flow cell methods, would follow acetate transformations in real time throughout the reaction identify intermediate acetate species not found in the hydroxyacetate polymer.

8.2.3 Acoustic wave devices

Acoustic device fabrication was only initially investigated in this work in order to prove the technology of acoustic wave device production from aqueous derived sol-gel routes is feasible making many opportunities for further investigation.

Deposition of thin films from unheated dispersions where a variation of acetate ligands (γ, η, and ι types) exist could result in differences of ZnO thin film properties. Thermal

decomposition properties of the coating material in alkoxide sol-gels has been shown to influence the zinc oxide thin film orientation - an important factor in acoustic wave devices. Variation of ratios of acetate ligand types by control of the Zn/NH_3 ratio of the initial condensation reaction so changing the composition, and hence thermal decomposition properties, of the hydroxyacetate polymer may be important. Further to this, investigations into zinc hydroxycarboxylate dispersions prepared from other zinc carboxylate salts than acetate (e.g. formate, stearate) may result in significant differences in the zinc oxide thin film properties. Alternatively addition of water soluble polymers or compounds of higher thermal stability, such as poly(ethyleneglycol), to the dispersion may assist in sol stabilisation and thin film orientation by a similar structural relaxation effect to alkylamines in alkoxide routes to highly oriented thin film formation.

The low temperature sulphate catalysed mechanism of zinc oxide formation may provide a novel route to zinc oxide thin films. Dip coating of substrates using dispersions of zinc oxide particles would result in layers of randomly oriented crystallites and would have poor surface acoustic wave carrying properties. A chemical bath approach of immersing the substrate during warming of the dispersion could feasibly by used to deposit zinc oxide thin films with little or no thermal treatment in curing the film. However a problem with this approach to overcome would be due to the simultaneous deposition of zinc hydroxyacetate material.

Substrate type greatly influences the crystal orientation of all types of thin films and so experiments using different substrates would be useful in perfecting the device. Extension of experiments using single crystal quartz, sapphire, and silicon wafers cut along different crystal faces to vary the film orientation properties could be made.

Appendix I

Spot test for acetates[1]

A drop of the test solution is mixed on a petri dish with a drop of 5% $LaNO_3$ and a drop of 0.01M iodine solution. A drop of 1M ammonia is added and after a few minutes a blue/ blue-brown ring develops around the drop of ammonia (limit of detection 50μM acetate).

Spot test for ammonium[2]

A drop of neutral or weakly acidic test solution is placed upon a petri dish. A drop of Nesslers reagent is added and formation of an orange/brown precipitate ($HgI_2.HgNH_2I$) indicates a positive result.

Nesslers reagent: Dissolve 10g mecury iodide and 5g of potassium iodide in 50ml of water and then add 20g of potassium hydroxide

Determination of Zn(II)[1]

Spot test

The presence of zinc(II) ions can be determined by additon of a solution of 3g of diammonium hydrogen phosphate in 5ml of water. A drop of the test solution is placed upon a petri dish and several drops of the diammonium hydrogen phosphate solution is added. Precipitation of white zinc ammonium phosphate indicates a positive result.

Quantitative determination of Zn(II) in saturated zinc acetate solution

1ml of the test solution was diluted into 30ml of water. The solution was cooled in ice. An excess of the ice cold diammonium hydrogen phosphate solution (20ml) was added and the resulting precipitate filtered and washed with ice water. The solid was then dried in air

at 100°C for 1 hour. This was repeated five times giving a mean mass of product of 0.2455g.

The reaction for the precipitation is;

$$Zn^{2+} + HPO_4^{2-} + NH_4^+ \longrightarrow \downarrow ZnNH_4PO_4 + H^+$$

$$H^+ + HPO_4^{2-} \rightleftharpoons H_2PO_4^-$$

The calculated concentration of Zn(II) in saturated zinc acetate solution is 1.38M.

References

1. "Spot tests in organic analysis, 7th Ed.", Fritz Feigl, Elsevier Scientific Publishing Company, (1966), pg. 454
2. "Spot test analysis: Clinical, Environmental, Forensic and Geochemical Applications", Ervin Jungreis, J. Wiley and Sons, (1984), pg. 57

Appendix II - Analysis of tetrahedral ZnO_4 by Far-IR

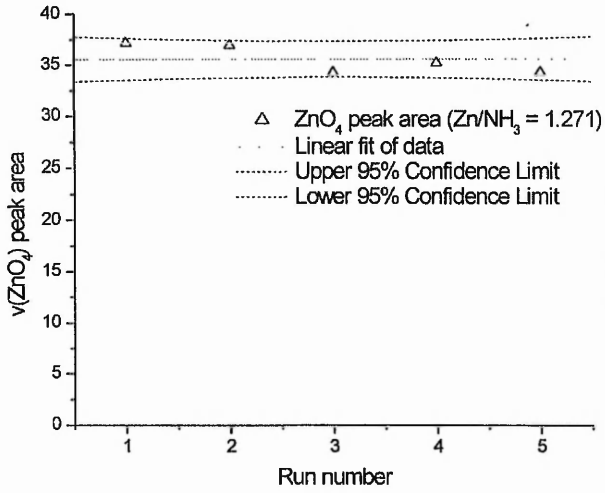

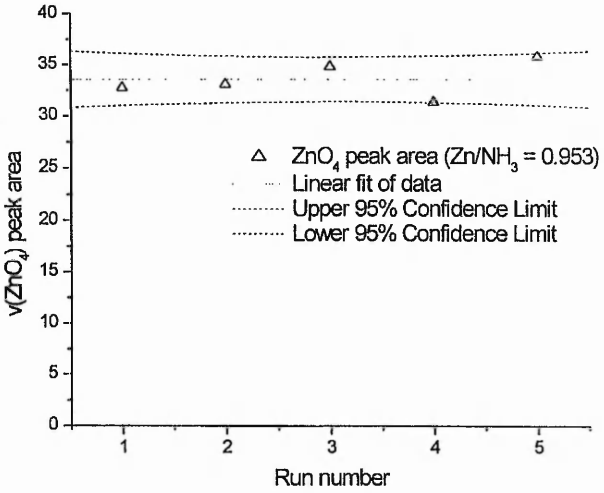

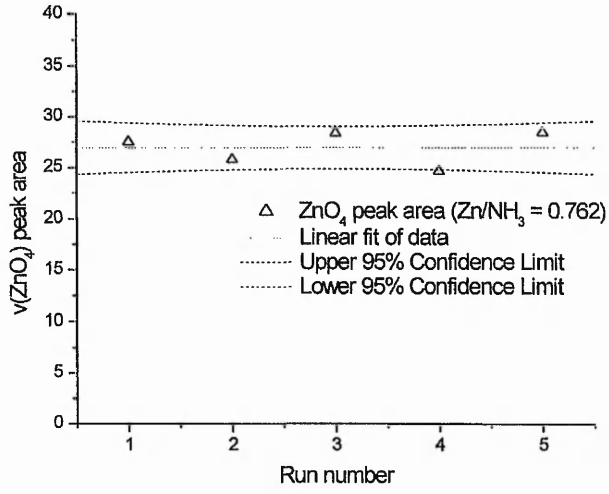

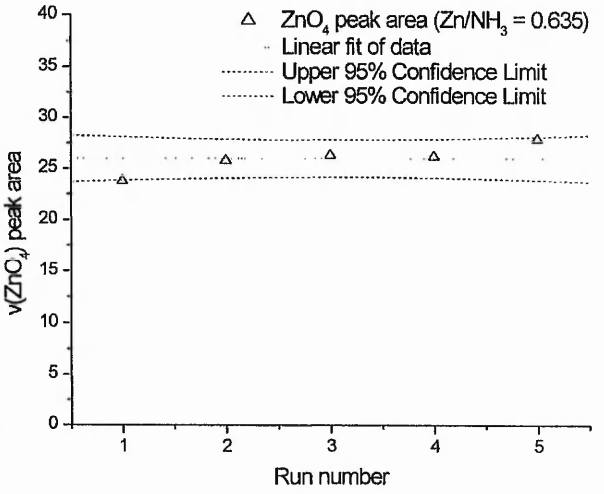

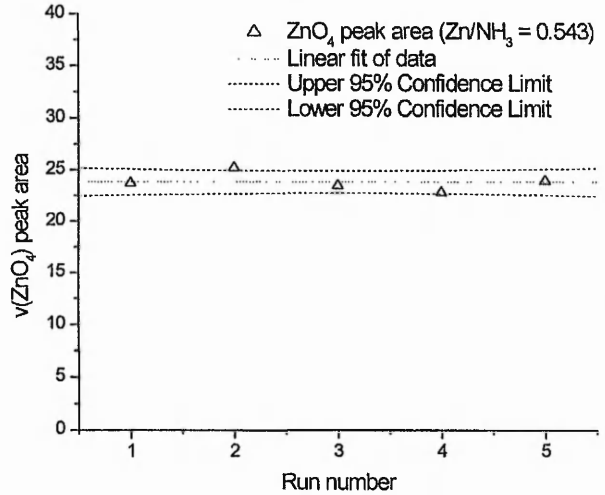

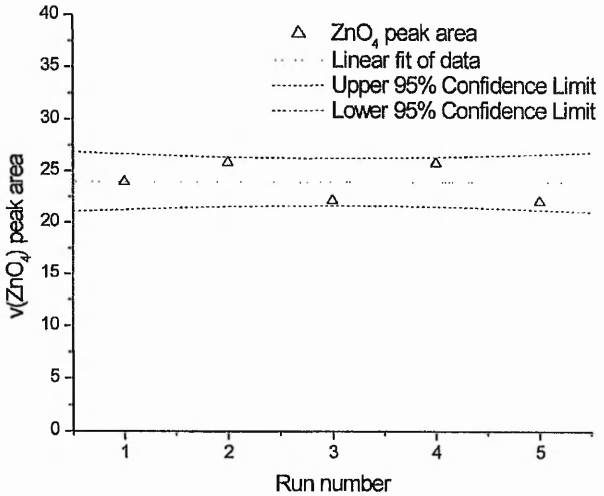

Appendix III – Crystal structure data

GREEN CRYSTALS

(1,2-diammoniumpropane)tetrachlorocuprate - $C_3H_{12}N_2CuCl_4$

X-ray refinement data

Temperature	: 281.49K
Wavelength	: 0.71073 Å
Crystal system	: Monoclinic
Space group	: $P2_1/c$
Unit cell dimensions	: a=16.72(4)Å alpha=90°
	: b=6.9(2)Å beta=88.37(2)°
	: c=8.42(2)Å gamma=90°
Volume	: 970(4)$Å^3$, 4
Density	: 1.921 Mg/m^3
Absorbtion coefficient	: 3.287 mm^{-1}
F(000)	: 564
Crystal size	: 0.14 x 0.14 x 0.1 mm
Range for data collection	: 2.44 to 23.22°
Limiting indices	: $-18 < h < 18, -7 < k < 5, -9 < l < 9$
Reflections collected	: 3846
Independent reflections	: 1376 (R_{int} = 0.0338)
Absorbtion correction	: Sadabs
Max. and min. transmission	: 1.00000 and 0.818582
Refinement method	: Full matrix on least squares on F^2
Data/ restraints/ parameters	: 1357 / 6 / 119
Goodness-of-fit on F^2	: 1.027
Final R indices [$I>2\sigma(I)$]	: R1 = 0.0305, wR2 = 0.0605
R indices (all data)	: R1 = 0.0310, wR2 = 0.0641
Extinction coefficient	: 0.0075(7)
Largest diff. Peak and hole	: 0.317 and -0.252 $eÅ^{-3}$

	x	y	z	U(eq)
Cu(1)	0	-5000	5000	31(1)
Cl(1)	231(1)	-2338(1)	3404(1)	37(1)
Cl(2)	1333(1)	-5560(1)	5102(1)	40(1)
Cu(2)	5000	0	0	29(1)
Cl(3)	5196(1)	-2656(1)	1597(1)	35(1)
Cl(4)	3650(1)	-513(1)	-109(1)	36(1)
N(1)	1372(2)	-4834(4)	1072(3)	37(1)
C(2)	2227(2)	-4378(5)	1382(4)	42(1)
C(3)	2767(2)	-5610(4)	416(4)	38(1)
N(3)	3616(1)	-5119(4)	870(3)	34(1)
C(4)	2627(2)	-5304(5)	-1360(4)	54(1)

ATOMIC CO-ORDINATES [X10^4] AND EQUIVALENT ISOTROPIC DISPLACEMENT PARAMETERS [Å X 10^3] FOR (1,2-DIAMMONIUMPROPANE)TETRACHLOROCUPRATE

Cu(1)-Cl(2)	2.2623 (7)	Cu(1)-Cl(2)#1	2.2624 (7)
Cu(1)-Cl(1)#1	2.3166 (6)	Cu(1)-Cl(1)	2.3167 (6)
Cu(2)-Cl(4)#2	2.2849 (6)	Cu(2)-Cl(4)	2.2850 (6)
Cu(2)-Cl(3)	2.2930 (6)	Cu(2)-Cl(3)#2	2.2930 (6)
N(1)-C(2)	1.482 (4)	C(2)-C(3)	1.498 (4)
C(3)-N(3)	1.500 (4)	C(3)-C(4)	1.523 (4)
Cl(2)-Cu(1)-Cl(2)#1	180.0	Cl(2)-Cu(1)-Cl(1)#1	91.34 (2)
Cl(2)#1-Cu(1)-Cl(1)#1	88.66 (2)	Cl(2)-Cu(1)-Cl(1)	88.66 (2)
Cl(2)#1-Cu(1)-Cl(1)	91.34 (2)	Cl(1)#1-Cu(1)-Cl(1)	180.0
Cl(4)#2-Cu(2)-Cl(4)	180.0	Cl(4)#2-Cu(2)-Cl(3)	88.60 (2)
Cl(4)-Cu(2)-Cl(3)	91.40 (2)	Cl(4)#2-Cu(2)-Cl(3)#2	91.40 (2)
Cl(4)-Cu(2)-Cl(3)#2	88.60 (2)	Cl(3)-Cu(2)-Cl(3)#2	180.0
N(1)-C(2)-C(3)	112.2 (2)	C(2)-C(3)-N(3)	108.3 (2)
C(2)-C(3)-C(4)	112.1 (3)	N(3)-C(3)-C(4)	109.8 (2)

BOND LENGTHS [Å] AND ANGLES [°] FOR (1,2-DIAMMONIUMPROPANE)TETRACHLOROCUPRATE

	x	y	z	U(eq)
H (1NA)	1176 (22)	-4228 (52)	185 (35)	70 (12)
H (1NB)	1245 (23)	-6143 (40)	978 (45)	85 (13)
H (1NC)	1038 (20)	-4372 (51)	1908 (37)	76 (12)
H (2A)	2356 (2)	-4574 (5)	2500 (4)	50
H (2B)	2321 (2)	-3026 (5)	1139 (4)	50
H (3A)	2671 (2)	-6975 (4)	666 (4)	45
H (3NA)	3690 (17)	-5306 (39)	1945 (28)	38 (9)
H (3NB)	3963 (22)	-5865 (56)	214 (41)	86 (14)
H (3NC)	3717 (19)	-3860 (37)	656 (37)	60 (11)
H (4A)	2983 (2)	-6117 (5)	-1934 (4)	81
H (4B)	2725 (2)	-3972 (5)	-1618 (4)	81
H (4C)	2084 (2)	-5629 (5)	-1647 (4)	81

HYDROGEN COORDINATES [X 10^4] AND ISOTRPIC DISPLACEMENT CO-ORDINATES ($Å^2$ X 10^3) FOR (1,2-DIAMMONIUMPROPANE)TETRACHLOROCUPRATE

YELLOW CRYSTALS (GREEN CRYSTALS HEATED TO 80°C FOR 1 HOUR)

(1,2-diammoniumpropane)tetrachlorocuprate - $C_3H_{12}N_2CuCl_4$

X-ray refinement data

Temperature	: 353(2)K
Wavelength	: 0.71073 Å
Crystal system	: Monoclinic
Space group	: $P2_1/c$
Unit cell dimensions	: a=16.66(5)Å alpha=90.00°
	: b=6.88(2)Å beta=89.18(3)°
	: c=8.40(3)Å gamma=90.00°
Volume	: 962(6)$Å^3$, 1
Density	: 1.944 Mg/m^3
Absorbtion coefficient	: 3.315 mm^{-1}
F(000)	: 564
Crystal size	: 0.14 x 0.14 x 0.1 mm
Range for data collection	: 2.44 to 23.42°
Limiting indices	: $-18 < h < 18, -7 < k < 5, -9 < l < 9$
Reflections collected	: 3851
Independent reflections	: 1377 (R_{int} = 0.0495)
Absorbtion correction	: Sadabs
Max. and min. transmission	: 1.00000 and 0.726242
Refinement method	: Full matrix on least squares on F^2
Data/ restraints/ parameters	: 1329 / 6 / 118
Goodness-of-fit on F^2	: 0.851
Final R indices [I>2σ(I)]	: R1 = 0.0476, wR2 = 0.1239
R indices (all data)	: R1 = 0.0933, wR2 = 0.2166
Extinction coefficient	: 0.851
Largest diff. Peak and hole	: 0.612 and -0.662 $eÅ^{-3}$

	X	y	z	U(eq)
Cu(1)	0	-5000	5000	31(1)
Cl(1)	1335(1)	-4442(3)	4955(3)	40(1)
Cl(2)	-224(1)	-2343(3)	3406(3)	35(1)
Cu(2)	-5000	5000	5000	28(1)
Cl(3)	-3656(1)	5525(3)	4944(3)	37(1)
Cl(4)	-4794(1)	2343(3)	3407(3)	34(1)
N(1)	-1372(5)	-134(11)	6018(10)	34(2)
C(2)	-2229(6)	-593(16)	6191(20)	82(5)
C(3)	-2768(6)	615(15)	5580(19)	84(5)
N(3)	-3622(4)	135(10)	5931(9)	29(2)
C(4)	-2574(9)	184(19)	3591(11)	73(4)

ATOMIC CO-ORDINATES [$X10^4$] AND EQUIVALENT ISOTROPIC DISPLACEMENT PARAMETERS [$Å \times 10^{-3}$] FOR HIGH TEMPERATURE PHASE OF (1,2-DIAMMONIUMPROPANE)TETRACHLOROCUPRATE

Cu(1)-Cl(1)#1	2.260 (5)	Cu(1)-Cl(1)	2.260 (5)
Cu(1)-Cl(2)#1	2.313 (4)	Cu(1)-Cl(2)	2.313 (4)
Cu(2)-Cl(3)#2	2.285 (6)	Cu(2)-Cl(3)	2.285 (6)
Cu(2)-Cl(4)	2.290 (4)	Cu(2)-Cl(4)#2	2.290 (4)
N(1)-C(2)	1.483 (7)	C(2)-C(3)	1.499 (7)
C(3)-N(3)	1.501 (7)	C(3)-C(4)	1.518 (7)
Cl(1)#1-Cu(1)-Cl(1)	180.0	Cl(1)#1-Cu(1)-Cl(2)#1	91.29 (7)
Cl(1)-Cu(1)-Cl(2)#1	88.71 (7)	Cl(1)#1-Cu(1)-Cl(2)	88.70 (7)
Cl(1)-Cu(1)-Cl(2)	91.29 (7)	Cl(2)#1-Cu(1)-Cl(2)	180.0
Cl(3)#2-Cu(2)-Cl(3)	180.0	Cl(3)#2-Cu(2)-Cl(4)	91.44 (6)
Cl(3)-Cu(2)-Cl(4)	88.56 (6)	Cl(3)#2-Cu(2)-Cl(4)#2	88.56 (6)
Cl(3)-Cu(2)-Cl(4)#2	91.44 (7)	Cl(4)-Cu(2)-Cl(4)#2	180.0
N(1)-C(2)-C(3)	112.1 (4)	C(2)-C(3)-N(3)	108.0 (4)
C(2)-C(3)-C(4)	112.3 (4)	N(3)-C(3)-C(4)	109.7 (4)

BOND LENGTHS [Å] AND ANGLES [°] FOR HIGH TEMPERATURE PHASE OF (1,2-DIAMMONIUMPROPANE)TETRACHLOROCUPRATE

	x	y	z	U(eq)
H (1NA)	-1151 (57)	-930 (127)	5150 (80)	60 (12)
H (1NB)	-1071 (57)	-625 (147)	6927 (83)	71 (13)
H (1NC)	-1194 (56)	1026 (50)	5832 (107)	57 (12)
H (2A)	-2313 (6)	-1863 (16)	5720 (20)	98
H (2B)	-2348 (6)	-714 (16)	7320 (20)	98
H (3A)	-2649 (6)	1968 (15)	5859 (19)	101
H (3NA)	-3971 (49)	579 (141)	5075 (81)	58 (31)
H (3NB)	-3726 (36)	364 (84)	7065 (19)	0 (16)
H (3NC)	-3679 (49)	-1258 (27)	5714 (92)	33 (23)
H (4A)	-2919 (9)	980 (19)	2958 (11)	110
H (4B)	-2671 (9)	-1162 (19)	3358 (11)	110
H (4C)	-2024 (9)	493 (19)	3348 (11)	110

HYDROGEN COORDINATES [X 10^4] AND ISOTRPIC DISPLACEMENT CO-ORDINATES ($Å^2$ X 10^3) FOR HIGH TEMPERATURE PHASE OF (1,2-DIAMMONIUMPROPANE)TETRACHLOROCUPRATE

YELLOW CRYSTALS

Tri(1,2-diammoniumpropane)tetrachlorocuprate(II) hexachloride - $C_9H_{48}N_6CuCl_{10}$

X-ray refinement data

Temperature	: 293(2)K
Wavelength	: 0.71073 Å
Crystal system	: Triclinic
Space group	: P1
Unit cell dimensions	: a=7.45(2)Å alpha=91.00(2)°
	: b=9.78(2)Å beta=100.14(2)°
	: c=11.44(3)Å gamma=100.68(2)°
Volume	: 805(3)$Å^3$, 1
Density	: 1.491 Mg/m^3
Absorbtion coefficient	: 1.5277 mm^{-1}
F(000)	: 375
Crystal size	: 0.17 x 0.13 x 0.1 mm
Range for data collection	: 1.81 to 23.27°
Limiting indices	: $-8 < h < 8$, $-10 < k < 10$, $-12 < l < 11$
Reflections collected	: 4179
Independent reflections	: 2292 (R_{int} = 0.0264)
Absorbtion correction	: Sadabs
Max. and min. transmission	: 1.00000 and 0.650741
Refinement method	: Full matrix on least squares on F^2
Data/ restraints/ parameters	: 2292 / 12 / 191
Goodness-of-fit on F^2	: 0.989
Final R indices [$I>2\sigma(I)$]	: R1 = 0.0277, wR2 = 0.0674
R indices (all data)	: R1 = 0.0434, wR2 = 0.0741
Extinction coefficient	: 0.0006(2)
Largest diff. Peak and hole	: 0.364 and -0.344 $eÅ^{-3}$

	x	y	z	U(eq)
Cu(1)	0	5000	0	29 (1)
Cl(1)	853 (1)	7122 (1)	-878 (1)	32 (1)
Cl(2)	2726 (1)	4426 (1)	-227 (1)	32 (1)
Cl(3)	3340 (1)	662 (1)	1164 (1)	36 (1)
Cl(4)	1696 (1)	3135 (1)	4971 91)	39 (1)
Cl(5)	8276 (1)	3628 (1)	-2351 (1)	35 (1)
N(1)	4972 (2)	2154 (2)	-1109 (2)	35 (1)
C(2)	3506 (3)	1749 (2)	-2172 (2)	40 (1)
C(3)	1839 (3)	704 (2)	-1982(2)	37 (1)
N(3)	647 (2)	1314 (2)	-1276 (2)	35 (1)
C(4)	648 (4)	126 (3)	-3160 (2)	62 (1)
N(11)	3261 (2)	3466 (2)	2597 (2)	32 (1)
C(12)	5180 (2)	4352 (2)	2795 (2)	33 (1)
C(13)	6587 (2)	3367 (2)	3255 (2)	34 (1)
N(13)	8446 (2)	4275 (2)	3351 (2)	36 (1)
C(14)	6375 (3)	2748 (3)	4423 (2)	56 (1)

ATOMIC CO-ORDINATES [$X10^4$] AND EQUIVALENT ISOTROPIC DISPLACEMENT PARAMETERS [Å X 10^{-3}] FOR TRI(1,2-DIAMMONIUMPROPANE)TETRACHLOROCUPRATE(II) HEXACHLORIDE

Cu(1)-Cl(2)	2.2639 (4)	Cu(1)-Cl(2)#1	2.2639 (4)
Cu(1)-Cl(1)	2.3535 (4)	Cu(1)-Cl(1)#1	2.3535 (4)
N(1)-C(2)	1.479 (3)	C(2)-C(3)	1.507 (3)
C(3)-N(3)	1.495 (2)	C(3)-C(4)	1.514 (3)
N(11)-C(12)	1.472 (2)	C(12)-C(13)	1.513 (3)
C(13)-N(13)	1.486 (2)	C(13)-C(14)	1.500 (3)
Cl(2)-Cu(1)-Cl(2)#1	180.0	Cl(2)-Cu(2)-Cl(1)	89.35 (2)
Cl(2)#1-Cu(1)-Cl(1)	90.65 (2)	Cl(2)-Cu(1)-Cl(1)#1	90.65 (2)
Cl(2)#1-Cu(1)-Cl(1)#1	89.35 (2)	Cl(1)-Cu(1)-Cl(1)#1	180.0
N(1)-C(2)-C(3)	115.4 (2)	N(3)-C(3)-C(2)	112.5 (2)
N(3)-C(3)-C(4)	108.0 (2)	C(2)-C(3)-C(4)	110.7 (2)
N(11)-C(12)-C(13)	112.6 (2)	N(13)-C(13)-C(14)	110.3 (2)
N(13)-C(13)-C(12)	106.4 (2)	C(14)-C(13)-C(12)	114.7 (2)

BOND LENGTHS [Å] AND ANGLES [°] FOR TRI(1,2-DIAMMONIUMPROPANE)TETRACHLOROCUPRATE(II) HEXACHLORIDE

	x	y	z	U(eq)
H (1NA)	5336 (34)	1456 (24)	-752 (21)	63 (8)
H (1NB)	5995 (29)	2756 (22)	-1277 (19)	54 (6)
H (1NC)	4533 (30)	2610 (23)	-558 (19)	50 (6)
H (2A)	4047 (3)	1367 (2)	-2784 (2)	48
H (2B)	3088 (3)	2581 (2)	-2467 (2)	48
H (3A)	2273 (3)	-66 (2)	-1554 (2)	44
H (3NA)	-427 (29)	698 (21)	-1230 (19)	51 (5)
H (3NB)	1283 (33)	1558 (24)	-546 (19)	61 (7)
H (3NC)	195 (41)	2025 (28)	-1581 (26)	91 (10)
H (4A)	-405 (4)	-536 (3)	-3021 (2)	93
H (4B)	1365 (4)	-324 (3)	-3609 (2)	93
H (4C)	231 (4)	872 (3)	-3595 (2)	93
H (11A)	2892 (27)	3266 (20)	3269 (18)	36 (5)
H (11B)	3211 (32)	2710 (22)	2192 (20)	57 (7)
H (11C)	2495 (30)	3963 (22)	2253 (20)	52 (7)
H (12A)	5301 (2)	5028 (2)	3362 (2)	40
H (12B)	5445 (2)	4633 (2)	2054 (2)	40
H (13D)	6483 (2)	2608 (2)	2664 (2)	41
H (13A)	8526 (29)	5056 (21)	3750 (18)	46 (6)
H (13B)	9339 (29)	3871 (22)	3730 (19)	47 (6)
H (13C)	8732 (37)	4470 (27)	2644 (21)	74 (8)
H (14A)	7315 (3)	2205 (3)	4650 (2)	83
H (14B)	5172 (3)	2163 (3)	4383 (2)	83
H (14C)	6503 (3)	3481 (3)	5017 (2)	83

HYDROGEN COORDINATES [X 10^4] AND ISOTRPIC DISPLACEMENT CO-ORDINATES ($Å^2$ X 10^3) for TRI(1,2-DIAMMONIUMPROPANE)TETRACHLOROCUPRATE(II) HEXACHLORIDE